MASTER

NAA-SR-1109
No. 3 OF 5
105 PAGES
SERIES C

74213

SODIUM GRAPHITE REACTOR

QUARTERLY PROGRESS REPORT

JULY-SEPTEMBER, 1954

RESTRICTED DATA

This document contains restricted data as defined in the Atomic Energy Act of 1946. Its transmittal or the disclosure of its contents in any manner to an unauthorized person is prohibited.

CLASSIFICATION CANCELLED
DATE 9-7-61
For The Atomic Energy Commission
H. F. Canell
Chief, Declassification Branch

NUCLEAR ENGINEERING AND MANUFACTURING
NORTH AMERICAN AVIATION, INC.

~~SECRET~~

NAA-SR-1109

REACTORS-RESEARCH AND POWER

SODIUM GRAPHITE REACTOR
QUARTERLY PROGRESS REPORT
JULY-SEPTEMBER, 1954

EDITED BY:
SIDNEY SIEGEL
GUY M. INMAN

NUCLEAR ENGINEERING AND MANUFACTURING
NORTH AMERICAN AVIATION, INC.
P. O. BOX 309 DOWNEY, CALIFORNIA

ISSUE DATE

DECEMBER 1, 1954

CONTRACT AT-11-1-GEN-8

662 003

~~SECRET~~

DO NOT PHOTOSTAT

DISTRIBUTION

Category: REACTORS-RESEARCH AND POWER (M-3679 15th Ed.)

Standard Distribution	Copy No.
AF Plant Representative, Burbank	1
AF Plant Representative, Seattle	2
AF Plant Representative, Wood-Ridge	3
American Machine and Foundry Company	4
ANP Project Office, Fort Worth	5
Argonne National Laboratory	6-16
Armed Forces Special Weapons Project (Sandia)	17
Armed Forces Special Weapons Project, Washington	18
Atomic Energy Commission, Washington	19-23
Babcock and Wilcox Company	24
Battelle Memorial Institute	25
Bendix Aviation Corporation	26
Brookhaven National Laboratory	27-29
Bureau of Ships	30
California Patent Group	31
Carbide and Carbon Chemicals Company (ORNL)	32-39
Chicago Patent Group	40
Chief of Naval Research	41
Commonwealth Edison Company	42
Department of the Navy - Op-362	43
Detroit Edison Company	44
duPont Company, Augusta	45-48
duPont Company, Wilmington	49
Duquesne Light Company	50
Foster Wheeler Corporation	51
General Electric Company (ANPD)	52-55
General Electric Company (APS)	56
General Electric Company, Richland	57-64
Hanford Operations Office	65
Iowa State College	66
Knolls Atomic Power Laboratory	67-70
Los Alamos Scientific Laboratory	71-72
Materials Laboratory (WADC)	73
Monsanto Chemical Company	74
Mound Laboratory	75
National Advisory Committee for Aeronautics, Cleveland	76
National Advisory Committee for Aeronautics, Washington	77
Naval Research Laboratory	78-79
Newport News Shipbuilding and Dry Dock Company	80
New York Operations Office	81
Nuclear Development Associates, Inc.	82
Nuclear Metals, Inc.	83
Pacific Northwest Power Group	84
Patent Branch, Washington	85
Phillips Petroleum Company (NRTS)	86-92
Powerplant Laboratory (WADC)	93
Pratt & Whitney Aircraft Division (Fox Project)	94
San Francisco Operations Office	95
Sylvania Electric Products, Inc.	96
Tennessee Valley Authority (Dean)	97
USAF Headquarters	98
USAF Project RAND	99
U. S. Naval Radiological Defense Laboratory	100
University of California Radiation Laboratory, Berkeley	101-102
University of California Radiation Laboratory, Livermore	103-104
Vitro Engineering Division	105
Walter Kidde Nuclear Laboratories, Inc.	106
Westinghouse Electric Corporation	107-112
Technical Information Service, Oak Ridge	113-129
File	130-150

TABLE OF CONTENTS

SECTION A
TECHNOLOGY OF THE SODIUM GRAPHITE REACTOR

(Section Editor - Sidney Siegel)

SECTION B
SODIUM REACTOR EXPERIMENT

(Section Editor - Guy Inman)

TABLE OF CONTENTS (Continued)

LIST OF FIGURES

LIST OF FIGURES (Continued)

LIST OF TABLES

This report is based upon studies conducted for the Atomic Energy Commission under Contract AT-11-1-GEN-8.

PREVIOUS SGR PROGRESS REPORTS

NAA-SR-227 Sodium Graphite Reactor Quarterly Progress Report, September-November, 1952

NAA-SR-260 Sodium Graphite Reactor Quarterly Progress Report, December, 1952-February, 1953

NAA-SR-274 Sodium Graphite Reactor Quarterly Progress Report, March-May, 1953

NAA-SR-878 Sodium Graphite Reactor Quarterly Progress Report, June-August, 1953

NAA-SR-956 Sodium Graphite Reactor Quarterly Progress Report, September-November, 1953

NAA-SR-1027 Sodium Graphite Reactor Quarterly Progress Report, December, 1953-February, 1954

NAA-SR-1049 Sodium Graphite Reactor Quarterly Progress Report, March-June, 1954

SECTION A

TECHNOLOGY OF THE SODIUM GRAPHITE REACTOR

I. FULL-SCALE REACTOR STUDIES

A. Analysis of Nuclear Performance (C. Roderick)

1. Plutonium Feedback Fuel Studies - To investigate the application of steady state plutonium feedback techniques to the use of diffusion plant tails for reactor fuel feed material, some reactivity calculations for this system have been performed. The fuel feed is considered to be a mixture of steady state plutonium[1] and uranium which is depleted to 0.25 per cent in the U^{235} isotope (2-1/2 grams of U^{235} per kilogram U^{238}). The variation in reactivity is estimated by calculating the ratio of the effective multiplication at any exposure to the effective multiplication initially; i.e., k_{eff}/k_{eff_o}

$$\frac{k_{eff}}{k_{eff_o}} = \frac{k_\infty e^{-\tau B_g^2}}{(1+L^2B_g^2)} \div \frac{k_\infty e^{-\tau_o B_g^2}}{(1+L_o^2B_g^2)} = \frac{(\eta f \epsilon p)\, e^{-\tau B_g^2}}{(1+L^2B_g^2)} \div \frac{(\eta f \epsilon p)_o\, e^{-\tau_o B_g^2}}{(1+L_o^2B_g^2)}$$

$$\frac{k_{eff}}{k_{eff_o}} = \frac{(\eta f)}{(\eta f)_o} \cdot \frac{(1+L_o^2B_g^2)}{(1+L^2B_g^2)} = \frac{(\eta f)}{(\eta f)_o} = \frac{\left(\frac{1}{L_o^2} + B_g^2\right)}{\left(\frac{1}{L_o^2} + \frac{\Sigma_{a\,total_o}}{\Sigma_{a\,total}} B_g^2\right)}$$

The values of ϵ and p are determined by the geometrical arrangement of the lattice and the concentration of U^{238}. Since the geometrical arrangement is fixed in any given instance, and the U^{238} concentration changes only slightly, the assumption is made that ϵp is independent of exposure. The slowing down area and geometrical buckling are also independent of exposure. The thermal diffusion area will change and therefore the thermal neutron leakage will change. The effect is particularly significant in the smaller reactors and cannot be neglected. For the larger reactors, the product $L^2B_g^2$ is small and the "correction factor" $(1 + L_o^2 B_g^2)/(1 + L^2B_g^2)$ is essentially unity.

Typical reactivity variations are shown for two cases in Figs. 1 through 6. The first case is for $R = \frac{N_{25_o}}{N_{28}} = 0.0025$ and $\alpha = \frac{N_{49_o}}{N_{25}} = 2$; the second case is for $R = 0.0025$ and $\alpha = 3$. The initial fuel composition for the first case is approximatel 2.5 grams U^{235}/kg, 5 grams Pu^{239}/kg, 3 grams Pu^{240}/kg and 1 gram Pu^{241}/kg; for the second case it is 2.5 grams U^{235}/kg, 7.5 grams Pu^{239}/kg, 4.5 grams Pu^{240}/kg and 1.5 grams Pu^{241}/kg.

The constants used in these calculations are for 20° C neutrons and are as follows:

$\upsilon(25) = 2.48$	$\upsilon(49) = 2.91$	$\upsilon(41) = 3.00$
$\sigma_a(25) = 680$ b	$\sigma_a(49) = 1065$ b	$\sigma_a(41) = 1480$ b
$\sigma_f(25) = 575$ b	$\sigma_f(49) = 745$ b	$\sigma_f(41) = 1080$ b
$\sigma_a(26) = 8$ b	$\sigma_a(40) = 530$ b	
$\sigma_a(28) = 2.77$ b		

B. Full-Scale Sodium-Graphite Power Plant (R. Balent)

The full-scale sodium graphite power plant study during the past quarter has been concerned primarily with the analysis and design of a plant which would involve the least amount of extrapolation from the Sodium-Graphite Experiment. It appears that a twin-core plant utilizing essentially all of SRE technology could be designed and constructed in the near future. The design is to be flexible so that it may take advantage of a number of anticipated improvements in reactor fuels, that is, as new fuel elements are tested and proven in the SRE they may be incorporated into the twin-core plant with a corresponding increase in the plant performance. The increase in power rating will not require major modification of the reactor system, but only the use of improved fuel elements and the addition of standard units of heat exchangers, steam generators, pumps, and turbo-generators.

The twin-core plant could operate initially with slightly enriched uranium fuel elements and produce weapons grade plutonium along with electrical power. At a later date the fuel assemblies could be changed to improved uranium assemblies or thorium assemblies and operate as a "power only" plant.

The performance of the twin-core plant when operated as a plutonium plus power and as a power only plant is given in Table I. It should be noted that the

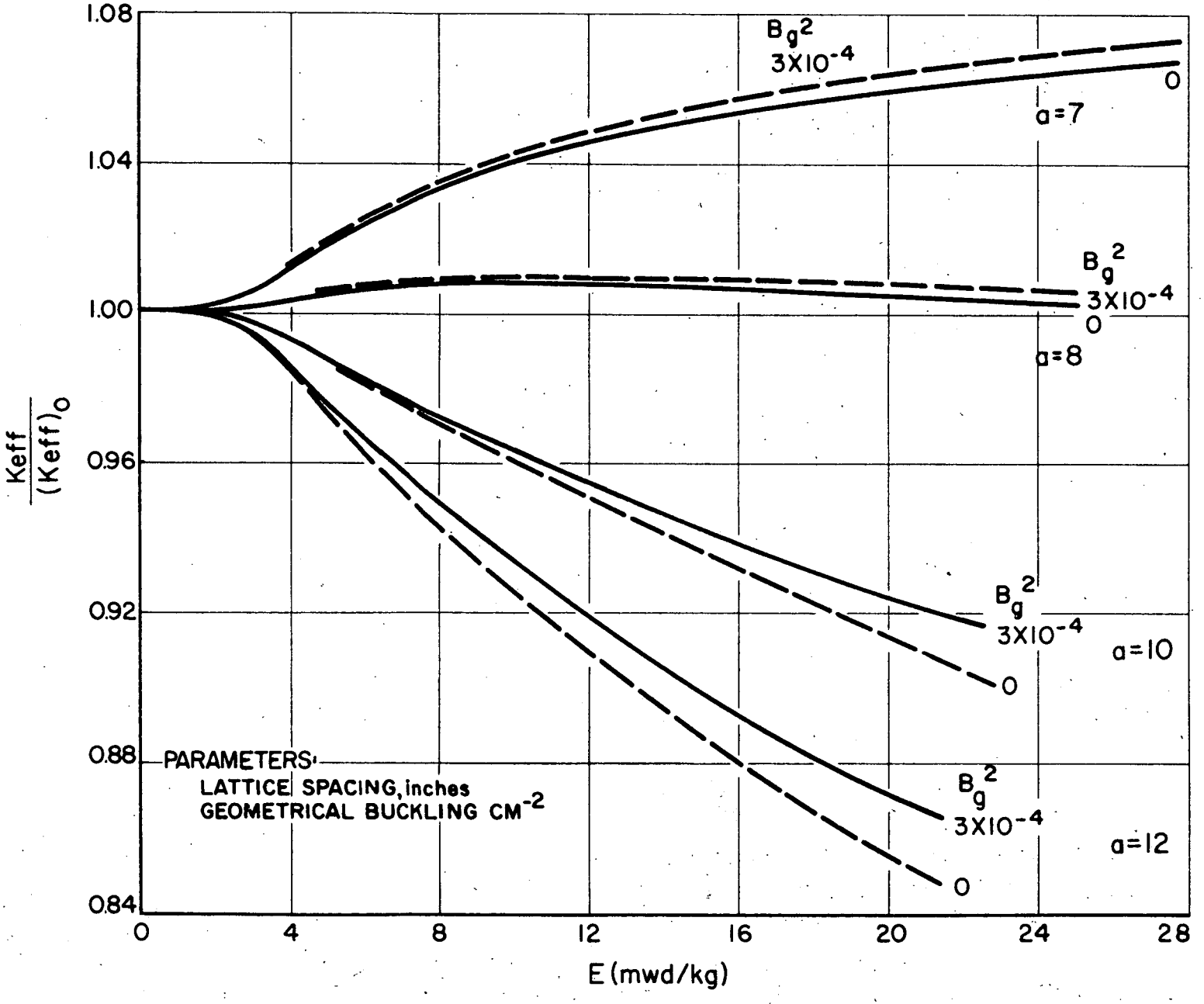

Fig. 1. Reactivity Changes vs Specific Energy, α = 2.00

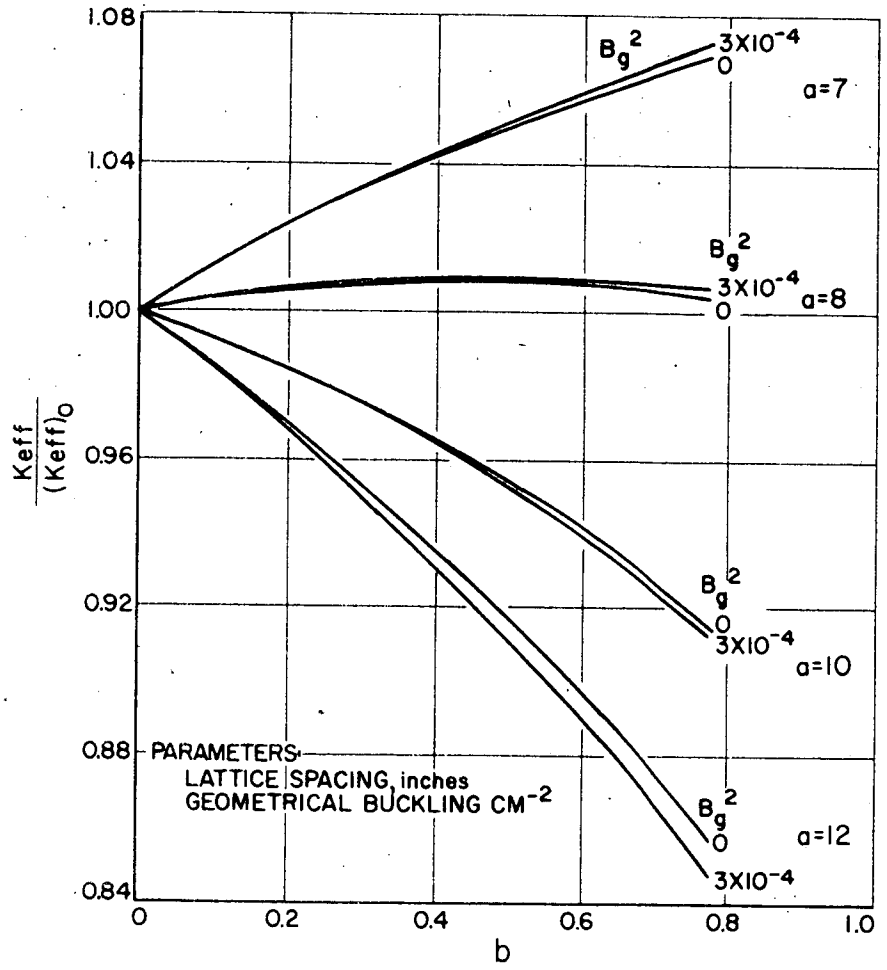

Fig. 2. Reactivity Changes vs Fractional Burnup of U^{235}, $\alpha = 2.00$

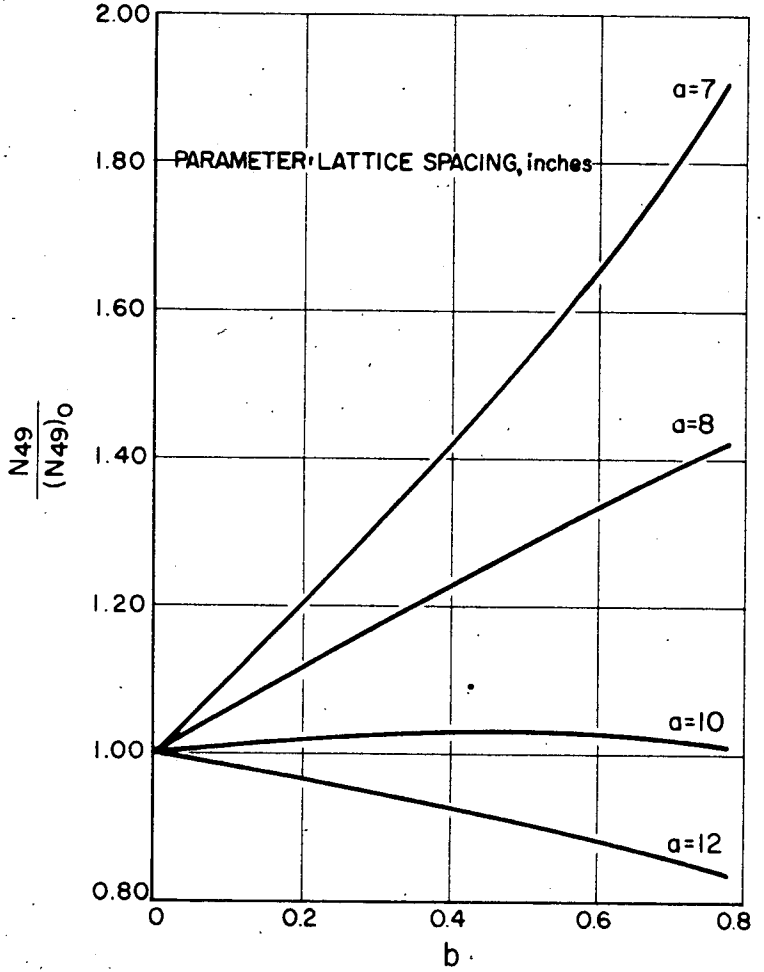

Fig. 3. Variation in Pu^{239} Concentration vs Fractional Burnup of U^{235} $\alpha = 2.00$

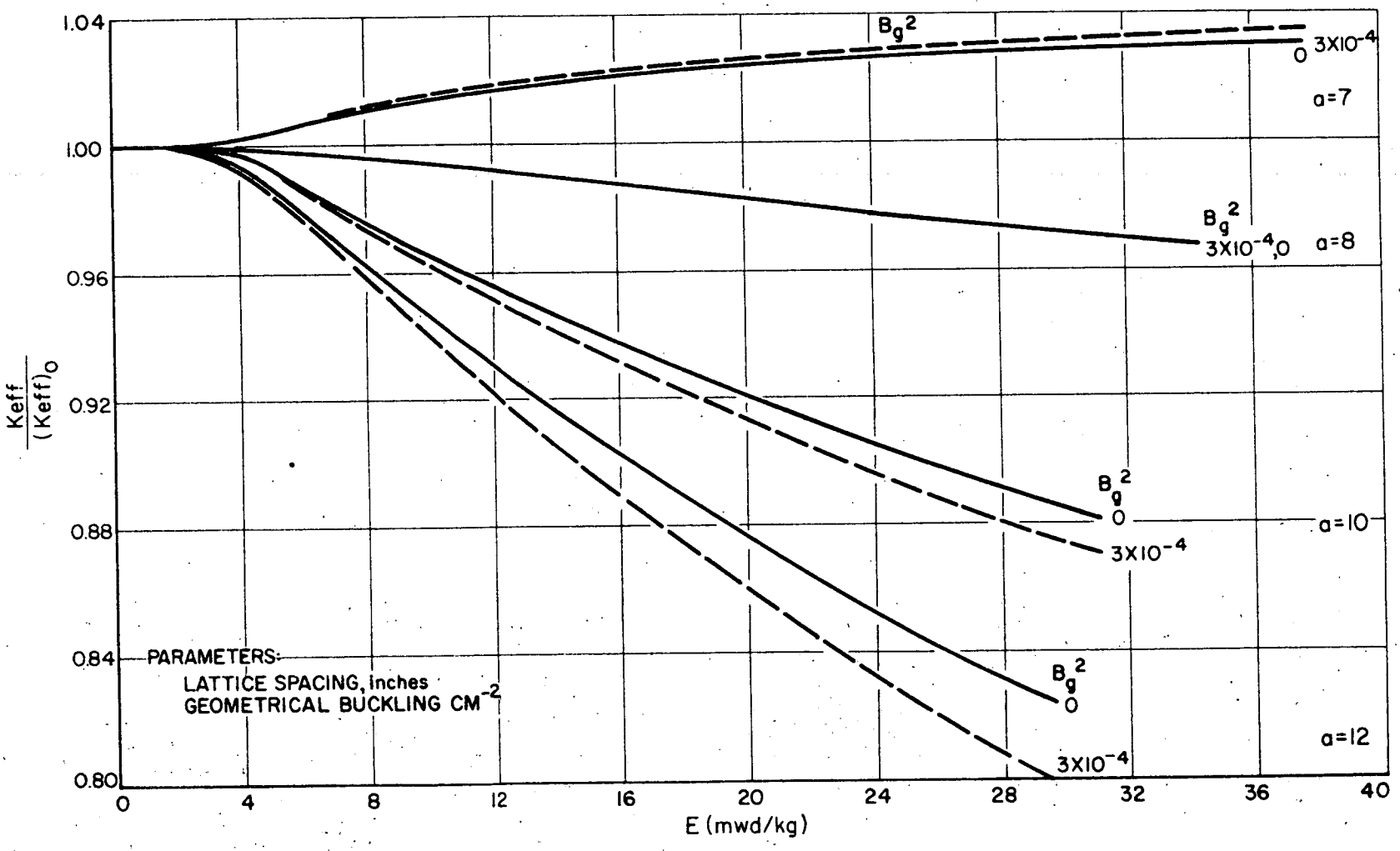

Fig. 4. Reactivity Changes vs Specific Energy, α = 3.00

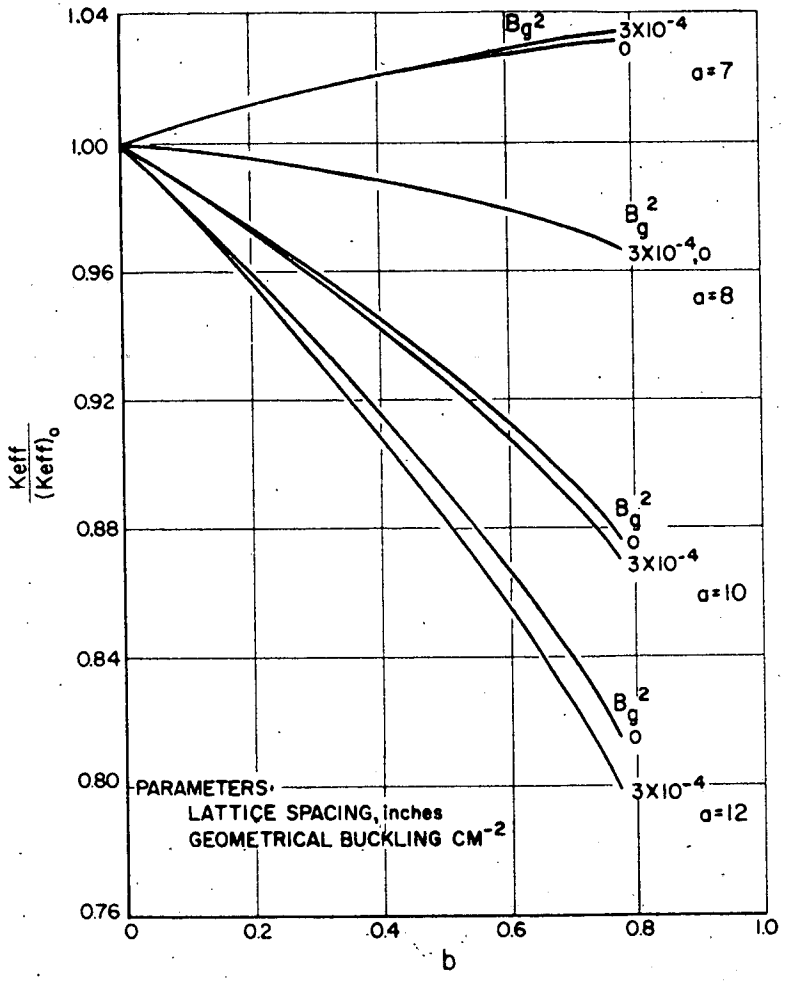

Fig. 5. Reactivity Changes vs Fractional Burnup of U^{235}, $\alpha = 3.00$

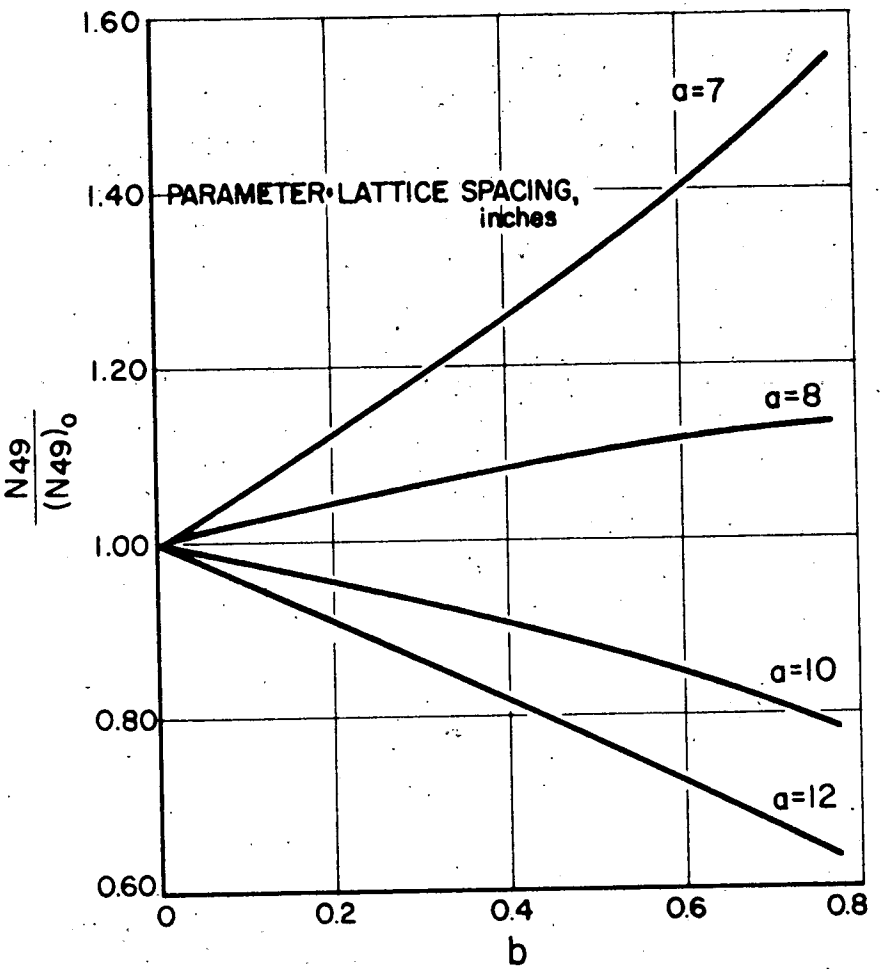

Fig. 6. Variation in Pu^{239} Concentration vs Fractional Burnup of U^{235}, $\alpha = 3.00$

TABLE I

TWIN CORE SODIUM-GRAPHITE REACTOR POWER PLANT

Design Designation	Twin Core Plutonium Plus Power SGR	Twin Core Power Only SGR
Core Dimensions Height x Diameter (ft)	10 x 11	10 x 11
Triangular Lattice Spacing (in.)	9	9
Number of Reactor Cores	2	2
Type of Fuel	U^{238} plus U^{235}	Thorium plus U^{233}
Number of Rods per Channel	19	7
Number of Loaded Coolant Channels	184	184
Maximum Center Temperature of Fuel Rods (° F)	1200	1950
Plant Thermal Power (Mw)	650	1000
Sodium Outlet Temperature (°F)	920	1090
Fuel Enrichment (Atom %)	2.25	2.70*
Fuel Investment per Core (tons)	23	14.8
Fissionable Mass per Core (kg)	470	365
Conversion Ratio	0.81	0.87
U Feed Rate for Weapons Grade Pu† (tons/yr)	132	
Pu Production Rate† (kg/yr)	155	
Steam Temperature (°F)	820	950
Steam Pressure (psig)	800	1250
Electric Power (Mw)	200	333

*1% excess k, which yields 10,000 mwd/ton

†80% plant factor

plant characteristics shown are those appropriate to optimum performance for the two different objectives shown. For example, if the U^{238} - U^{235} design had been optimized for initial power-only operation, the fuel enrichment required is 1.6 per cent, rather than 2.25 per cent.

The general arrangement of the reactor for the twin-core plant is shown in Fig. 7. The reactors are similar to the SRE in that they are of the tank type using hexagonal canned graphite moderator elements and a rotating upper shield. The over-all plant layout is shown in Figs. 8 and 9, and coolant system layout is shown in Fig. 10. The use of two cores rather than one large reactor results in a plant with a higher availability. The plant can be operated to 50 per cent rating during fuel loading and unloading operations or at times of low power demand. Each reactor will have its own controls, piping, pumps, and heat exchangers so that it can operate independently of the other; however, the same building, loading and unloading mechanism, and fuel storage facilities will serve both reactors.

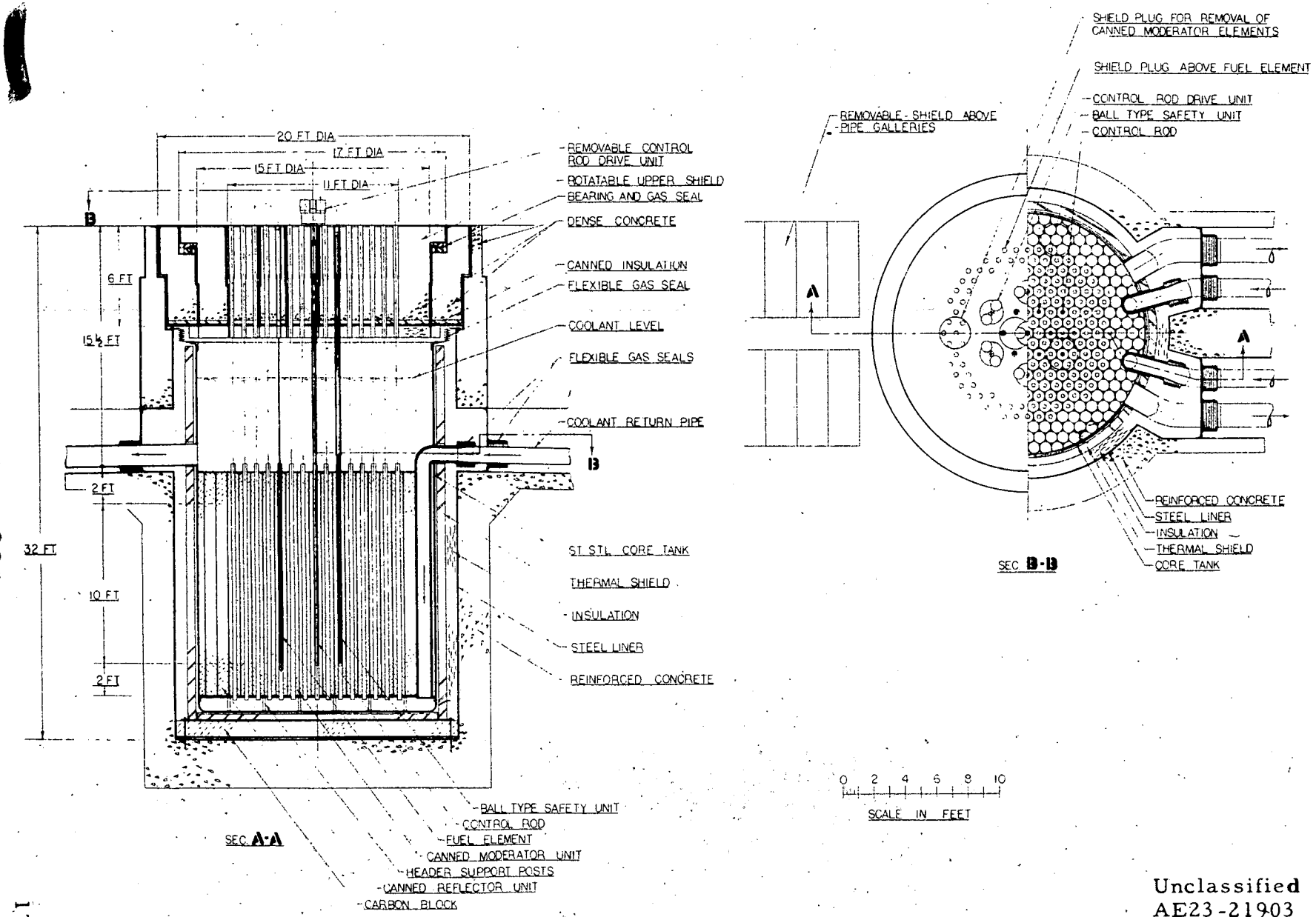

Unclassified
AE23-21903

Fig. 7. Layout - SGR Twin Core Reactor

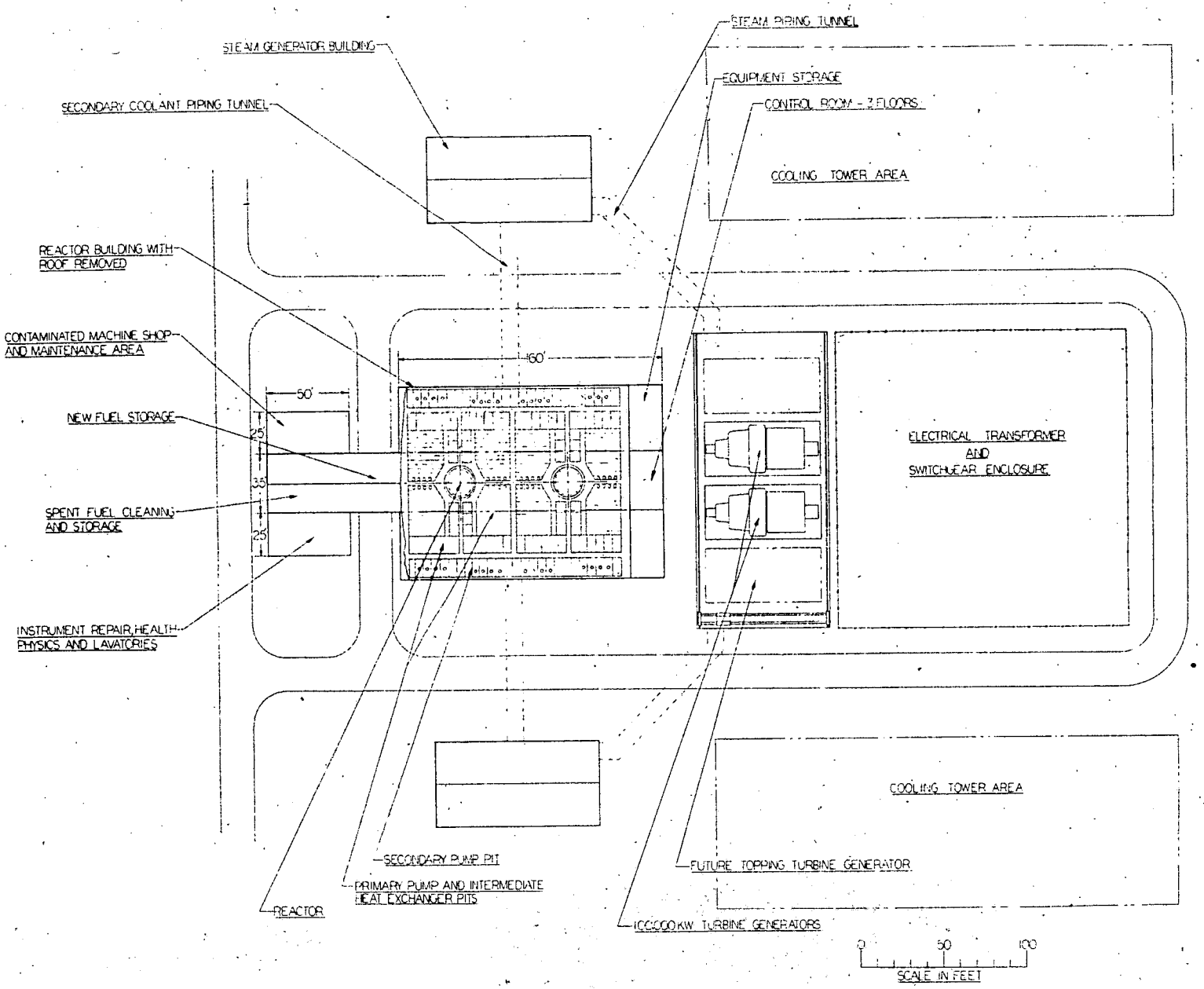

Fig. 8. Plant Arrangement - SGR Twin Core Reactor

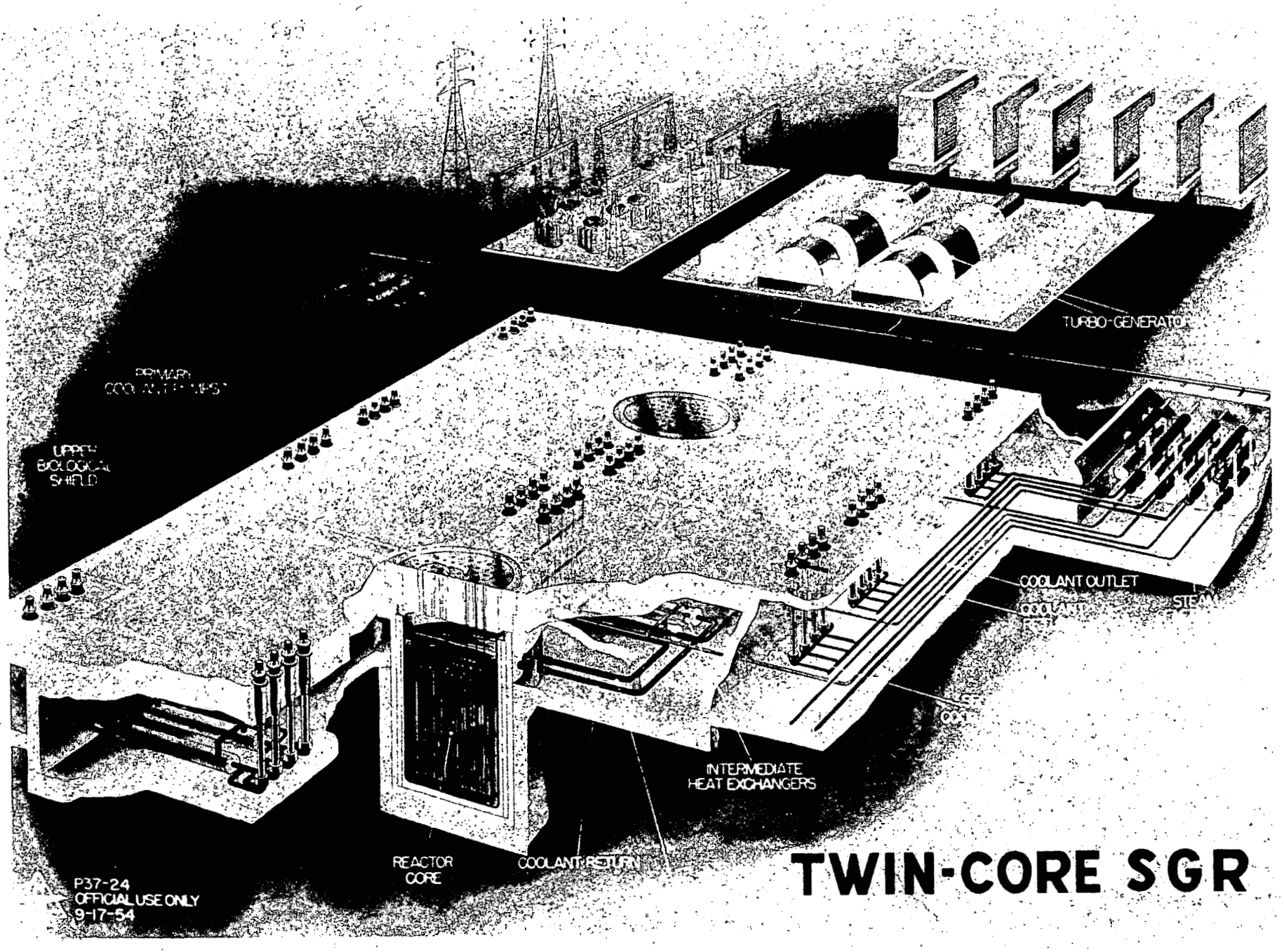

Fig. 9. Twin Core SGR

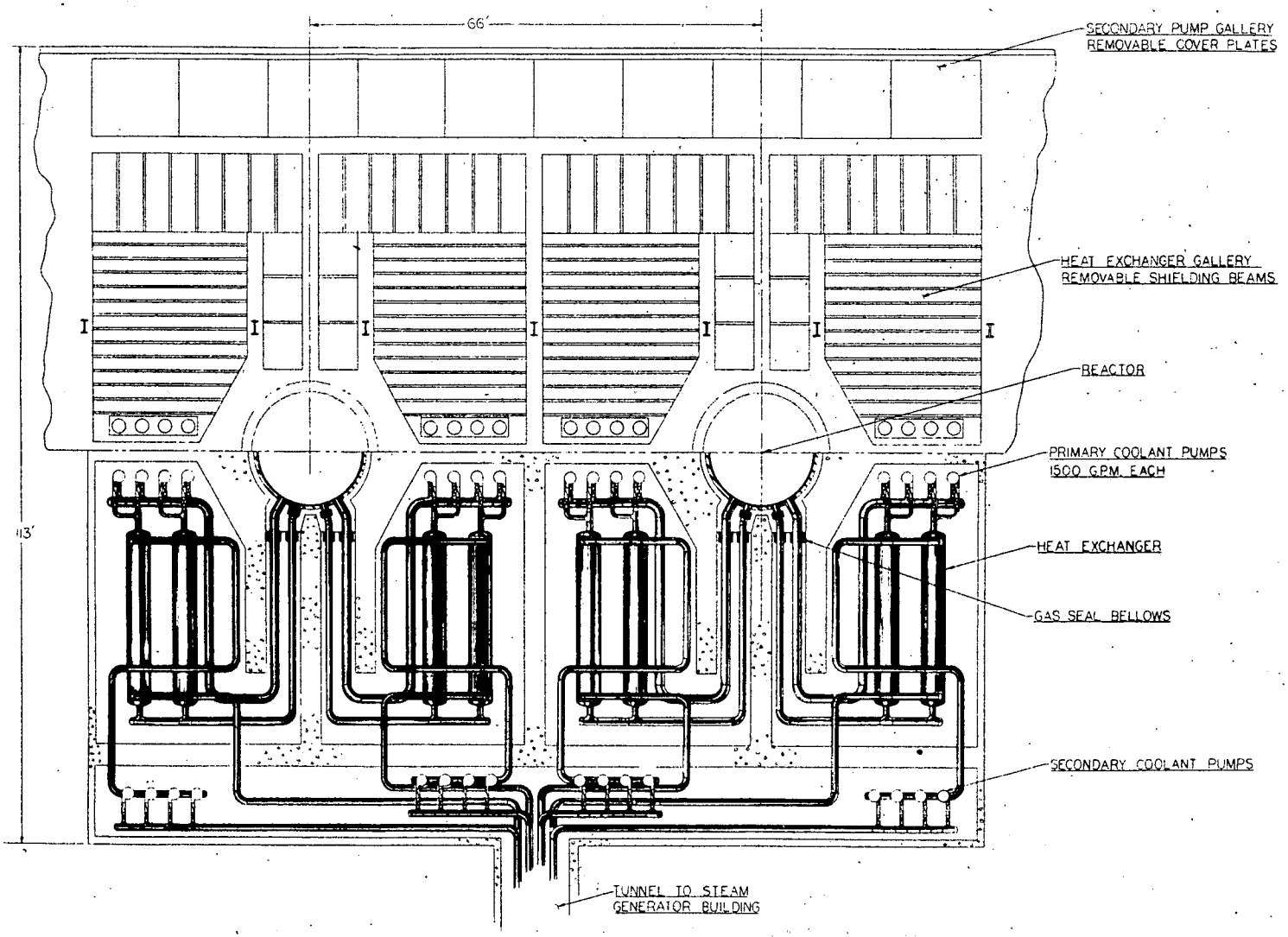

Official Use Only
AE23-21904

Fig. 10. Coolant System Plan View SGR Twin Core Reactor

II. REACTOR PHYSICS

A. Determination of Power and Temperature Coefficient of Reactivity

(G. W. Rodeback)

The essential features of the apparatus to measure the temperature coefficient of the effective resonance integral of U^{238} were described in detail in the previous progress report (NAA-SR-1049). The temperature coefficient is measured by comparing the activation of U^{238} foils (highly depleted in U^{235}) which have been irradiated at various elevated temperatures. This is accomplished by placing a thin sector shaped depleted foil in the central diametral plane of a short slug of normal uranium. The entire slug is heated by means of a small concentrically mounted heater and the whole assembly is mounted concentrically in an evacuated aluminum capsule. The latter is a water-cooled cylinder lined with cadmium and a thin inside plating of chromium.

Arrangements have been made to use the facilities of the SUPO reactor at Los Alamos for the irradiations. The original design has been modified so as to provide a quick disconnection of the slug from the capsule. The equipment is under construction and laboratory tests of the components and procedures are underway in preparation for the activation measurements.

B. Thermal Neutron Flux Distribution Measurements in Fuel Elements

1. Six Rod Fuel Cluster (E. Martin, B. A. Engholm) - Measurements of the thermal neutron flux distribution within a cluster of seven uranium rods were described in the previous quarterly report. These measurements were for the purpose of providing a check on the calculational procedure used to obtain the theoretical flux distribution within seven-rod fuel assemblies. The uranium rods which were used were one inch in diameter and had a U^{235} content of 0.9 per cent. They were contained in a 9.86 centimeter diameter aluminum cylinder with seven holes drilled lengthwise in it.

The measurements showed that the average flux in the central rod was only about 60 per cent that of the average flux in any of the other rods. Because of the comparatively low flux observed in the central rod, additional measurements were made to determine the effect of replacing the central uranium rod by a one-inch diameter graphite rod. The experimental details for the six-rod cluster were in most respects similar to those employed for the seven-rod cluster, however, the

substitution of dysprosium oxide foils for lead-indium foils eliminated the need for cadmium covered measurements.

A comparison of the thermal flux along a radius of the six-, and seven-rod clusters is shown in Fig. 11. The results of the measurements for the two clusters is summarized in Table II. The correlation of the data was based upon the assumption that foils placed in the buffer lattice, remote from the cluster, would be relatively unaffected by the change in the central rod. The last numbers shown in the table represent the average flux for all rods of the cluster normalized to the surface of the cluster. If these flux values are multiplied by the respective number of uranium rods in the cluster, the result is 3.3 for the six- and 3.5 for the seven-rod cluster. If a further correction is made for the fact that the over-all flux is less depressed by the six-rod cluster (the flux at the cluster surface is somewhat higher for the six-rod cluster), the comparison is more like 3.4 to 3.5.

It is clear that the over-all absorption of the cluster has been only slightly affected by the removal of the central rod. This is reasonable, since a thermal neutron which reaches the central graphite rod is very likely to be captured by an outer rod before it can leave the cluster. It is worth noting that the additional neutron absorption by the outside rods in the six-rod cluster takes place predominantly at the inner portions of the rods.

2. Hollow Fuel Elements (D. H. Martin) - Thermal neutron flux distribution measurements have been made in a hollow rod of natural uranium. Dimensions of the rod were 2.420 inches outside diameter and 1.389 inches inside diameter which is approximately the dimensions of the hollow slug which could be used to replace the seven-rod fuel cluster of the SRE. The flux measurements were made with the hollow fuel element positioned at the center of a buffer lattice of enriched uranium rods in the D_2O tank which is the same arrangement used for the six- and seven-rod fuel clusters. An aluminum rod was used to fill the space inside the fuel element and mock up the sodium coolant which would be present if the element were cooled internally.

Results of the flux measurements are shown in Fig. 12. A slight peak in the flux was observed at the center of the aluminum rod. The disadvantage factor, or ratio of flux at the outside surface of the rod to average flux in the uranium, was found to be 1.34. For a solid uranium rod with the same outside diameter, the disadvantage factor obtained by extrapolation from other data was estimated to be 1.62.

TABLE II

DISADVANTAGE FACTORS FOR SIX- AND SEVEN-ROD CLUSTERS

	6 U Rods	7 U Rods
Outside Uranium Rods		
$\frac{\text{Average flux over rod surface}}{\text{Average flux in rod}}$	$\frac{2.36}{1.93} = 1.22$	1.19
$\frac{\text{Average flux over cluster surface}}{\text{Average flux in rod}}$	$\frac{3.50}{1.93} = 1.81$	1.88
Central Uranium Rod		
$\frac{\text{Average flux in central rod}}{\text{Average flux in outside rods}}$	- -	0.63
All Uranium Rods		
$\frac{\text{Average flux in uranium rods}}{\text{Average flux over cluster surface}}$	$\frac{1.93}{3.50} = 0.55$	$\frac{1.72}{3.43} = 0.50$

C. Nuclear Parameters of Sodium-Graphite Lattices, Thorium-Uranium Fuel (W. J. Houghton)

The most economical full-scale sodium graphite reactor is believed to be one which operates on the Th-U^{233} breeder cycle. However, there is a problem in getting the reactor started since large quantities of U^{233} are not available. The presently favored method consists of loading the reactor with Th-U^{235} (highly enriched) alloy. With proper design, the U^{235} is then converted into U^{233} and breeding becomes established. Since there are no experimental data available on heterogeneous lattices using thorium-U^{235} alloy fuel elements, it is planned to do exponential experiments to provide the desired information on the nuclear parameters of these start-up lattices. The range of parameters which would be of interest in this experimental work was determined by considering the cost of power as a function of lattice spacing. Calculations were made extending a previously reported cost calculation[2] so that a definite minimum cost was found.

The basis of the cost calculation was a 1000 megawatt sodium-graphite breeder reactor which starts up on thorium-U^{235} alloy. The fuel rods are in the

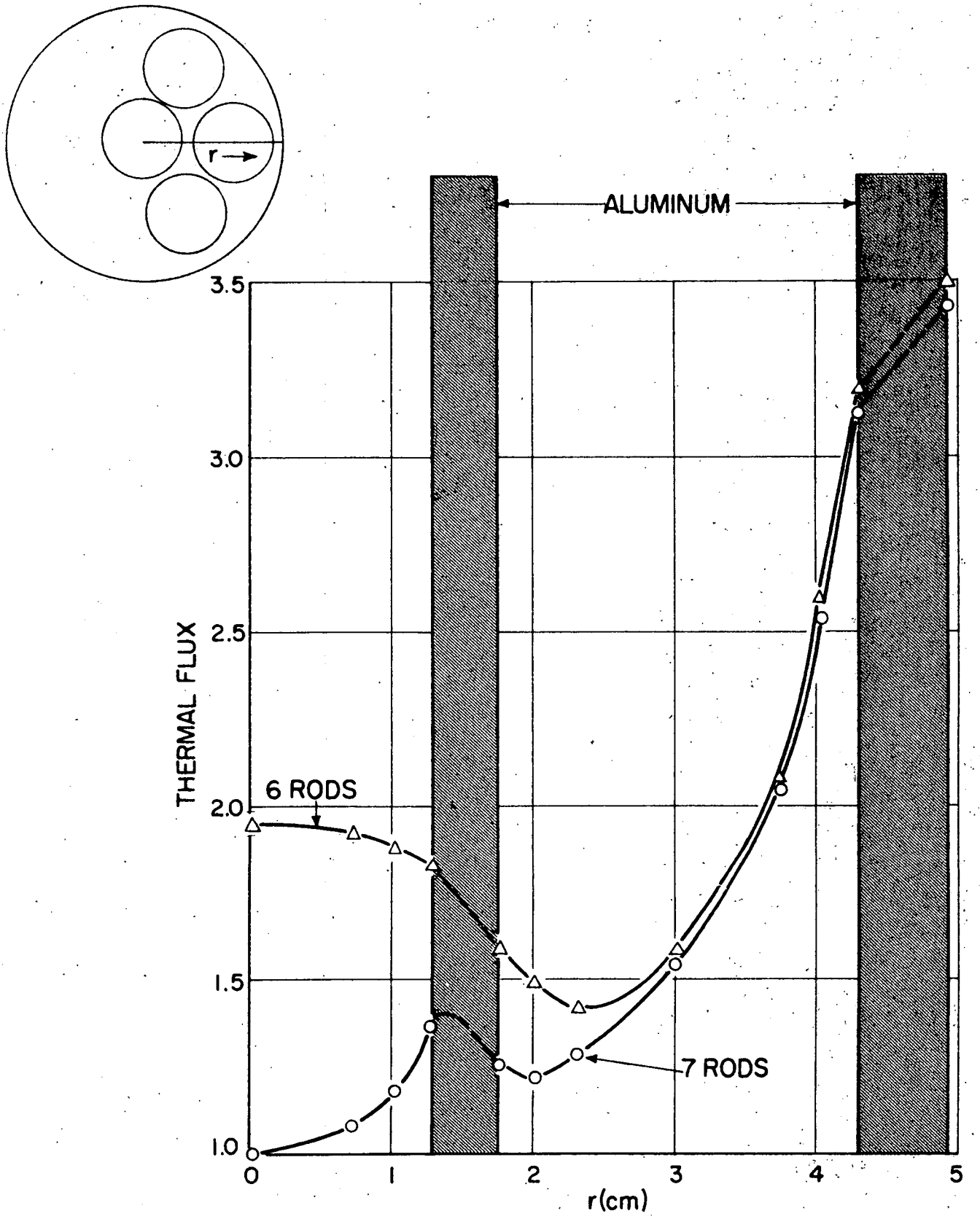

Fig. 11. Thermal Flux Through the Seven-Rod and Six-Rod (Graphite Center) Clusters

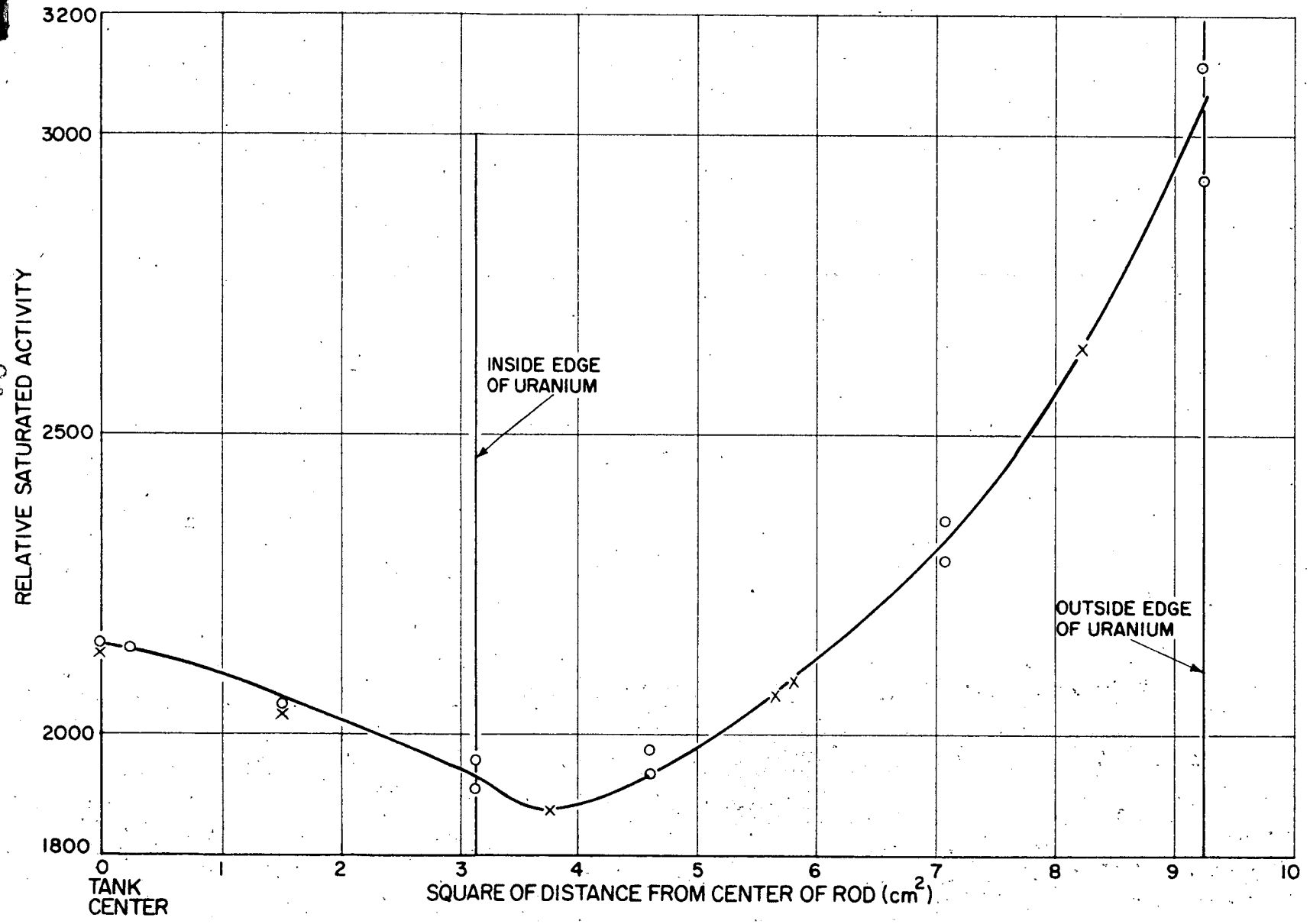

Fig. 12. Thermal Flux Through Wall of Hollow Uranium Rod

form of seven-rod clusters. A peak fuel temperature of 1800° F was assumed and the processing of the core was assumed to be done in a batch process with removal of fission products only. A net power conversion efficiency of 32 per cent was used. The reactor core structure and fuel cladding was assumed to be zirconium.

Figure 13 shows the calculated power cost as a function of lattice spacing. An optimum square lattice spacing between 8 and 9 inches was obtained. The sum of all charges except that for U^{235} investment makes up about 80 per cent of the power cost and these charges increase only gradually with lattice spacing. The rise in cost for the smaller lattice spacings is caused by the investment charge on the larger amount of U^{235} needed to make the reactor critical. The absolute value of the power cost is based upon present estimates of construction costs and operating performance; the principal purpose of this study was to locate the approximate position of the minimum, rather than its absolute value.

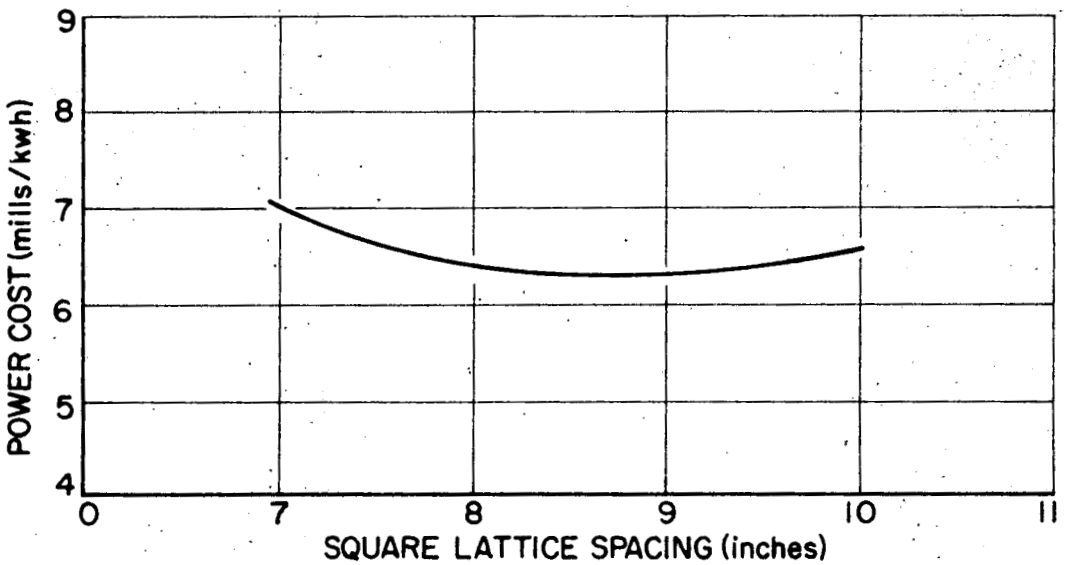

Fig. 13. Power Cost for 1000 Mw SGR Th-U^{233} Breeder Which Starts Up on Th-U^{235} Alloy

D. Neutron Leakage Through SRE Shield (F. L. Fillmore)

A method of calculating the flux in a reactor shield was described in the last progress report. Six-group calculations have now been completed for the radial and top shields of the SRE. Since each shield consists of several homogeneous regions, it was necessary to proceed stepwise through the shield taking two regions at a time. In each two-region problem, the thickness of the region

nearest the core is taken to be that actually occurring in the reactor structure while the second region is taken to be of infinite thickness. The first two-region problem consists of the reflector and the next material outside the reflector. For the top shield this is sodium, and for the side shield it is iron. The boundary condition at the entrance to the reflector is taken to be the flux at the core-reflector interface as was obtained from a two-region criticality problem. The other boundary conditions are continuity of flux and current at the interface between the two regions and vanishing of the flux at infinity. This problem is now solved and the current at the interface between the two regions is found which is then used as the boundary condition at the entrance to the first region in the next two-region problem. The physical basis for this choice is that modification of the shield regions of a reactor does not appreciably alter the conditions required for criticality, and hence the neutron current at a boundary inside the modified region cannot be greatly altered by such changes.

The next two-region problem has as its first region the material which made up the infinite region of the preceding problem. The thickness of this material is that actually occurring in the reactor structure. The second region of this problem is infinite and consists of the material which lies just outside the former material in the reactor. The boundary condition at the entrance to the first region is the current which was found in the preceding problem. The other boundary conditions are the same as before. This problem is now solved and the current at the interface between the two regions is found.

One proceeds in this manner until the problem consisting of the last two materials on the outside of the shield is solved. The flux near the other boundary of the final region will not be represented very well by the curves appropriate to the infinite outer region. Hence, the final step is to now solve a one-region problem with the flux vanishing at the outer surface of the shield. The boundary condition at the entrance to this region is the current which was found in the preceding problem.

The radial geometry was assumed to consist of three homogeneous regions exclusive of the core, namely reflector, iron thermal shield, and ordinary concrete biological shield. Hence, two two-region problems and a one-region problem were required. The axial geometry above the reactor was assumed to consist of four homogeneous regions exclusive of the core, namely reflector, sodium reservoir, iron thermal shield, and magnetite concrete biological shield. Hence,

three two-region problems and a one-region problem were required. The effect of neutron streaming through ducts was not considered nor were thin layers of material which had negligible effect on the attenuation of neutrons considered. Average values for the operating temperatures of the various materials were estimated. Recent design changes have modified some of these temperatures, so in view of this and the other factors which were neglected, the results of this study must be corrected in order to apply to the present SRE design. However, the curves presented herein can be used as a starting point for the SRE shield design.

The six-group constants for each material which were used in the calculations are listed in Table III. Figures 14 and 15 show the axial and radial fluxes, respectively. The radial flux has been corrected to cylindrical geometry by multiplying the calculated flux by $\sqrt{R/x}$, where R is the core radius and x is the distance from the reactor axis.

It will be noted that the fluxes are discontinuous at the boundaries, but these discontinuities are small in most cases (especially for the thermal flux) so their effect is relatively unimportant in an analysis of shield performance. The flux discontinuities appear because of the way in which the problem was formulated, namely the requirement of continuity of current at all boundaries in the shield. The requirement of continuity of flux would overdetermine the problem, so this requirement was dropped. Physically the flux is continuous, of course, so the absence of serious jumps in the calculated fluxes may be interpreted to mean that the method chosen was a satisfactory one.

Another interesting feature shown by the curves is the dip of the thermal flux in the iron region and its peaking in the concrete region. This is to be expected since the iron is a better absorber of thermal neutrons and a poorer moderator of fast neutrons than is the concrete. This feature would not be brought out by a calculation based only on fast neutron removal cross sections.

The attenuation of neutrons by slabs of iron, magnetite concrete, and ordinary concrete has been measured. The procedure was to place slabs of the above materials which were approximately 5 feet square upon the 28-inch thick graphite reflector of the WBNS and observe the activity induced in indium foils (cadmium covered and bare) distributed at various distances within the slabs of materials. Measurements were made on 6 inches of iron, 2 inches of iron followed by ordinary and magnetite concrete, and 6 inches of iron followed by

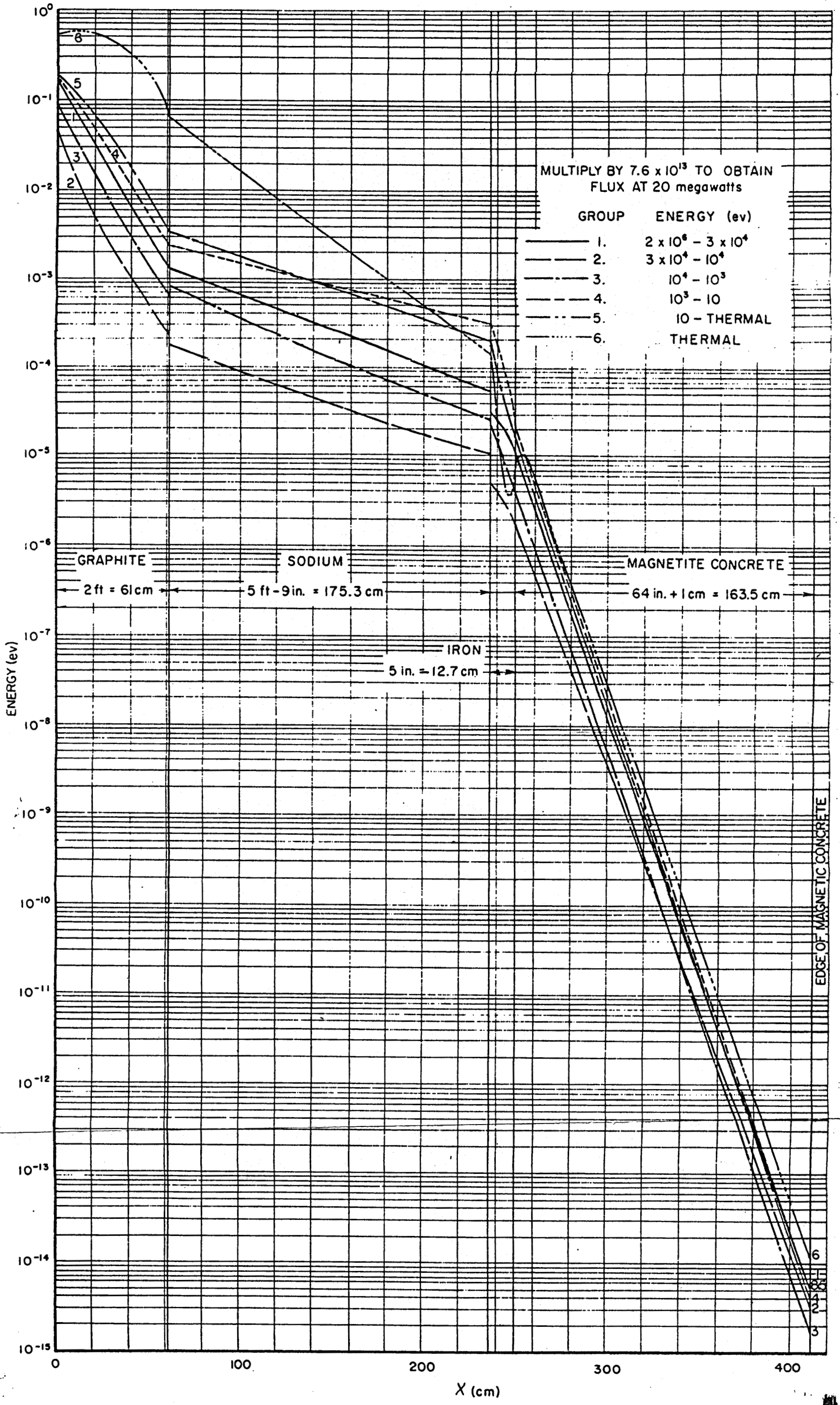

Fig. 14. Axial Flux above Reactor Normalized to Unit Thermal Flux at Center of Core

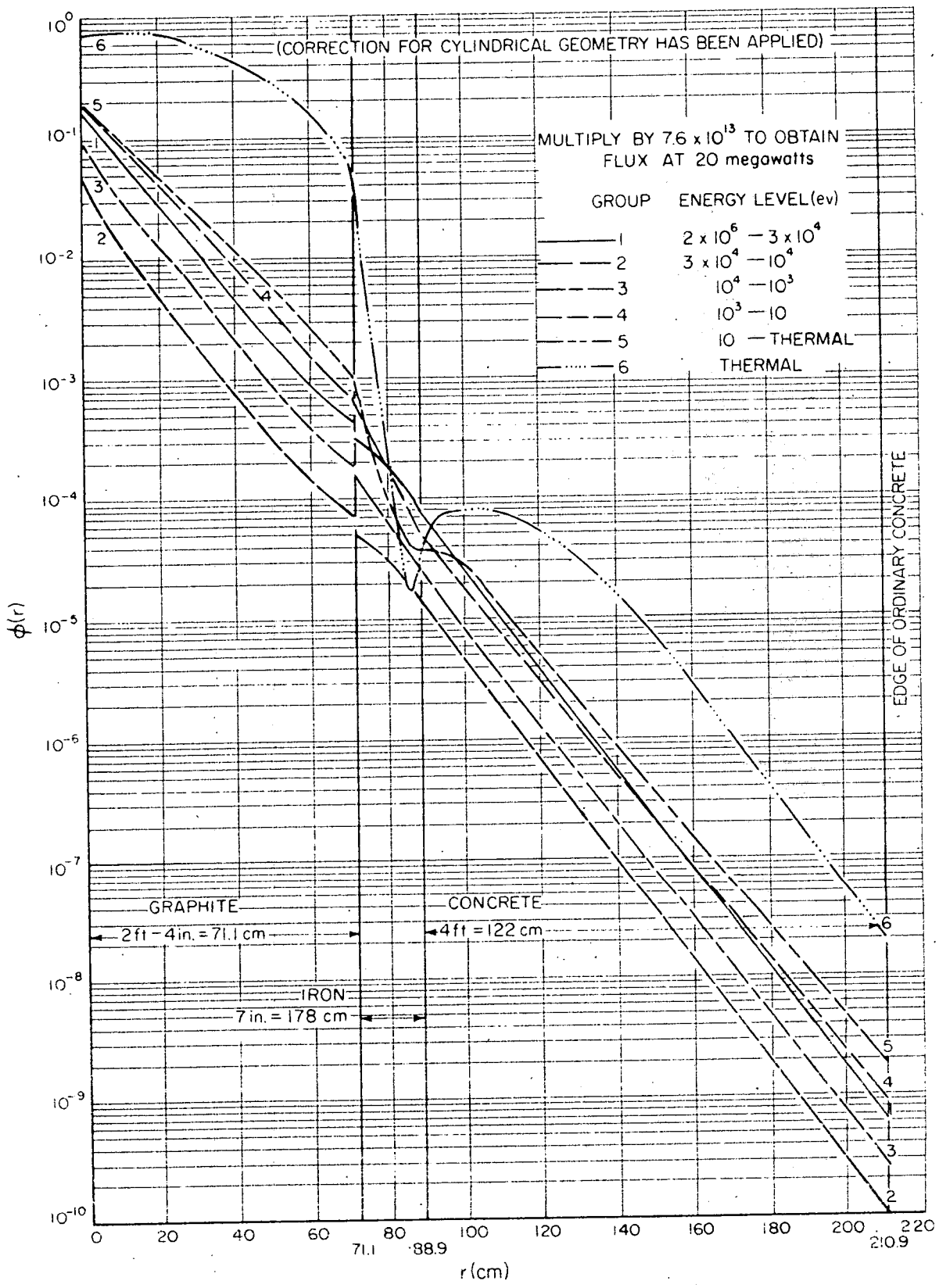

Fig. 15. Radial Flux Normalized to Unit Thermal Flux at Center of Core

TABLE III

SIX-GROUP CONSTANTS USED IN THE CALCULATIONS

Material	Quantity Tabulated						
	Group	1	2	3	4	5	6
	Group Energy (ev)	Fission - 3×10^4	3×10^4 - 1×10^4	10^4 - 10^3	10^3 - 10	10 - 1.a	Thermal
Axial	χ^2 (cm^{-2})	0.00655	0.05668	0.02705	0.01353	0.01353	0.00080
Reflector	D (cm)	1.153	0.928	0.928	0.928	0.928	0.914
T = 468° C	p	1.000	1.000	1.000	1.000	0.990	-
Sodium	χ^2 (cm^{-2})	0.000387	0.002777	0.001311	0.002608	0.000567	0.001358
T = 468° C	D (cm)	3.453	2.955	3.071	5.180	4.694	4.390
ρ = 0.84 g/cm^3	p	0.999	0.999	0.998	0.956	0.643	-
	Σ_a (cm^{-1})	0	0.00001	0.00003	0.00014	0.00145	0.00596
Iron	χ^2 (cm^{-2})	0.001450	0.007007	0.016429	0.025384	0.092569	0.3290
T = 400° C	D (cm)	1.156	1.259	0.577	0.375	0.366	0.359
ρ = 7.74 g/cm^3	p	0.992	0.993	0.983	0.866	0.215	-
	Σ_a (cm^{-1})	0.00005	0.00024	0.00054	0.00260	0.02727	0.11823
Magnetite	χ^2 (cm^{-2})	0.01776	0.2740	0.1665	0.1026	0.1189	0.0814
Concrete	D (cm)	1.245	1.152	0.772	0.646	0.620	0.600
T = 70° C	p	1.000	1.000	1.000	0.995	0.953	-
ρ = 3.60 g/cm^3	Σ_a (cm^{-1})	0.00003	0.00014	0.00032	0.00153	0.01786	0.04879
Radial	χ^2 (cm^{-2})	0.00704	0.06094	0.02908	0.01454	0.01413	0.000367
Reflector	D (cm)	1.153	0.928	0.928	0.928	0.928	0.914
T = 400° C	p	1.000	1.000	1.000	1.000	0.997	-
Ordinary	χ^2 (cm^{-2})	0.00923	0.12555	0.05883	0.03239	0.03181	0.00639
Concrete	D (cm)	1.539	1.240	1.324	1.215	1.149	1.156
T = 70° C	p	1.000	1.000	1.000	0.999	0.987	-
ρ = 2.32 g/cm^3	Σ_a (cm^{-1})	0	0.00002	0.00005	0.00025	0.00291	0.00739

ordinary concrete. The activity of foils placed in magnetite concrete proceeded by 6 inches of iron would have been too low to give reliable results, so this case was not studied.

The measured attenuation constants ($\mathcal{X}$) were obtained by fitting a simple exponential to the observed data and correcting the result for the finite transverse geometry. Two values were obtained for iron, namely, those for neutrons above and below the cadmium cutoff. These are compared to calculated values of $\mathcal{X}$-thermal and $\mathcal{X}$-intermediate in Table IV. The discrepancy between the experimental and calculated values of $\mathcal{X}$-thermal can probably be explained by the well-known phenomenon of neutron hardening in an absorbing medium and also an incomplete thermalization of neutrons by the 28-inch graphite reflector. A neutron temperature of about 150° C would bring these values into close agreement. The uncertainty in the thermal scattering cross section for iron (11 $\pm$ 1 barns) leads to about a 5 per cent uncertainty in the calculated value of $\mathcal{X}$-thermal so only about half of the discrepancy need be attributed to the first two effects.

It was found that the thermal and epi-cadmium neutron fluxes in the concrete were both attenuated by the same factors. The explanation for this is that neutrons of all energies arriving at a point deep in a material which contains much hydrogen must necessarily have penetrated to this point as fast neutrons. They remain fast until a head-on collision with hydrogen is made which thermalizes them, then they are quickly absorbed. Consequently, only the fast neutron attenuation constant is measured by this method. Good agreement was obtained between the experimental and calculated values of $\mathcal{X}$-fast for magnetite concrete. The exact composition of the ordinary concrete has not been determined, so a comparison is not possible for this case.

Fast neutron measurements using U^{238} and Np fission counters were also made but the data are still being analyzed.

TABLE IV

COMPARISON OF EXPERIMENTAL AND THEORETICAL ATTENUATION CONSTANTS

	$\mathcal{L}$ -thermal	$\mathcal{L}$ -intermediate	$\mathcal{L}$ -fast
Iron:			
Experimental	0.66 cm^{-1}	0.24 cm^{-1}	
Theoretical	0.72	0.23	
Magnetite Concrete:			
Experimental	-	-	0.134 cm^{-1}
Theoretical	-	-	0.130 cm^{-1}
Ordinary Concrete:			
Experimental	-	-	0.11 cm^{-1}

III. REACTOR FUEL ELEMENTS

A. Metallurgy of SGR Fuel (F. E. Bowman, B. R. Hayward)

1. Hollow Slugs - An internally and externally cooled large hollow uranium cylinder is being considered as a promising alternate fuel element to the seven-rod cluster. The element is made up of a series of powder-compacted hollow slugs approximately 2.42 inches O. D. by 1.38 inches I. D. by 4 inches long.

A sample slug was completely sectioned and metallographically examined for uniformity of structure, grain size, and hardness. The results showed uniform small grains and uniform microporosity throughout. Hardness values ranged from R_c20 to R_c25 with no apparent pattern.

The apparatus for thermal cycling these slugs, described in the previous period, required modification for satisfactory performance. The major changes involved the replacement of the glass container with steel and the cycle time was reduced to 1 hour. One specimen was thermal cycled 500 times between 100° and 500° C with an examination midway through the test. The data are shown in Table V.

TABLE V

THERMAL CYCLING OF HOLLOW URANIUM SLUGS

	After 243 cycles	After 500 cycles
Maximum Δd (O. D.)	+0. 008 in.	+0. 021 in.
Maximum Δd (I. D. , ends only)	+0. 004 in.	+0. 011 in.
Maximum Δl	+0. 002 in.	-0. 002 in.
Warp	+0. 006 in.	+0. 008 in.

It is important to note that the slug was cycled in a vertical position. Also, there was a small amount of oxidation of the slug after cycling which may cause some error in the measurements. The seam from the split die was very noticeable after cycling. One point along the seam was badly pitted. The greatest distortion occurred on one small arc on the top edge, which flared. Another large slug is currently being cycled; no results are available.

2. Dimensional Stability of Uranium Alloys at High Temperatures - Another series of powder-compacted uranium specimens were thermal cycled 500 times between 200° and 700° C. This high temperature cycling results in transforming the specimen from the low temperature alpha phase to a high temperature beta phase and back again. These specimens, which consisted of uranium alloys of Cr, Sn, Si, Mo, Bi, Zr, and Nb, were either hot pressed or cold pressed and sintered as indicated by the results in Figs. 16, 17, and 18. All of these powder-compacted alloys have been cycled at least in duplicate, except for the U-Zr alloys, with reasonable similarity of results. The other results were previously reported. The following observations are of interest:

a. The U-Cr alloys shown in Figs. 16 and 18 should not be interpreted as duplicate specimens since the origin of the specimens is different. The specimen shown in Fig. 16 was fabricated from a mixture of U and Cr powders while the other specimen was fabricated from prealloyed powder.

b. The hot-pressed alloys of U-Sn and U-Bi have all given poor results from the high temperature cycling tests. None of these alloys have been prepared by cold pressing and sintering.

c. Some of the hot-pressed U-Si alloys show severe distortion as illustrated in Fig. 16. Cold-pressed and sintered U-Si alloys of the same

U-Cr, 1.0 w/o Cr

Change in diameter = +2%

Change in length = +0.3%

Surface appearance = Sand blasted

Internal appearance = Solid

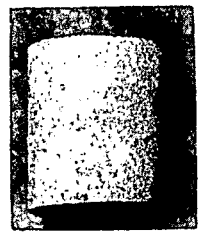

U-Si, 0.42 w/o Si (duplicate samples)

Change in diameter = +30% +20%

Change in length = -12% +7%

Surface appearance = Wrinkles & edges curled (both)

Internal appearance = Not examined (both)

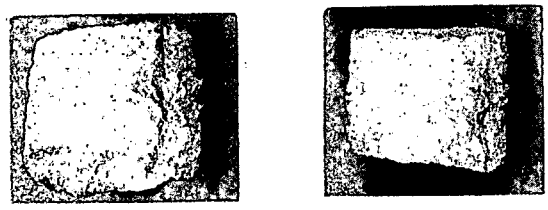

U-Sn, 2.0 w/o Sn (duplicate samples)

Change in diameter = +37% +42%

Change in length = +8% -7%

Surface appearance = Severely cracked (both)

Internal appearance = Porous (both)

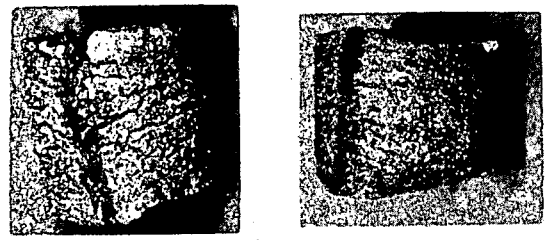

U-Bi, 1.0 w/o Bi

Change in diameter = +31%

Change in length = +19%

Surface appearance = Severely cracked

Internal appearance = Very porous

Fig. 16. Results of 500 Thermal Cycles (200°-700° C) on Hot-Pressed Powder-Compacted Uranium Alloys

U-Mo, 0.8 w/o Mo

Change in diameter = From -1% to + 6%

Change in length = -2%

Surface appearance = Smooth

Internal appearance = Solid

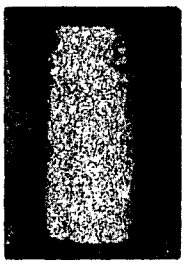

U-Mo, 1.2 w/o Mo

Change in diameter = +1%

Change in length = +0.6%

Surface appearance = Smooth

Internal appearance = Not examined

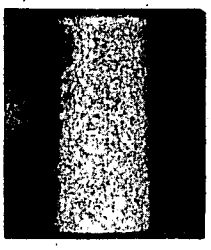

U-Nb, 3.0 w/o Nb

Change in diameter =	+3%	+1%
Change in length =	-0.1%	+2%
Surface appearance =	Bumpy	Smooth
Internal appearance =	Not examined	Solid

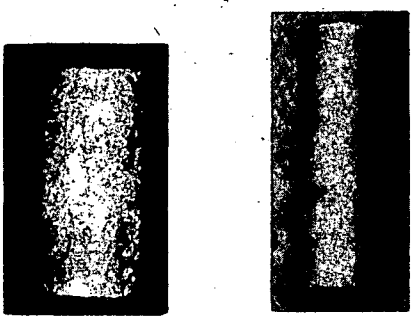

Fig. 17. Results of 500 Thermal Cycles (200°-700° C) on Cold Pressed and Sintered Powder-Compacted Uranium Alloys

U-Mo, 0.35 w/o Mo

Fabrication	=	Hot pressed
Change in diameter	=	+7%
Change in length	=	+13%
Surface appearance	=	Sand blasted

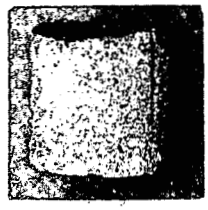

U-Si, 0.42 w/o Si

Fabrication	=	Cold pressed and sintered
Change in diameter	=	+6%
Change in length	=	+6%
Surface appearance	=	Sand blasted

U-Zr, 7.0 w/o Zr

Fabrication	=	Cold pressed and sintered
Change in diameter	=	+3%
Change in length	=	+2%
Surface appearance	=	Somewhat rough

U-Cr, 1.0 w/o Cr

Fabrication	=	Hot pressed, pre-alloyed powder
Change in diameter	=	+8%
Change in length	=	+3%
Surface appearance	=	A few large wrinkles and a few cracks

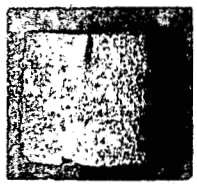

Fig. 18. Results of 500 Thermal Cycles (200°-700° C) on Powder-Compacted Uranium Alloys

composition, previously reported, indicate much less distortion. Sylvania has observed that the U-Si alloys require quite careful preparation during fabrication.

d. The cold-pressed and sintered U-Nb alloy specimens shown in Fig. 17 are appreciably more stable than the hot-pressed specimens described in other periods.

e. The cold-pressed and sintered U-Mo alloy specimens shown in Fig. 17 contained a slightly higher concentration of Mo than the hot-pressed specimen in Fig. 18. Both of the former specimens are quite stable, with the specimen of lower Mo content having some warp.

The results to date show the cold-pressed and sintered alloys to be superior to similar alloys which were hot pressed; this would indicate that complete dispersion of the alloying element brings about the stability noted. The most promising specimens have been the cold-pressed and sintered U-Mo, U-Si, and U-Cr alloys with the U-Nb and U-Zr alloys as promising alternates. Metallographic results on the above specimens are incomplete. The samples used in this study were prepared by powder metallurgy methods by Sylvania Electric Products.

3. Fission Gas Study - A theoretical analysis of the possible effects of gaseous fission products in SRE fuel slugs after relatively high burnup indicates potentially serious problems at the proposed temperature conditions. A series of MTR irradiation experiments are being designed to obtain a more realistic basis for evaluating these problems. This study is being made in conjunction with the MTR experiments for evaluating the temperature limits of SGR fuels described in Section III, C, 2. The data for both studies will be taken from the same capsule with the same specimens.

Design studies indicate that to obtain a 0.5 per cent burnup within a reasonable period while maintaining the 1200° F center and 900° F surface temperature of the slug imposes rather severe restriction on slug size. A 3/8-inch diameter specimen has been selected; this will give the desired burnup in 13 to 15 weeks irradiation. A 10 per cent enrichment was imposed by the desire to minimize the decrease in power generation with burnup. It has been decided to include heaters in the capsules in order to provide a means of compensating for temperature changes in the slug resulting from the inherent fluctuations in the reactor flux level. Provision is being made to monitor gas pressure in the capsule during the irradiation.

B. Metallurgy of Breeder Fuels (F. E. Bowman)

As a preliminary attempt to establish the solid solubility of uranium in thorium, a solid diffusion couple has been prepared by heating small cylinders of arc melted thorium and powder compacted uranium under axial pressure at 850° C for 24 hours. This treatment, which produced severe upsetting in both materials, resulted in what appears to be a satisfactory weld. The specimen, sealed in an evacuated vicor capsule, is being held for 30 days at 850° C. Subsequent to the treatment a thorough metallographic, X-ray diffraction, and chemical analysis will be made.

Additional couples pressure welded and diffused at other temperatures will be prepared, dependent upon the results obtained in the current experiment.

C. Determine Maximum Operating Temperature Limits of SGR Fuel

1. Restrained Slugs (B. R. Hayward) - Uranium fuel elements which operate with the peak internal temperature greater than 1220° F may have two phases (alpha and beta) coexistent within the fuel slug. Due to the density differences between these two phases, large internal stresses will develop. It is important to evaluate these stresses with both new fuel slug designs and new fuel slug materials. Previous thermal cycling of stainless-steel-jacketed alpha-rolled uranium slugs between 630° and 680° C resulted in various degrees of distortion of the jacket. As the jacket thickness decreased the distortion increased. The distortion increased as the number of cycles increased.

One of the promising approaches to help relieve these internal stresses is through use of a hollow slug with a small diameter axial hole. Jacketed specimens have been prepared with axial holes of varying size. These similar specimens are being cycled by the same technique as mentioned above for a direct comparison with solid slugs. There are no results to date. Hollow specimens are also being prepared for this test by other methods of uranium metal fabrication and from uranium alloys.

2. MTR Experiment (B. R. Hayward, R. R. Eggleston) - Experiments are being designed for SRE fuel slugs simulating the temperature level and temperature differences anticipated in SRE fuel materials. This includes tests both with the maximum fuel temperature of 1200° F and with temperatures greater than 1200° F. In order to get a reasonable burnup in a short period of time (0.5 per cent of total atoms in 17 weeks) the specimens will be enriched to about

10 per cent U^{235}. This fairly high U^{235} content helps to stabilize the temperature fluctuations anticipated within the specimens. The specimens will be made by the same technique and of the same material compositions as are expected to be used in the full-scale reactor. Among those fuels to be tested are uranium-rich alloys of Mo, Si, Cr, and Nb. If it appears feasible, Th-U alloys will also be studied.

The experimental specimen size is approximately 3/8 inch by 1-1/2 inch. Thus with the same ΔT as expected in the SRE 3/4-inch diameter slugs, this will actually be a more severe test. These tests are being designed for simplicity and economy with some variation in the results anticipated. A minimum of six tests (18 specimens) are planned. The capsule design is well advanced with current consideration being given to the use of heaters to maintain the desired temperatures. Each sample will have an internal thermocouple for temperature studies. A cobalt wire will be used to monitor the exposure.

IV. REACTOR MATERIALS

A. Engineering Evaluation of Graphite (D. Klein)

The second thimble of the MTR-NAA-3 experiment to determine the thermal conductivity of graphite was exposed. An attempt was made to minimize fluctuations in the thermocouple readings by cementing the thermocouples into their insulating tubes. This attempt was largely unsuccessful; and the fluctuations were, if anything, worse during this run than during the first. In spite of the large scatter in the data, order of magnitude agreement was shown between the data of this run and the first one (see NAA-SR-1049). Sample temperatures at the end of the second run were 450, 655, and 665° C. Post irradiation measurements of the samples exposed in both runs are expected to give better information on the state of damage of the graphite. Dissection of the experimental thimbles is under way at present at the MTR site; and the laboratory measurements will be carried out at NAA

B. Corrosion and Transfer of Radioactivity by Sodium (S. Nakazato, A. M. Saul)

1. Transfer of Radioactivity from Zirconium - The third capsule of the first series of three mini-harps to study the transfer of radioactive zirconium in sodium has been opened and analyzed. The first two of this set ruptured, one due to weld failure and the second capsule probably due to accidental overheating.

The power input to the furnace was approximately tripled over a period of 15 minutes while an emergency generator was in use. Rupture appeared to have resulted from an erosion of the stainless steel wall in the hottest zone, possibly a melting of a eutectic formed between zirconium and one of the components of the stainless steel. A mass of metal was found in the bottom of the capsule; this appeared to have a eutectic type microstructure. Since the third capsule experienced the same overheating, it was opened for analysis.

The third capsule had been heated for a period of 408.5 hours. The oxygen content of the sodium in this capsule was analyzed to be 0.07 per cent O_2 by weight.

Table VI shows the data for this capsule. The activities in the sodium and one the wall are seen to be concentrated on the lower hot portion of the capsule. No conclusions are drawn at this time as to why the activity should be concentrated in this lower section, or whether or not the activity on the wall is due to Zr^{95} diffusion into stainless steel. Possible mechanisms for this activity gradient have been postulated and will be checked during future experiments.

Three more capsules were prepared to replace the first series. One of these has already ruptured due to weld failure at the hot end.

TABLE VI

CAPSULE ANALYSIS -

TRANSFER OF RADIOACTIVE ZIRCONIUM

Capsule Section from Bottom to Top Inch	Temp. °C	Sodium Activity, d/m/cc	Wall Activity, d/m/cm^2
0 - 1	725	25,500	*
1 - 2	715	19,900	42,800
2 - 3	700	13,000	29,300
3 - 4	665	2,260	19,200
4 - 5	615	**	328
5 - 6	575	**	192
6 - 7	540	**	133
7 - 8	515	**	100
8 - 9	995	**	126
9 - 10	475	**	66
10 - 11	440	**	117
11 - 12	385	**	158

* Sample given to metallurgy group for metallographic analysis.
** Activity in these sections is below background for the dilution used in this analysis.

C. Organic Coolant Investigations (E. L. Colichman)

1. Toluene - Irradiation studies are being performed on toluene in relation to its proposed use as the shield coolant in the SRE. Some work completed on this project can now be summarized. Three metals Al, Cu, steel, (structural parts of cooling system) were immersed in toluene which was then irradiated at 150° F in the MTR-Gamma canal. Corrosion and irradiation damage data were obtained for three levels of gamma dosage, 6.6×10^6 to 3×10^7 R. It has been estimated that the maximum fast neutron flux impinging upon toluene in the SRE shield will be about 2.7×10^8 neutrons/sec-cm^2 with an average energy of 0.40 Mev and a cross section equal to 0.22 cm^{-1}, corresponding to about 0.5R/sec or 5×10^7R/3 years. Gamma facility experimental data has been extrapolated to estimate damage to toluene and the various metals for a service life of 3 years equivalent to 5×10^7R. Results are given below:

DAMAGE (PER 3 YEARS or 5×10^7 ROENTGEN)

Metal Samples (3/16 inch by 1/16 inch by 1 inch)	Corrosion		Gas Evolved, ml/gm Toluene
	Wt. Loss, mg	Penetration, mils	
Iron	2.2	.05	$0.20 \pm .12$
Al	1.0	.07	$0.20 \pm .12$
Cu	0.8	.02	$0.20 \pm .12$

On the basis of this experiment, it appears that radiation induced corrosion in the SRE shield cooling system will be negligible.

An MTR in-pile experiment on toluene and p-xylene now in progress, will offer an independent check on the extent of damage to be expected in the SRE shield cooling system.

2. Terphenyls - Pyrolysis and 1-Mev electron irradiation studies have been completed on the terphenyls at 400-450° C. Analyses of per cent polymer formed are still in progress on the ortho-terphenyl samples. The following summary of the results can be given at this time:

a. G_{gas}, $G_{polymer}$ and pyrolysis runs indicate that para-terphenyl is the most stable terphenyl isomer.

b. G_{gas} values for the terphenyls over the temperature range 30-350° C and at doses from 2-100 μah were:

para, 0.001-0.006
meta, 0.005-0.010
ortho, 0.005-0.009

c. $G_{polymer}$ and per cent polymer values for the terphenyls over the temperature range 400-450° C and at doses from 10-90 $\frac{\mu ah}{gm}$ were:

para, 0.020-0.022 and 4-31%, respectively
meta, 0.033-0.085 and 14-45%, respectively

d. Per cent polymer formed in the terphenyls in the pyrolysis runs at 400 and 450° C were:

para, 0.4-0.7% at 15-90 hr and
0.3-2.4% at 8-66 hr, respectively
meta, 0.1-0.3% at 10-84 hr and
4-12% at 7-74 hr, respectively

These electron irradiation results and pyrolyses indicate the following order of stability for the terphenyls: para>meta>ortho. Emphasis in this work has now shifted to similar studies with mixtures.

Gas volume measurements on terphenyls irradiated in MTR reactor hole VH-3 for 10^{19} nvt have been completed and are:

meta-, 1.21 ml/gm $\pm$ 0.09;
ortho-, 2.33 ml/gm $\pm$ 0.15;
and para-, 3.76 ml/gm $\pm$ 0.14.

It is planned to run another series of these samples to confirm the results obtained These in-pile irradiations at ambient (near room) temperature indicate the following order of stability based on gas evolution: meta>ortho>para.

Results on the order of stability of the various isomers under different conditions of irradiation and temperature are not only of scientific interest but also are necessary if an attempt is to be made to develop the most stable organic mixture for ultimate testing in an in-pile loop at high temperatures.

Further details in regard to present irradiation work are given in NAA-SR-1087.

Construction of the loop for circulating organic fluids at up to 900° F was completed and tested. The two major components, the heated test section and the pump, were found to perform unsatisfactorily at 800° F, the highest temperature reached. The capacity of the pump (Viking Pump Company) falls off rapidly in the 750-800° F region. In an effort to overcome this difficulty, work has begun on repiping the loop in such a manner that line loss will be held to a minimum. Difficulty with thermocouples and with the calrod heaters were encountered in the heated test section. Refabrication of this heated test section and construction of alternate models has been started. It has been found necessary to make these changes in the original pump loop scheme in an attempt to obtain a system that will operate for extended periods up to about 900° F.

SECTION B
SODIUM REACTOR EXPERIMENT
V. REACTOR DESIGN AND EVALUATION (LAND, BUILDINGS, SERVICES)

A. Site

The site selected and approved for the SRE Project has been surveyed to include layout of site boundaries, Reactor Building, Engineering Test Building, on-site roads and paved areas, drainage control system, and water distribution tank.

Preliminary grubbing and establishment of construction roads is now complete (Fig. 19). Insofar as possible, routing of these roads has followed final road layout.

Security planning requires the Reactor Building and Engineering Test Building to be enclosed in a limited area bounded by a perimeter fence of chain link type. The remainder of the site shall be considered a controlled area.

Communications at site will be furnished by commercial telephone and a radio facility similar to that in present use by North American Aviation Inc. at adjacent site areas. These will be tied into North American Aviation Inc.'s existing facilities to fully coordinate security and fire protection for total area.

A soil survey has been completed which generally indicates a solid sandstone with a sand overburden varying from 15 to 24 feet deep. No ground water was encountered in the 50-foot boring. This investigation substantiated practically all of the preliminary foundation design assumptions made previously, based on adjacent site foundation information.

Site grading, excavation and paving bid requests have been released as has the 50,000 gallon water distribution tank.

B. Reactor Building

Architectural layout has now reflected changes required by changing irradiated fuel storage from a wet to a dry type system. An underfloor fuel element and cleaning system together with a new hot cell location has been approved. The hot cell now shall be underground to receive irradiated fuel elements. Here the

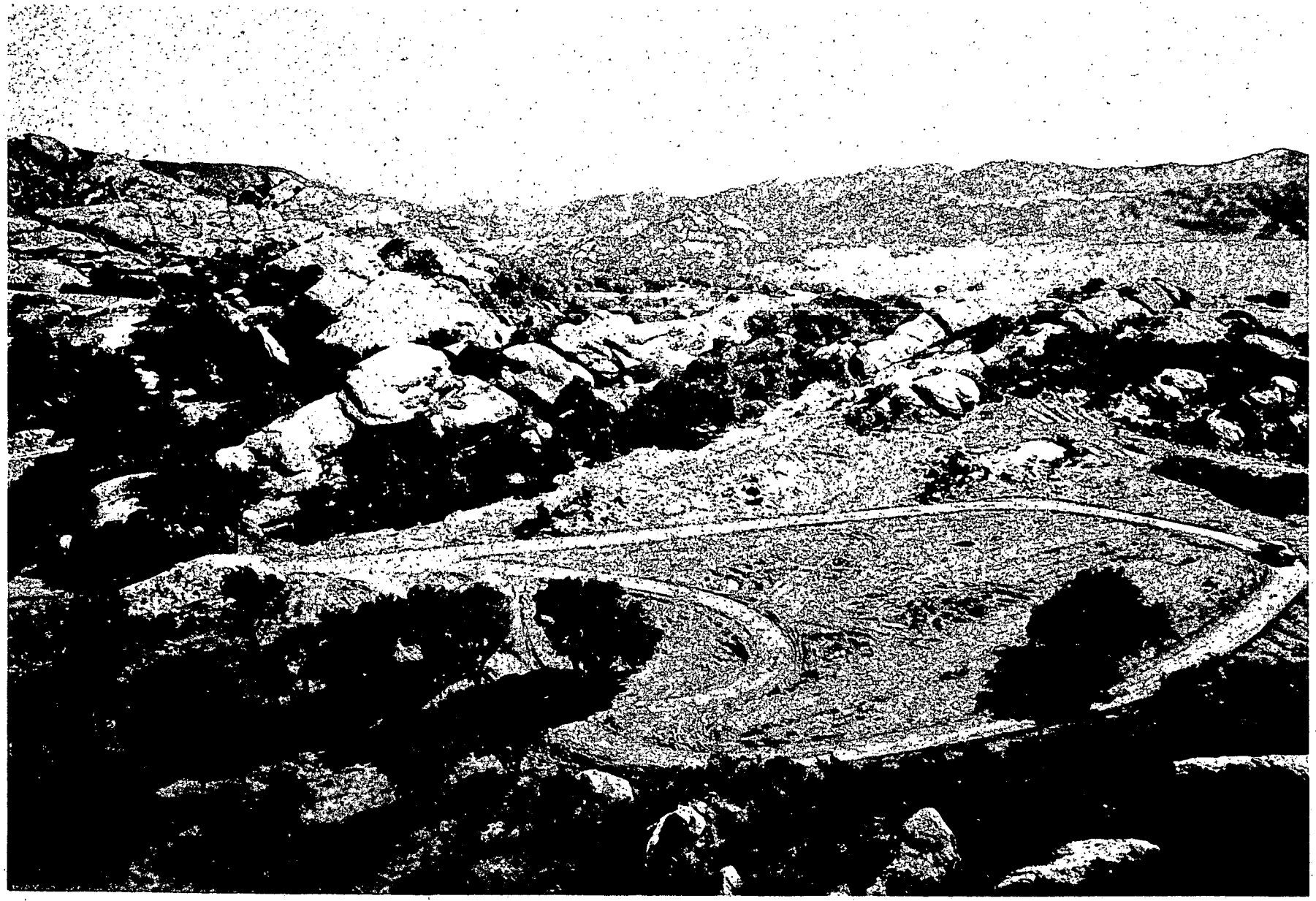

Fig. 19. Reactor Site

elements shall be prepared for the shipping coffin or disassembled and opened for examination in an adjacent metallurgical hot cell.

The handling bridge for the coffins and related services has been submitted for bids. Completion of this bridge and auxiliary trolley should be in time to handle the installation of heavier reactor components.

C. Engineering Test Building

Final architectural layout is in progress together with mechanical, electrical, and structural design.

The superstructural contract of the building has been awarded and preliminary construction drawings have been completed by the fabricator subject to North American Aviation Inc. approval.

VI. FUEL ELEMENTS

A. Fuel Material (B. R. Hayward, W. J. Hallett)

Specifications have been prepared for the uranium for the initial loading and routine operation of the SRE. These specifications have been submitted to the AEC for approval and procurement from FMPC. The material required consists of 4300 kilograms of 2.75 per cent enriched uranium metal in the form of slugs 6 inches long by 0.750 inch diameter (a total of 5230 slugs). The metal will be beta heat treated while in the rod stage, according to present practice at FMPC.

B. Fuel Rod Jackets (J. J. Droher, T. E. Stephens, W. J. Hallett)

Tentative specifications for the stainless steel jacket tubing have been prepared. With few exceptions, these are similar to existing military specifications. The major deviation will be the addition of specifications for non-metallic inclusions.

Since the wall of the fuel jacket is only 10 mils in thickness, it is important that this tubing have no regions of potential failure. Pin hole failure might allow the escape of fission products into the primary coolant. To detect whether such regions exist in the tubing, effort has been directed towards attempting to induce failure by extreme chemical and mechanical means.

Further metallographic examination of tubing both in the as-received condition and exposed to 800° F sodium was carried out both at NAA and at Allegheney

Ludlum. This steel was not excessively dirty and would rate as average or slightly better as far as cleanliness for stainless steel is concerned. The inclusions are primarily chromites which are mixtures of iron oxide and chromium oxide. Upon etching, many more dark particles were seen; these, however, are not inclusions but are the chromium carbides which have not been dissolved by annealing. These carbides could be removed by proper high temperature annealing, but is not believed that these carbides cause pitting in molten sodium.

To determine the presence of any areas of excessive carbide precipitation the Strauss test was utilized. Specimens of as-received tubing and tubing which had been heated in sodium for 100 hours at 800° F were subjected to immersion in a boiling solution of 3 per cent cupric sulphate, 10 per cent sulphuric acid, and 87 per cent distilled water for 72 hours. No evidence of excessive carbide precipitation or intergranular corrosion was noted upon metallographic examination.

To determine whether heavily oxidized sodium at high temperature would cause pitting or selective attack, the following tests were performed. Four specimens of tubing were sealed in a stainless steel capsule in contact with sodium which had been heavily oxidized. The capsule was maintained at 800° F for a total of 450 hours. The capsule was opened after 100, 200, and 450 hours at which times the specimens were water washed in air and visually examined. Neither of the aggravated conditions resulting from exposure to the oxidized sodium or the cleaning in air (which was done to deliberately develop high local surface temperatures where the burning sodium contacted the stainless steel) contributed to localized surface attack.

Hydraulic pressure tests of the tubing were conducted as a basis for establishing a non-destructive test in which the tubing is pressurized to 90 per cent of yield strength and examined for dimensional change and for leakage through flaws or inclusions. The yield and ultimate strengths and elongation values agreed with handbook data for Type 304 stainless steel. The majority of the test specimens failed with longitudinal split although several pinhole failures were obtained as shown in Fig. 20. The tubing at the top of the figure had been heated in sodium at 800° F for 100 hours and subsequently used in drop testing.[3] This tubing had visual pits at the start of pressure loading and failed with a pinhole leak. However, the increase in diameter of this tubing was significantly less than that of the other tubes tested due to the loss in ductility caused by the work hardening obtained in the drop test. Despite the presence of these known flaws the tubing did not fail at

90 per cent yield and reached the same ultimate load as the other tubes tested. This indicates that it is doubtful that this type of test could be adopted as a means of detecting minor flaws that were not visible prior to testing. It may have application in detecting thin-walled areas of significant size.

Preliminary tests of the welded joint between the fuel jacket and the end plug had indicated that a partial atmosphere of argon was necessary to strike an arc, while helium was added for purposes of leak testing the weld. Techniques have now been developed for making satisfactory welds in helium alone both at 1 atmosphere and 1/2 atmosphere. Tensile tests of these joints indicate that they are stronger than the jacket tubing.

Proof tests of the welded joint have been carried out by applying a load sufficient to stress the weld joint without permanently deforming the thin-wall tubing. It was found that a tensile load of 700 pounds would not cause permanent deformation of the tubing, while a load of slightly over 1000 pounds was required to reduce the tubing diameter 0.001 inch. Fracture of the tubing required a 2500 pound tensile load and the tubing diameter decreased along its entire length uniformly until just before fracture. It is suggested that a dead load of 700 pounds or less be used to test all fuel rods to detect extremely poor welds and to aggravate any minute flaws so that they may be more easily found in the leak detection test.

C. Spacer Wire (H. Strahl)

The wire wraps to be used for spacing the fuel elements have been preformed by Pacific Wire Rope Co. As shown in Fig. 21, the wire used was hard drawn Type 304L stainless steel. The wires are 0.091 inch in diameter, 100 inches long, and have a pitch of 10 inches. The wires fit snugly to the tubing but are difficult to install and will spring from the tubing if not restrained.

VII. MODERATOR, REFLECTOR, STRUCTURE

A. Reactor Core Tank and Supporting Structure (W. J. Sanders)

Changes in the material of both the core tank and the intermediate tank were incorporated into the design. Studies have been made of the stresses in the core tank and in the intermediate tank which proved that the wall thicknesses are adequate to withstand the loads involved without excessive creep of the material at the maximum temperature at which these parts will operate.

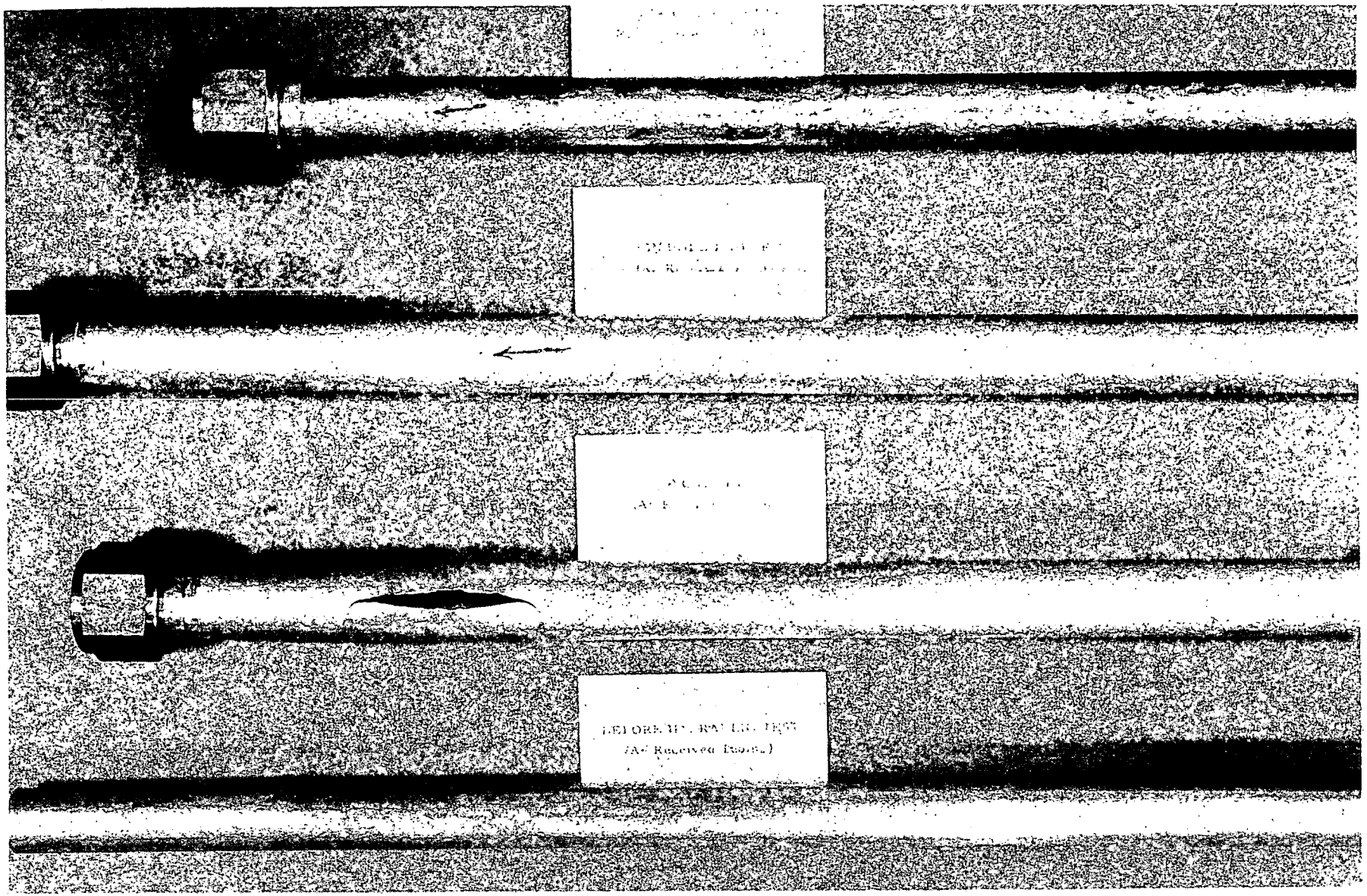

Fig. 20. Fuel Rod Cladding - Hydraulic Test Specimens

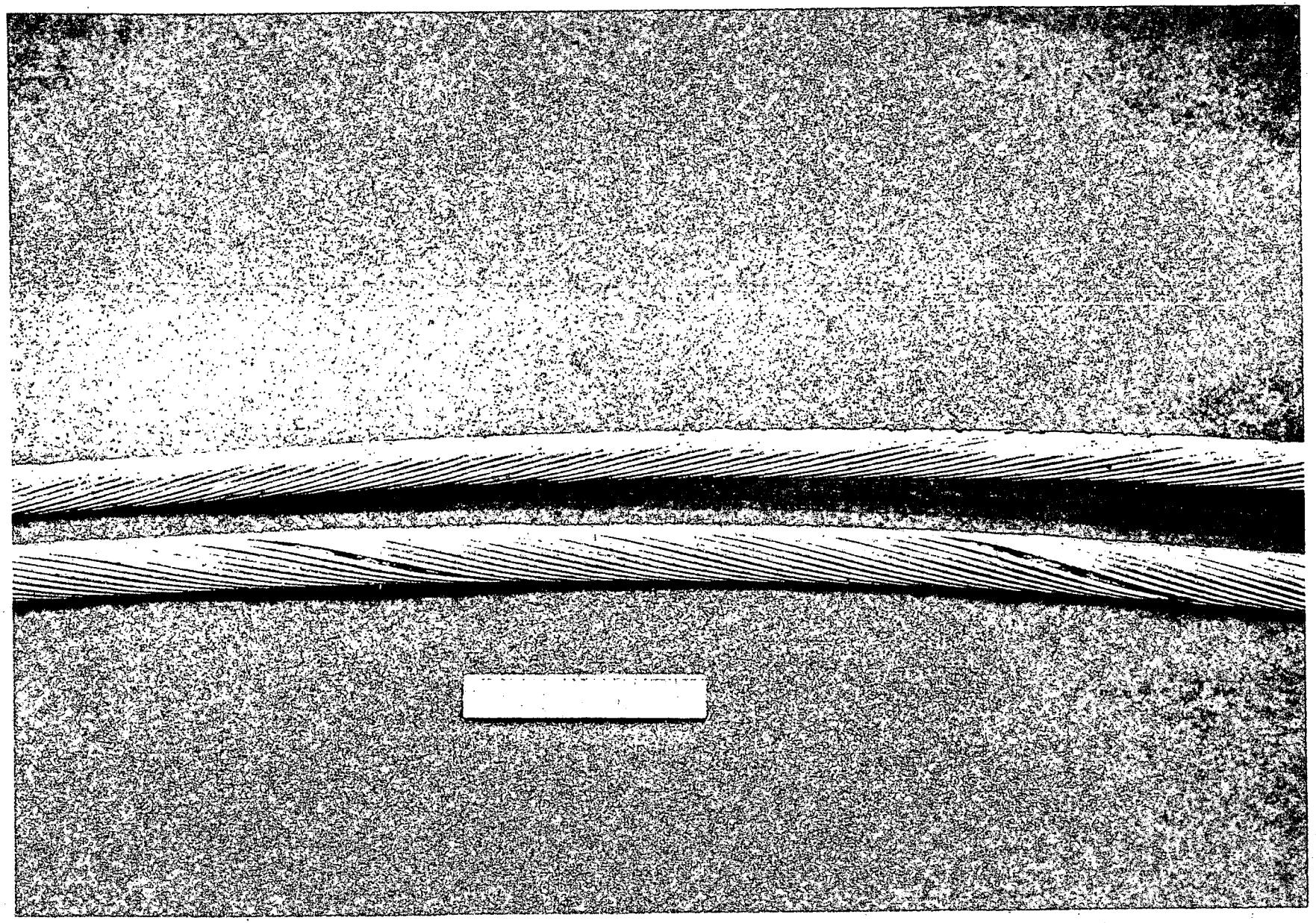

Fig. 21. Fuel Rod Spacer Wire

A study is being made of the heat transfer characteristics of the coolant with respect to the core and the core tank to insure that no excessive thermal stresses will be imposed on the wall of the core tank. Layouts have been made of some alternate schemes of the arrangement of the inner thermal shield and core clamps between the core tank and the core.

Further studies of the thermal shield material have corroborated the selection of the high temperature resistant gray cast iron originally specified.

Insulation cells have been designed to fit the annular space between the intermediate tank and the core cavity liner. These consist of long rectangular sheet metal containers which may be filled with either a granular or fibrous type of insulation and which may be installed from the top after the tanks, thermal shield, and piping have been placed. Insulation at the bottom of the cavity will be arranged similarly except that the cells will be smaller and of a modified cubical shape. Selection of the insulating material will be predicated upon the results of tests now being conducted on the compatibility of liquid sodium with various types and brands of insulation (See Section VIII, B, 1).

Studies are in progress of the arrangement of the large bellows gas seal at the top of the core tank and intermediate tank to insure that neither mechanical nor thermal stresses are excessive in the bellows or their attaching members. Bellows manufacturers have been contacted in an effort to determine successful bellows attachment methods in similar installations.

Detail drawings have been made for the following items; core tank, thermal shield, outer tank, and supporting structure. Some of these are complete and ready for purchase. Others are being checked.

B. Development of Zirconium Moderator Cell Cans (R. C. Brumfield, W. L. Cockrell)

Work performed this quarter was concerned principally with the following: design of a breathing tube for the moderator cans, calculations on the transport of sodium vapor, rolling of the zirconium billets into sheet form, machining of graphite billets, procurement of a welding stake, and installation of an outgassing furnace and vacuum equipment.

1. Design - The vent tube system shown in Fig. 22 was designed to allow the moderator can to breathe into the helium plenum chamber above the sodium

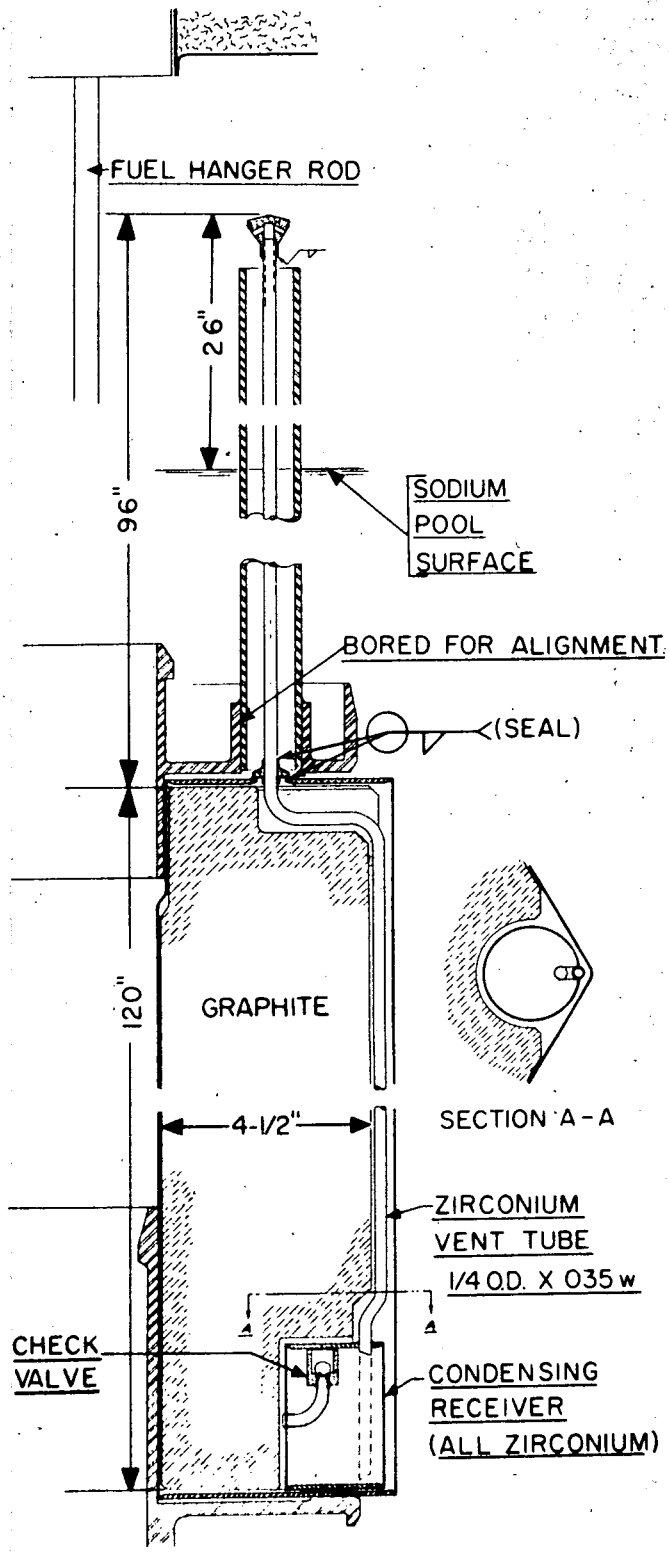

Fig. 22. Moderator Cell Vent Tube Arrangement

reservoir. A "snorkel" of this type would allow discharge of gases which will be released from the graphite by thermal agitation and radiation during reactor operation. It would also release gas pressure from thermal expansion of gases contained in pores and clearances in and around the graphite, thus protecting the can from structural damage by pressure buildup. A condenser has been attached to the lower (cooler) end of the breather tube to trap sodium vapor before it reaches the graphite. The trap shown is probably adequate for ten years of normal operation. A check valve is shown between the condenser and graphite chambers. In the final analysis this valve might be omitted.

The transport of sodium vapor into the moderator can during cooling and by the actions of normal and thermal diffusion has been studied and found to be very small and acceptable in practice. However, an experiment will be run to check these effects under simulated operating conditions (excepting the influences of radiation).

A vent tube support has been designed to maintain the lateral position of the vent tube in relation to the moderator can. This is to prevent spacial interference of the tube with the fuel cluster and adjacent can during removal and replacement of these units.

A model of a flat-plate can head has been built of aluminum for bonded-wire strain gage measurements with pressure and thermal strain loadings. A chamber has been built for the testing of can heads under load at high temperature in contact with sodium in order to determine the effects of stress corrosion and corrosion-fatigue, particularly in weld areas. Data are not yet available from either of these experiments.

2. Zirconium and Fabrication - The conversion of two ingots of zirconium started early in July is nearly complete. The small character of the lot and necessity of making more than one size product from an ingot made for poor yield, which will be approximately 60 to 65 per cent. Some difficulty has been experienced in scale removal, resulting in time delays. There will be sufficient materia to make the six development cans and to conduct physical testing at 1000° and 1200° F.

The fabrication of metal parts for the six development cans has been scheduled for the Los Angeles Plant. The necessary orders will be issued by the time material can be released for manufacturing operations about October 1. A

jig has been designed for the location and attachment of the studs on the end closures.

The welding machine and some of its equipment require further shakedown before welding of the development cans can be made on a routine basis. The welding stake with a moderator can (.050-inch wall) is shown in Fig. 23.

Work has been initiated on measuring the strength and creep characteristics (at 1000 and 1200° F) of the zirconium to be used in development cans.

C. Graphite

The hexagonal graphite blocks for six development cans have been received from the vendor and dimensional inspection has been completed. The present indications are that the blocks are dimensionally satisfactory; the inspection operation is shown in Fig. 24.

The values for ash content reported by the manufacturer and checks obtained with our laboratory indicate the ash content to be well within the specified 0.10 per cent maximum.

The density values reported by the manufacturer and checks made in our laboratory are slightly lower than specified. The actual range of densities is 1.60 to 1.68, whereas the value specified to the producer was 1.65 minimum. Measurement of the magnetic susceptibility indicates this graphite to be equivalent in degree of graphitization and orientation to AGOT, as specified in the purchase order. The measurement of nuclear properties of the graphite in the Hanford 305 pile has been scheduled.

D. Heat and Vacuum Treatment

Installation of the 150-kilowatt electric furnace and handling equipment (Fig. 25) was completed. The furnace performed and controlled satisfactorily during the drying and heating cycle and during sustained high temperature operation. This furnace will be used for thermal outgassing of the graphite moderator, annealing of zirconium strip, and high temperature tests on moderator elements. Assembly of the vacuum retort, which mounts in the furnace, has been started following the rework of leaky components.

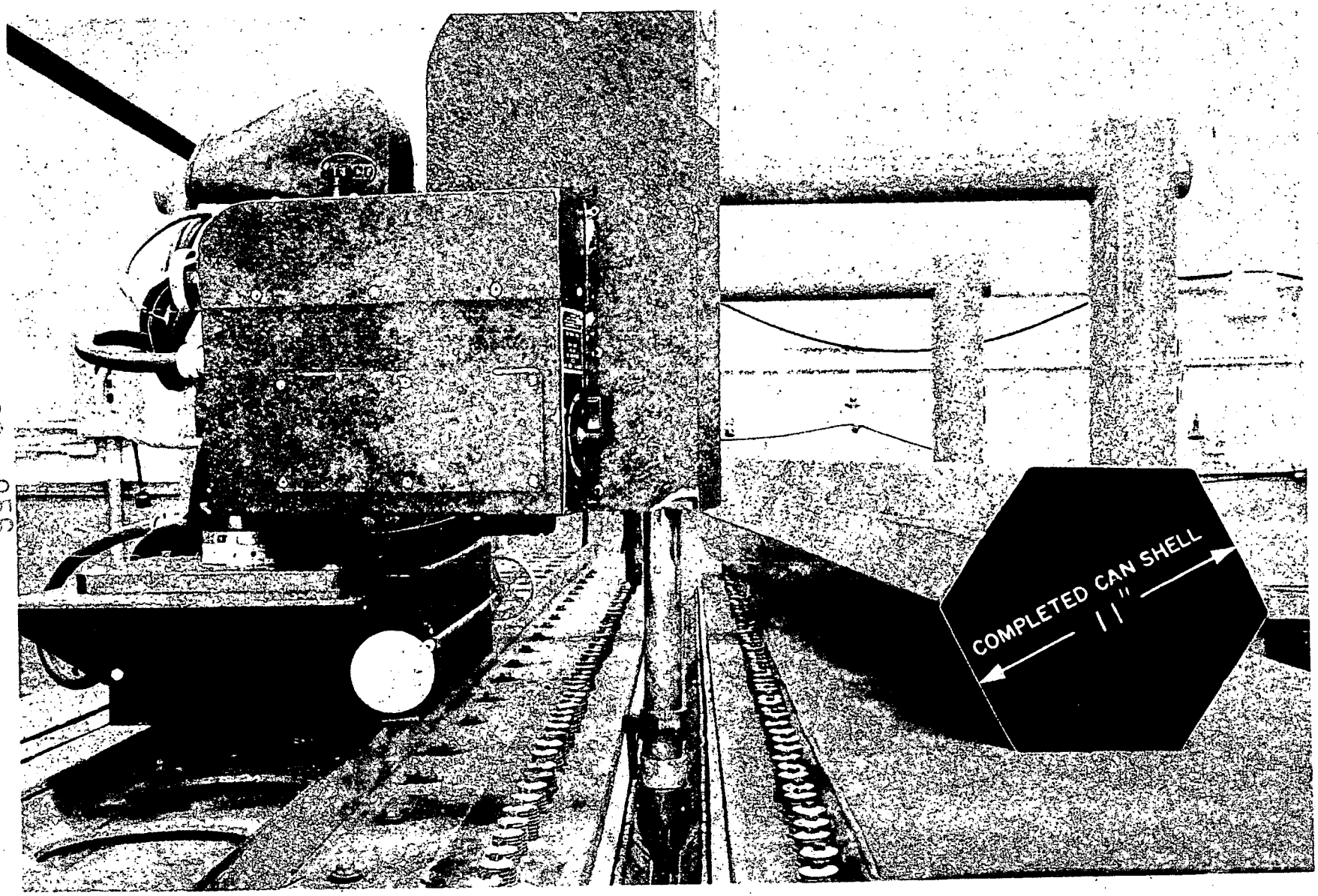

Fig. 23. Welding Stake Assembly for Fabricating Hexagonal Zirconium Moderator Cans

Unclassified
SRP47-113A

Fig. 24. Graphite Moderator Block - Inspection Procedure

Unclassified
SRP47-111D

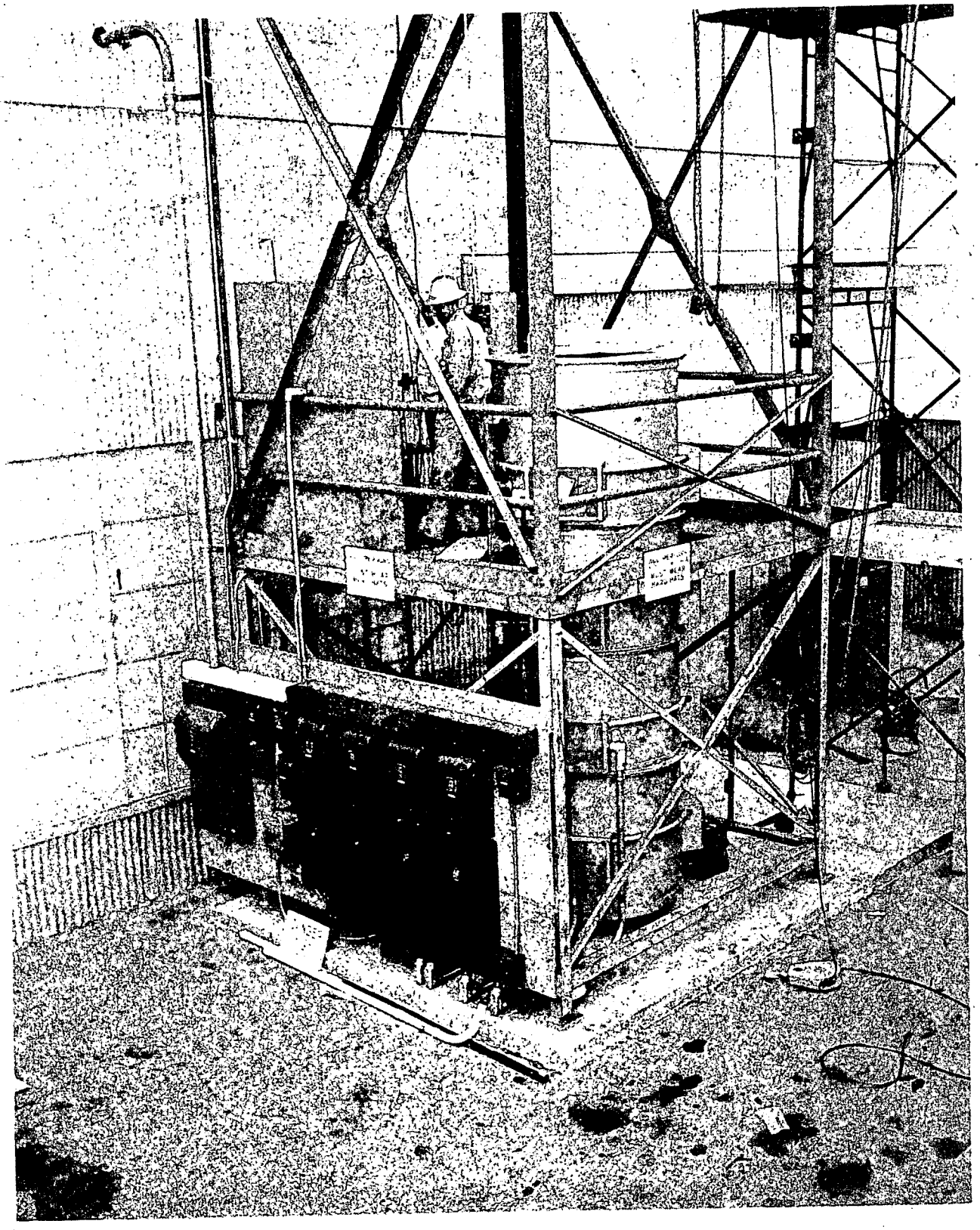

Unclassified
SRP21-55A

Fig. 25. Moderator Cell Outgassing Furnace

VIII. REACTOR COOLING AND HEAT TRANSFER

A. Engineering and Tests on SRE Components

1. Insulation

a. Insulating Brick and Fiber Tests in Sodium (M. Tarpinian) - Various types of insulating materials were subjected to liquid sodium to study deterioration effects. The specimens were sealed in steel pipes with provisions for flushing with inert gas and for introducing the liquid sodium. Heater wire was wrapped around the tanks and chromel-alumel thermocouples were peened into the tank walls.

The first specimen consisted of Johns-Manville Sil-O-Cel Brick #C-16 cut into a cylinder 2 inches high and 4 inches in diameter. The temperature of the brick was 740° F; sodium at 907° F was dripped onto the specimen. After removal and before an alcohol bath, the sample had a dull black to gray color, and exhibited large pores. However, after dissolving out the sodium the specimen disintegrated into a gray-black sludge.

Another cylinder (Fig. 26) of Sil-O-Cel Brick #C-16 was cut in half, cemented together with Sil-O-Cel mortar and subjected to the same conditions described above. The specimen, upon removal, separated at the cemented joint, the sodium having completely destroyed the cement. Again after an alcohol bath the black-gray sludge resulted.

The next two materials, Johns-Manville Superex paste (Fig. 27) and Eagle-Pitcher mineral wool (Fig. 28) were run under different conditions. Instead of dripping the liquid sodium on to the samples, a cube of sodium was placed on each specimen. After evacuation, the chambers were heated to 900° F and maintained at temperature for 1-1/2 hours. Both specimens were removed intact without a complete penetration of the sodium. The Superex showed some flaking tendency as well as a slight whitish discoloration (Fig. 27). The gray color of the mineral wool had become black in the areas where sodium made contact (Fig. 28).

b. Stainless Steel Wool (F. E. Bowman) - The current SRE design calls for a 12-inch layer of stainless steel wool thermal insulation between the outer tank and the core cavity liner. This material is to operate in a nitrogen atmosphere at temperatures which may reach 1500° F.

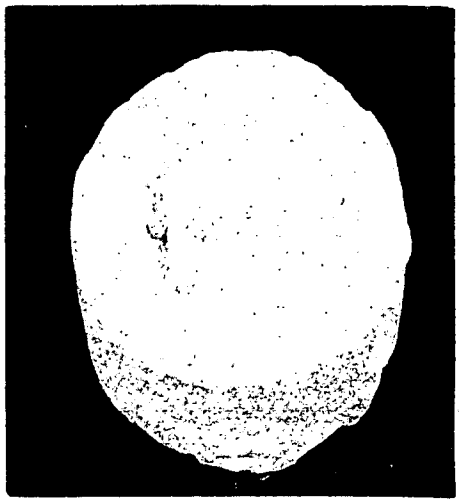

SRP29-29G

SPECIMEN BEFORE TEST

SRP29-34B

SPECIMEN VERTICALLY SECTIONED AFTER TEST

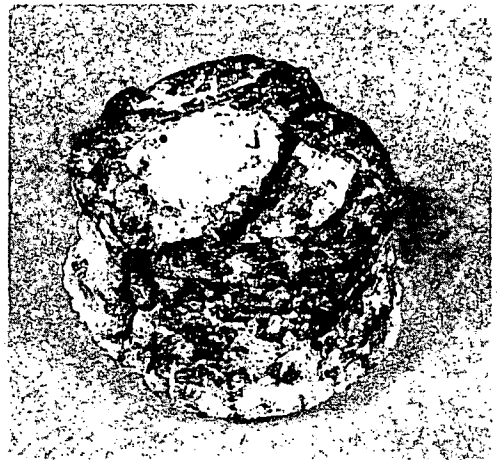

SRP29-34A

SPECIMEN AFTER TEST

Fig. 26. Thermal Insulation Tests - Johns-Manville Brick No. C-16 Sil-O-Cel Mortar

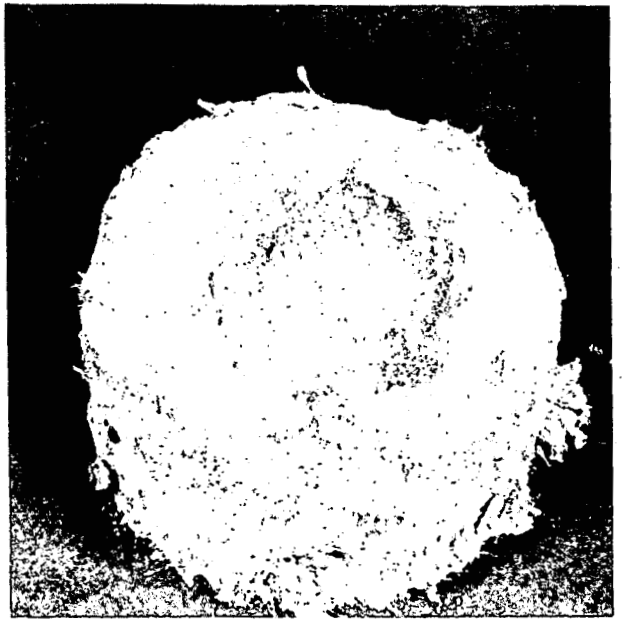

SRP29-28H

SPECIMEN BEFORE TEST

SRP29-36A

SPECIMEN AFTER TEST

SRP29-36D

SPECIMEN VERTICALLY SECTIONED AFTER TEST

Fig. 27. Thermal Insulation Tests - Johns-Manville Superex Paste

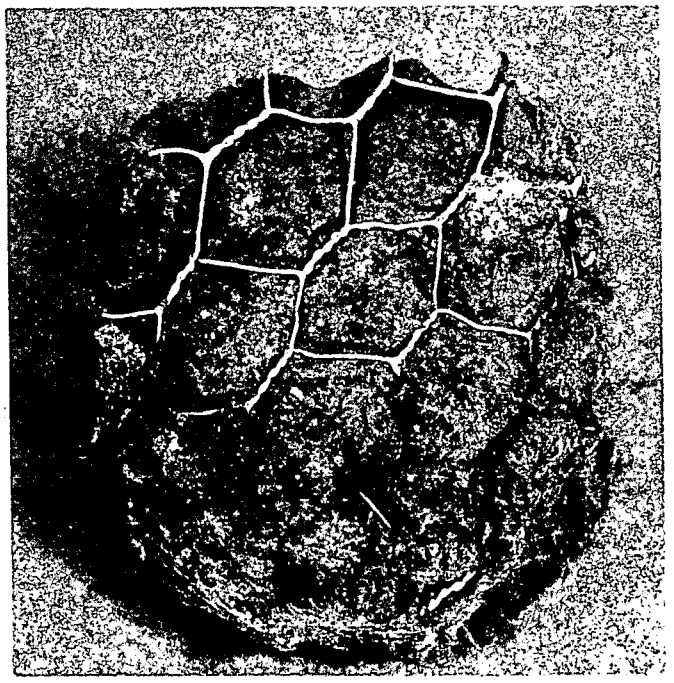

SRP29-28F

SPECIMEN BEFORE TEST

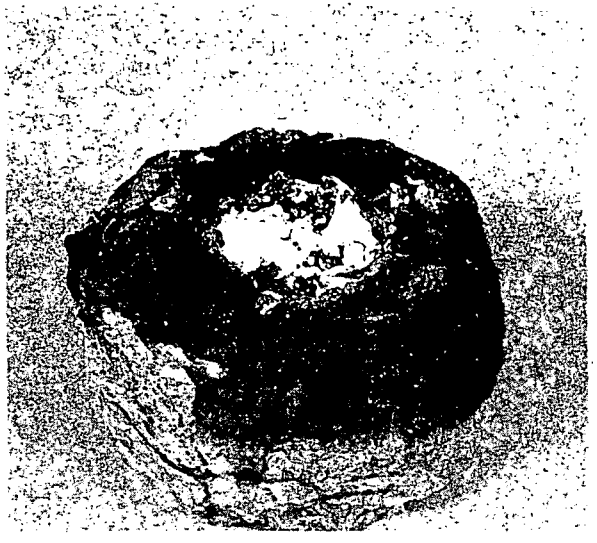

SRP29-36B

SPECIMEN AFTER TEST

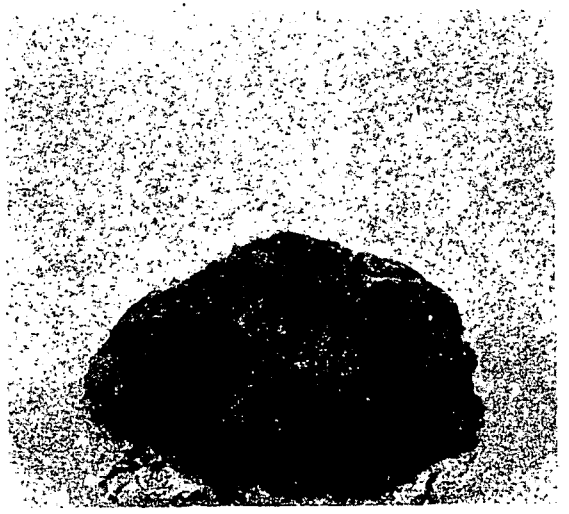

SRP29-36C

SPECIMEN VERTICALLY SECTIONED AFTER TEST

Fig. 28. Thermal Insulation Tests - Eagle Pitcher Co. - Mineral Wool

In order to establish the feasibility of such operation, a series of tests have been run exposing steel wool and massive 304L specimen to both static and flowing tank nitrogen and air at temperatures of 1200° F and 1500° F for periods up to 6 weeks. The nitrogen flow rate was maintained at about 20 cubic centimeters per minute. No attempt was made to obtain quantitative data, since it was felt that the necessary decision could be made on the basis of qualitative information.

The results obtained were as follows:

1. In static atmosphere both types of material are completely satisfactory. With the exception of a change in surface appearance (gray in nitrogen and black in air), there was no significant alteration observable. The static atmosphere implies, of course, a restricted amount of gas available for reaction.

2. With a continuous supply of fresh gas as provided in the dynamic atmosphere tests, the results were much less encouraging. At 1500° F all grades of the stainless wool (coarse, medium, and fine) were converted completely to a friable material in 1 month. Although during the test the specimens retained their original form, they were reduced to powder even by the most careful handling. X-ray diffraction patterns of the resulting powder revealed only the oxides of iron and chromium. It is felt, however, that the oxide is a secondary product resulting from a prior reaction of nitrogen with the chromium. The formation of chromium nitride would effectively remove the element which imparts the oxidation resistance to stainless steel, thus permitting the entire material to react with the impurity oxygen in the nitrogen gas.

The results at 1200° F were, as might be expected, much less severe. However, there was evidence to indicate that with time the same end result could be anticipated.

2. Inert Gas System

a. System Arrangement (E. Thomas) - Piping layouts have been prepared to establish pipe trenches for distributing the inert gases within the reactor building. It has been decided to replace nitrogen in the double wall sodium inlet pipes to the core tank with helium and to use nitrogen as an inert atmosphere in the disposable cold trap gallery outside the reactor building. The gas pressures in the insulation annulus, within the outer tank, and above the sodium pool in the core tank have been set at 3 psig. The difference in gas pressure between these

components and the connecting piping galleries, which have a gas pressure of 1/4 psig, will be taken up at the gallery seal diaphragm.

Helium gas will be purchased from the Bureau of Mines in Amarillo, Texas and will be stored in special bottles of 920 SCF capacity at a storage pressure of 2000 psig. This capacity is approximately four times the amount stored in a standard gas cylinder.

Nitrogen gas will be stored in standard cylinders for normal usage and nitrogen trailers will be brought to the reactor site for the purging of the piping galleries.

b. Helium Analysis System for Oxygen Determination (W. G. Bradshaw, L. Silverman) - The Brady method is to be used in the experimental studies of the SRE program, to determine the oxygen content of the helium gas blanket maintained over liquid sodium. It offers a rapid method of analysis with suitable precision, in the range of zero to 10 parts per million of oxygen in the helium.

The apparatus of Brady has been modified to make a mobile unit and the mode of operation has been changed. By improving the pumping system and by using graphical computation, as little as 15 to 20 liters of gas may be used to obtain results for oxygen in helium in the 0 to 12 parts per million range within 45 minutes.

In principle, a water solution of a red dye (anthraquinone-beta-sulfonate) is directed through glass tubing by the helium gas. At the start of the test, the red color of the solution is measured by a Beckman spectrophotometer, and the oxygen in the helium gas reacts to decolorize the red solution. The measure of the change from red to colorless is the measure of the oxygen content.

The spectrophotometer was independently calibrated, first, by using gases of known oxygen content and second, by electrically generating known quantities of oxygen gas. Using gases of known oxygen content, a precision of ± 0.25 parts per million oxygen in the 0 to 12 parts per million range was obtained. The results agree within ± 0.1 part per million of the Winkler method as described by Silverman and Bradshaw.[5]

When in continuous operation, a change in oxygen content of the gas may be detected within 15 to 30 minutes. If the oxygen content is sufficiently low, about 8 determinations may be made per day.

c. Winkler System - A modification of the Winkler method, in which oxygen is absorbed into alkaline manganous hydroxide and then determined as iodine, has been described by Silverman and Bradshaw.[5]

A precision ranges from 0.4 to 0.7 part per million for bottled gases varying in oxygen content from 2 to 23 parts per million. The method can be used from zero to 150 parts per million oxygen.

The time to complete one analysis is 6 hours. A series of analyses can be combined so that four may be made in one day. The volume of oxygen required for one analysis is one liter. The Winkler method is recommended when only small amounts of sample gas are available and a rapid answer is not required.

d. Purification of Inert Gases - A series of helium samples, taken before and after passing through a NaK bubbler, were analyzed by a modified Winkler method.[5] The lowest oxygen concentration obtained after passing through the NaK bubbler was 1.1 parts per million.

Bottled helium and hydrogen gases were passed through systems of gas-bubblers containing concentrated sodium anthraquinone-beta-sulfonate reagent. The oxygen content of hydrogen was reduced from 2.7 parts per million to 0.3 part per million; the oxygen content of helium was reduced from 6.6 parts per million to 0.5 part per million, according to the Brady system and the Winkler method.

e. Helium Purification (R. Cygan) - Spargers consisting of flat stainless steel cans have been incorporated into the NaK bubblers in place of a previously used perforated tube. Two new sets of NaK bubblers have been ordered for use on the fuel loading apparatus and the handling experiments. One of these will be used for further tests on the optimization of design for NaK bubblers.

Tests have been started to determine back diffusion of oxygen into helium service lines. This system will test the effective sealing of valves, fittings, and pipes used in the design of the reactor gas service system.

3. Sodium System Components

a. Calibration of E-M Flowmeters (D. F. Barker) - Five electromagnetic flowmeters for general use in the Engineering Test Program were fabricated and calibrated. They were calibrated by placing them in series in a pipe loop with a calibrated flowmeter.

Five surplus radar magnets were acquired to supply the magnetic field at five different locations in a closed pipe loop. This was constructed with 1-inch nominal 304 ELC stainless steel that had been electropolished inside to improve sodium wetting. A standard electromagnetic flowmeter and an electromagnetic pump cell were welded in the loop in series with the five uncalibrated flowmeters. The voltage probes of 304 ELC wire, 40 mils in diameter, were welded 180° apart on a plane perpendicular to the magnetic flux. These leads were connected to a multipoint recorder with a range of 0 to 10 millivolts. Two thermocouples were welded on the pipe itself at points intermediate between flowmeters and two thermocouples were welded on each flowmeter, one at a pole piece and another on the base. These were connected to a selector switch and read with a portable precision potentiometer. The exposed stainless steel pipe was then wrapped with heating cable and then insulated with Superex. The loop was then brought up to 600° F and the electromagnetic pump was energized. As sodium was not wetting the pipe, very little flow was recorded. The pump was then turned off for 5 minutes and then turned on again. This procedure was repeated several times with a slight increase of flow each time until a maximum flow rate of 8 GPM was obtained at 110 volts on the pump. It was evident that the pipe was not wetting completely.

The temperature of the loop was raised to 800° F to promote better wetting. The pump was then turned on at 110 volts and immediately a flow rate of about 19 GPM was recorded. A number of calibration runs were made with the loop at 800° F at different pump voltages to obtain different flow rates.

b. Sodium Cleaning with Anhydrous Ammonia (D. F. Barker) - Sodium has a solubility in anhydrous ammonia of about 10 per cent. This would indicate that liquid ammonia might offer considerable promise for cleaning parts coated with sodium. To determine the effectiveness of the method, a batch cleaning system using liquid ammonia was assembled at Santa Susana. A glass capsule of sodium and a sintered stainless steel filter loaded with sodium were both effectively cleaned in two separate trials. Based upon these encouraging results, a circulating ammonia cleaning system is now being fabricated.

(1) Apparatus for Batch Cleaning - The cleaning container consisted of a 4-inch nominal schedule 80 black iron pipe 12 inches long. A #300 weld cap was welded on one end and a flange welded on the other end. All 3/8-inch piping was of schedule 80 pipe with heavy duty union valves and elbows. Two sight glasses and a pressure gage were incorporated in the system. A stirring rod was

installed through the 1 1/2 inch thick cover. The stirring rod was driven by a 1/4 horsepower motor mounted on the cover. The ammonia was drained directly from a larger commercial cylinder.

(2) Test-Tube Cleaning Experiment - In order to get an idea of the cleaning time required, 10 grams of sodium were poured in a test tube. The open end of the test tube was then cut off 3/4 inch above the sodium. The diameter of this test tube was about 1/2 inch. The test tube was then put in the cleaning tank and the tank filled with ammonia. The dissolving time of the 10 grams in the capsule was 5 hours with continuous ammonia stirring. The ammonia was changed as soon as its color appeared as an opaque blue-black; these ammonia changes were necessary about every hour. Because of the small opening of the test tube, only a small area of the sodium was exposed to the ammonia. Since the cleaning time is proportional to the area of sodium exposed, this explains the long cleaning time.

(3) Cleaning of Sintered Stainless Steel Filter - A sintered stainless steel Surfamax filter that had been used in emptying the fill pot at Santa Susana was obtained to test the cleaning method. It was evident on inspection that it was badly loaded with sodium. The combined weight of the filter and sodium was 718.3 grams. The filter was placed in the cleaning tank and the tank was then filled with liquid anhydrous ammonia. The stirring rod motor was turned on and left running for one hour. Ammonia was then drained into the sight glass on the drain line. As seen through the sight glass, the ammonia no longer was clear but blue-black in color to the point of being opaque. This particular color indicated that the solution of ammonia was near sodium saturation. The tank was then completely drained into a drum of water through a submerged nozzle. No explosive reaction was involved. The tank was again filled and the procedure repeated until the ammonia drained into the sight glass remained clear. The total cleaning time was five hours.

It is interesting to note that six times more sodium was dissolved in this test over the previous experiment with the same time and volume of ammonia. This is due to the larger area exposed to the ammonia in this experiment.

The filter was removed from the cleaning tank and immersed in butyl alcohol. No visible reaction occurred and after 1/2 hour the filter was removed from the butyl alcohol and immersed in ethyl alcohol. A very slight reaction was visible. The filter was left in the alcohol for 1 hour and water was then added

to the alcohol with no reaction. Filter was removed, washed thoroughly in plain water, dried and weighed. The weight of the dry filter was 658.5 grams; the ammonia cleaning had dissolved 59.8 grams of sodium in five hours.

(4) Circulating Ammonia System for Sodium Cleaning - The good results obtained in cleaning the stainless steel filter makes it plausible to build a closed circulation ammonia cleaning system. Fabrication of such a system is now in progress.

B. Engineering Tests of Sodium Flow Under SRE Conditions (R. Cygan, W. J. Freede, T. T. Shimazaki)

Pressure drop measurements for the latest design SRE fuel element were completed. A composite photograph of this assembly is shown in Fig. 29. The chief differences between this assembly and the SGR elements previously tested are its shorter active length, additional spiral wire wrapping, and addition of an orifice plate at the lower end of the cluster.

The location of pressure taps used in the measurements is shown in Fig. 30. Using these taps the pressure drop in the fuel element section and the combined pressure drop of the orifice and entrance section was observed. Five different orifice plate sizes from 2.250 inches to 2.750 inches were used. For the 2.750-inch diameter orifice plate, measurements were taken with the plate in the extreme eccentric position as well as in the centered position.

Friction factor data for isothermal turbulent flow through the fuel element section are shown in Fig. 31. The results can be approximated by the expression:

$$F = \frac{0.0376}{Re\ 0.1} \text{ where } f \text{ is defined by } h = \frac{4fV^2L}{2g\ D_e}$$

The friction factor for the SRE fuel element is higher than for the SGR element previously described.[6] The difference is due to the greater number of wire spacers used in the SRE design.

The orifice coefficient data are plotted in Fig. 32, where the coefficient C is defined by $h_o = \frac{1}{C^2}\frac{V_o^2}{2g}$ where h_o is the combined head loss of the orifice and entrance section and V_o is the velocity through the orifice. The orifice coefficient increases with decrease in orifice plate diameter. The data indicate that for a given orifice plate diameter, the orifice coefficient decreases with increase in

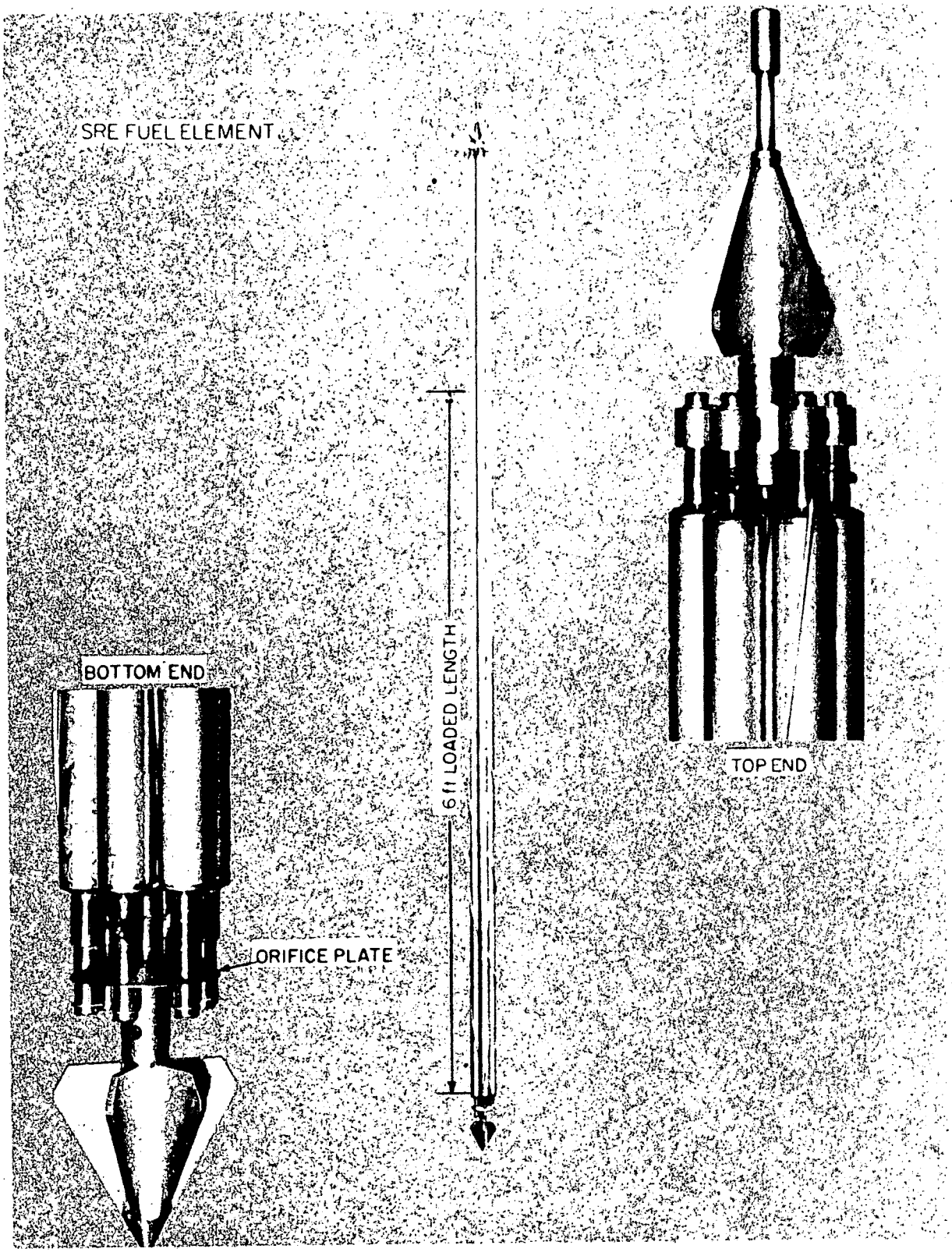

Fig. 29. SRE Fuel Element

SRP29-27@
Confidential

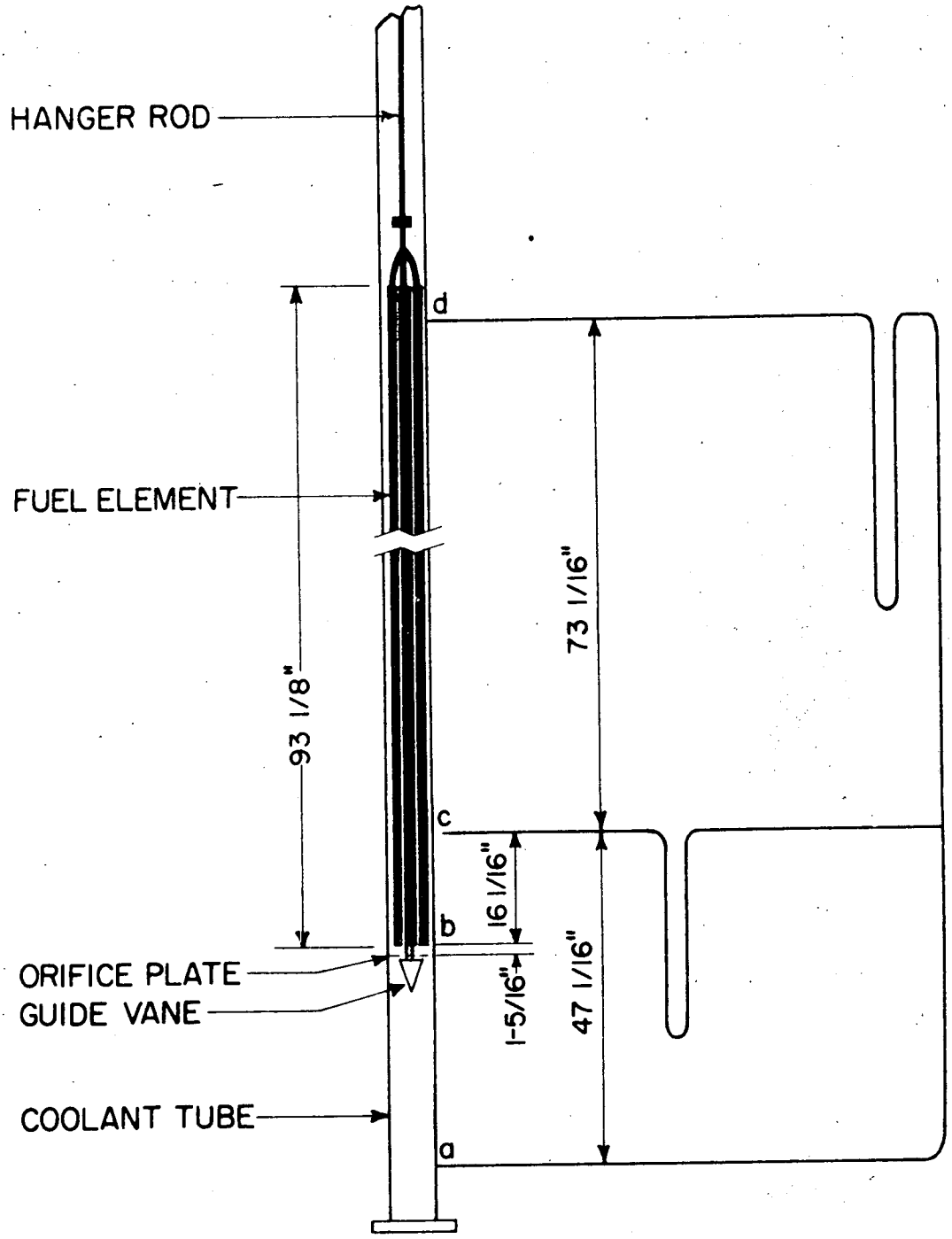

Fig. 30. Location of Pressure Taps on SRE Fuel Element Coolant Tube

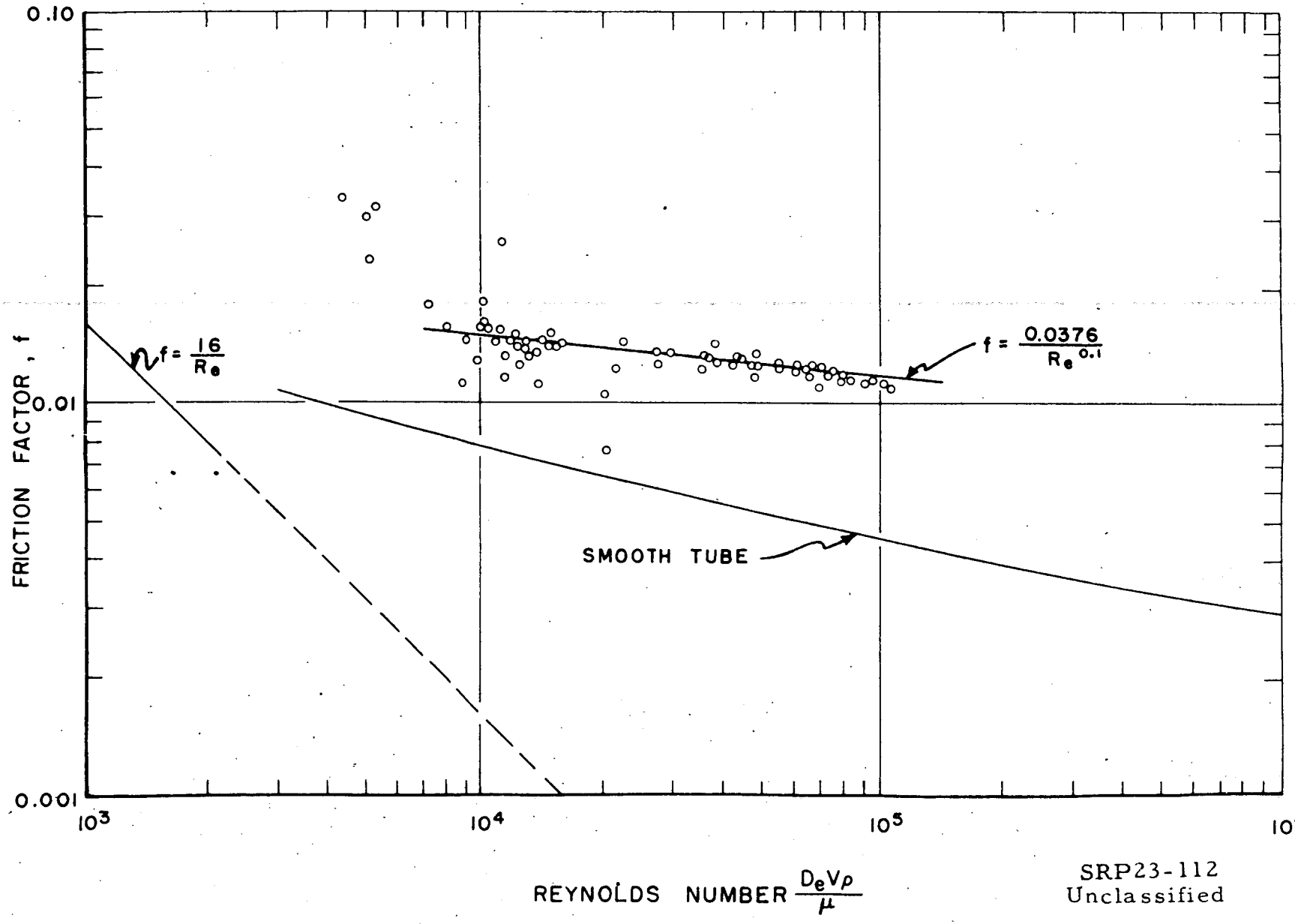

Fig. 31. Friction Factor for Isothermal Flow in Fuel Element Section of SRE Coolant Tube

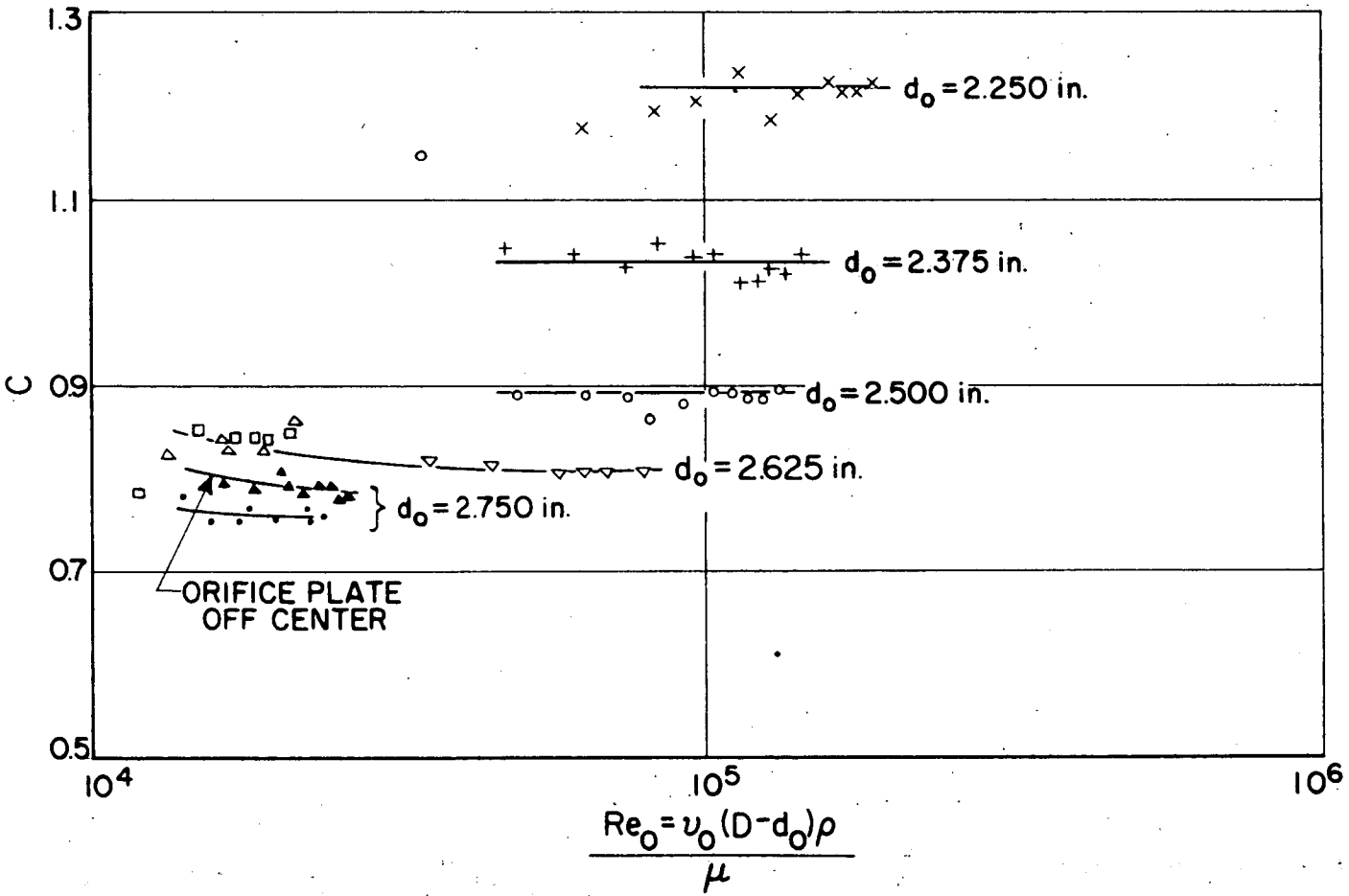

Fig. 32. Orifice Coefficient vs Re_o for SRE Fuel Element

Reynold's number up to a value of Reynold's number above which the orifice coefficient becomes approximately constant.

Figure 32 also shows that if the orifice plate is eccentric, the coefficient increases. For the 2.750-inch diameter orifice plate in the extreme eccentric position, the orifice coefficient increases about 4 per cent. Figure 33 is a cross plot of the results shown in Fig. 32 for the concentrically positioned orifice plates.

There is considerable scatter of experimental data in the lower Reynold's number region, which introduces some uncertainty in the interpreted results for this region. The scatter results from the pump and valve sizing made originally for the higher flow rates applicable to SGR, which resulted in poor control characteristics at very low flows. Since this flow rate region is below normal flow for SRE, revision of equipment to get better data is unwarranted.

More exact flow pattern studies have been carried out using larger suspended particles (sawdust), high intensity lighting and Fastex cameras. The photographs and data are being analyzed.

C. Sodium Pump Development and Test (R. Cygan)

During the past quarter the sodium pump loop (Fig. 38, NAA-SR-878) has been installed and instrumented and the auxiliary equipment has been added (Figs. 34 and 35). Pipe preheating is provided using General Electric flexible heating cable (nichrome covered with asbestos-glass insulation with monel braid over-all). The heating cable is held in place using steel wire and plumber's tape. For sodium leak detection, two stainless wires imbedded in loosely woven glass yarn tape are fastened to the underside of the horizontal piping.

Thermocouples are peened directly into the pipe wall except for low temperature regions, where they are soldered to the surfaces. Thermostats maintain the drain line and dump tank above the melting point of sodium at all times. Helium supply is bubbled through NaK columns to remove trace oxygen present in tank helium.

Preliminary checkouts are finished and the loop is now ready for the initial sodium charge.

D. Stainless Steel Metallurgy for SRE (D. T. Eggen)

During the last quarter it was decided that the standard material for systems in contact with sodium or sodium vapor should be 304 stainless steel. Prior to

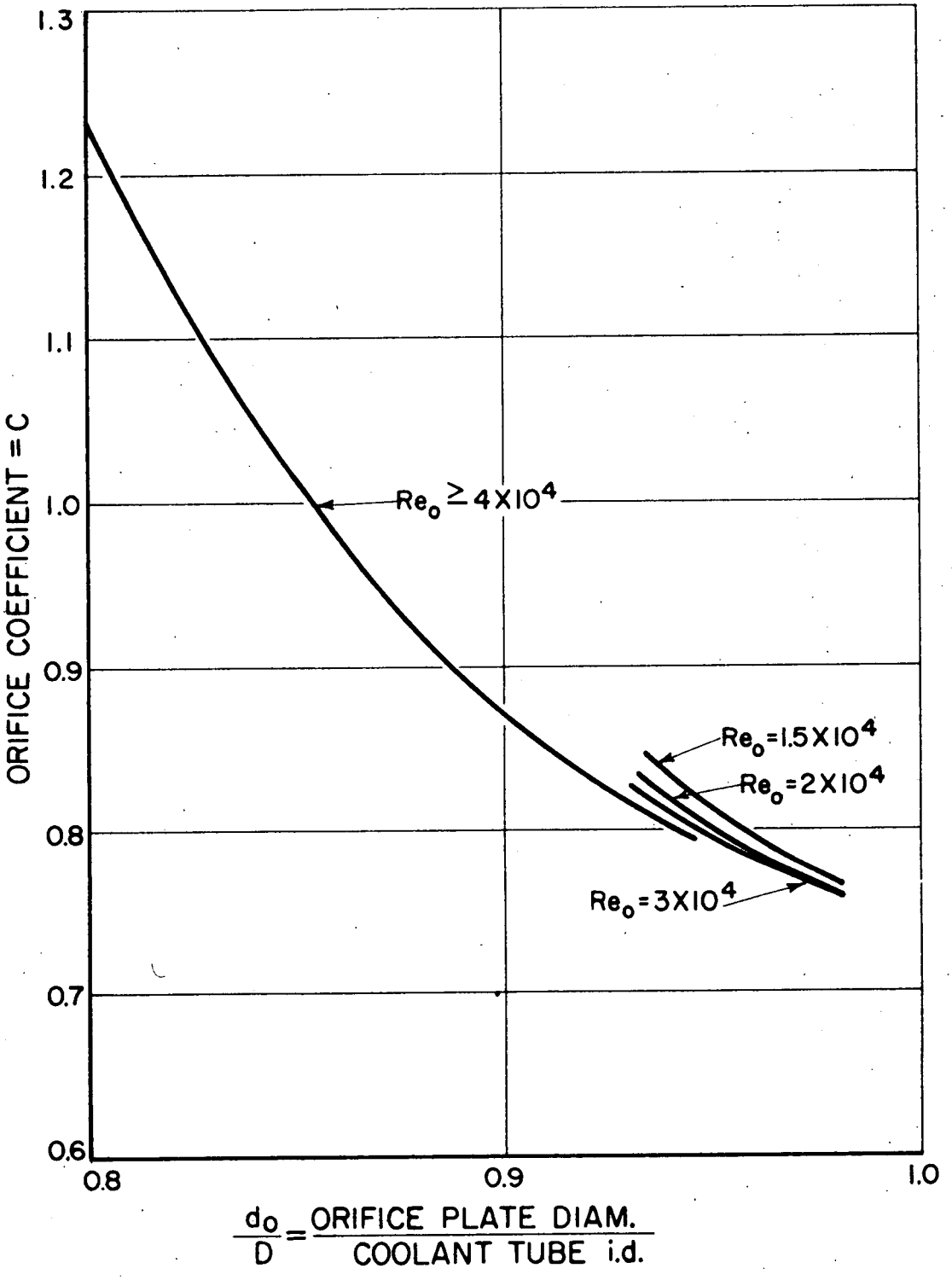

Fig. 33. Orifice Coefficient vs d_o/D for SRE Fuel Element

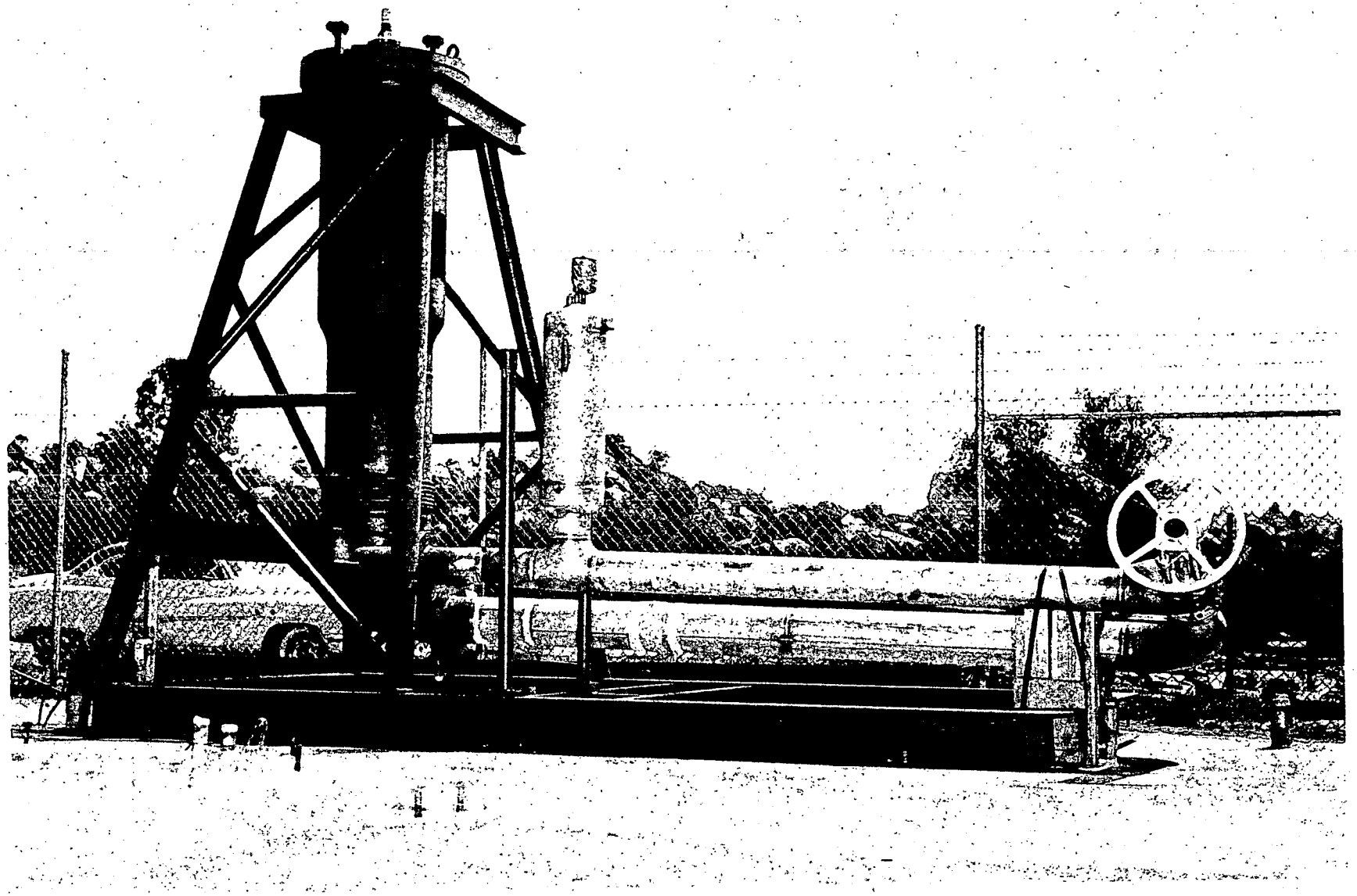

Fig. 34. 1200 gpm Sodium Pump Loop Assembly

Unclassified
SRP29-17A

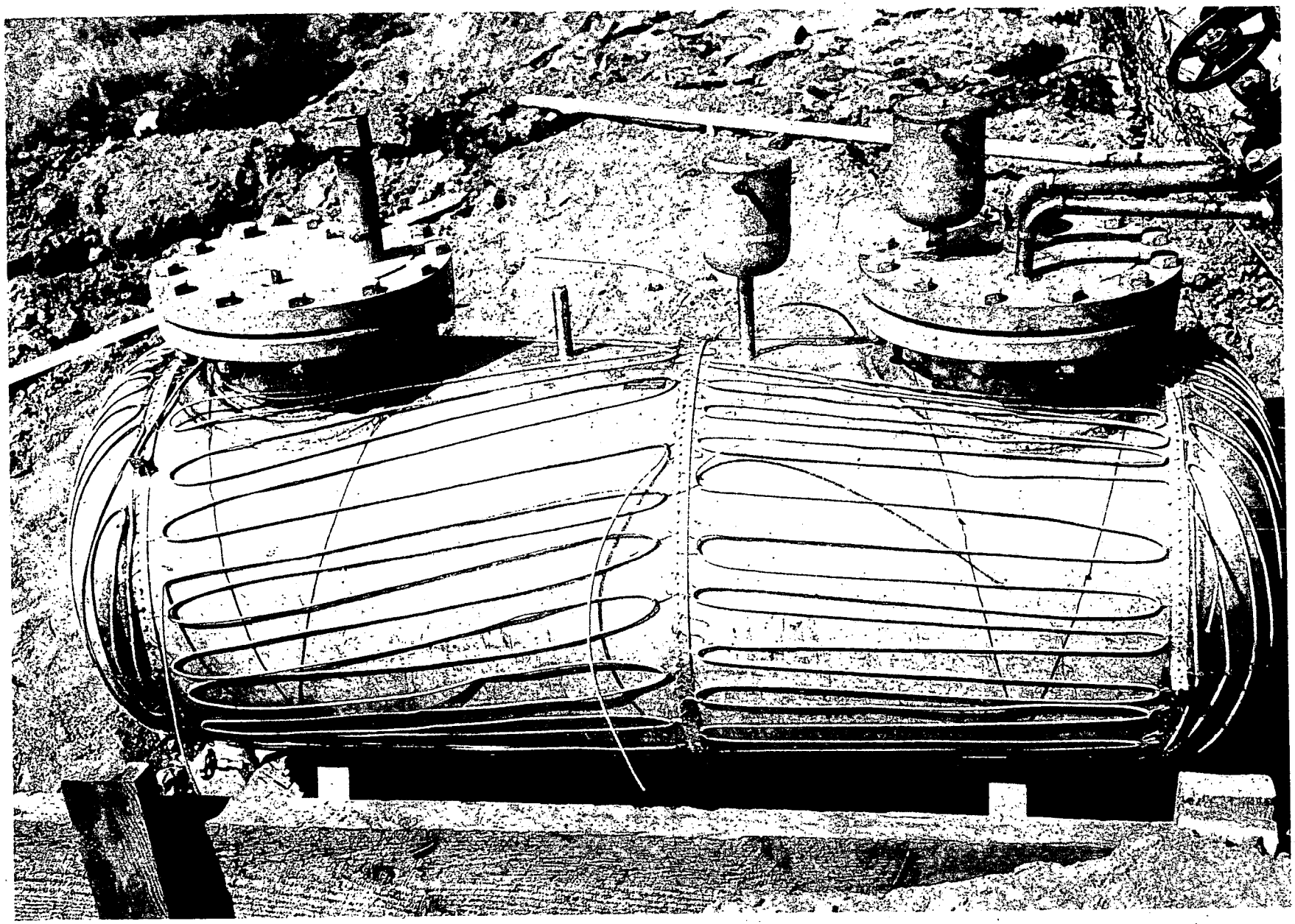

Fig. 35. Sodium Fill Tank for Sodium Pump Loop

Unclassified
SRP29-20A

this decision, it had been general practice to specify 304L (extra low carbon, 0.030 per cent) for this service. This choice was made after investigations which indicated carbon precipitation even with the extra low carbon material. It was felt that the little advantage gained over commercial 304 did not warrant the increased cost. Exceptions to this general case will be made under certain conditions where extra toughness, strength, or cleanliness are required; e.g., sodium pump impeller and the jacket tubing for fuel rods.

The backup ring developed by the Electric Boat Company for use in inert gas welding of stainless steel for sodium service has been added to preferred methods of welding. The other accepted methods are gas backup, consumable backup ring, and temporary copper backup. These methods are used in order to reduce oxidation on the inside of weldments.

IX. INSTRUMENTATION AND CONTROL

A. Control Rod Systems

1. Control Rod Drive Mechanism (M. Mueller, R. E. Douglas) - As previously reported,[1] the four control rods will be used as shim rods and two of the four will be arranged to have an override on the shim movement so they might function as regulating rods. The shim movement will be manually operated while the regulating rod will be instrument controlled.

Travel of the shim rod is tentatively fixed at 0.24 ft/min. Using a 1.00 diameter worm with a lead of 0.20 inch requires a slow speed of 14.4 rpm. Travel as a regulating rod is tentatively limited to a maximum of 3.0 ft/min. This requires a fast speed of 180 rpm.

The required speeds for the two-speed drive (Fig. 36) are obtained using two 1200 rpm, constant speed, reversing motors driving through friction type, adjustable torque, slip couplings coupled to a gear reducer. The gear reducer uses a planetary gear system. Two input shafts, one for each of the two motors, are provided. The planetary gears are arranged to utilize the two ratios normally available. The high ratio is obtained by driving the sun gear through the planet gears against a fixed annulus or ring gear held by the inactive motor on brake. The low ratio is obtained by driving the ring gear through the planet gears against the fixed sun gear held by the opposite motor brake. With this arrangement two

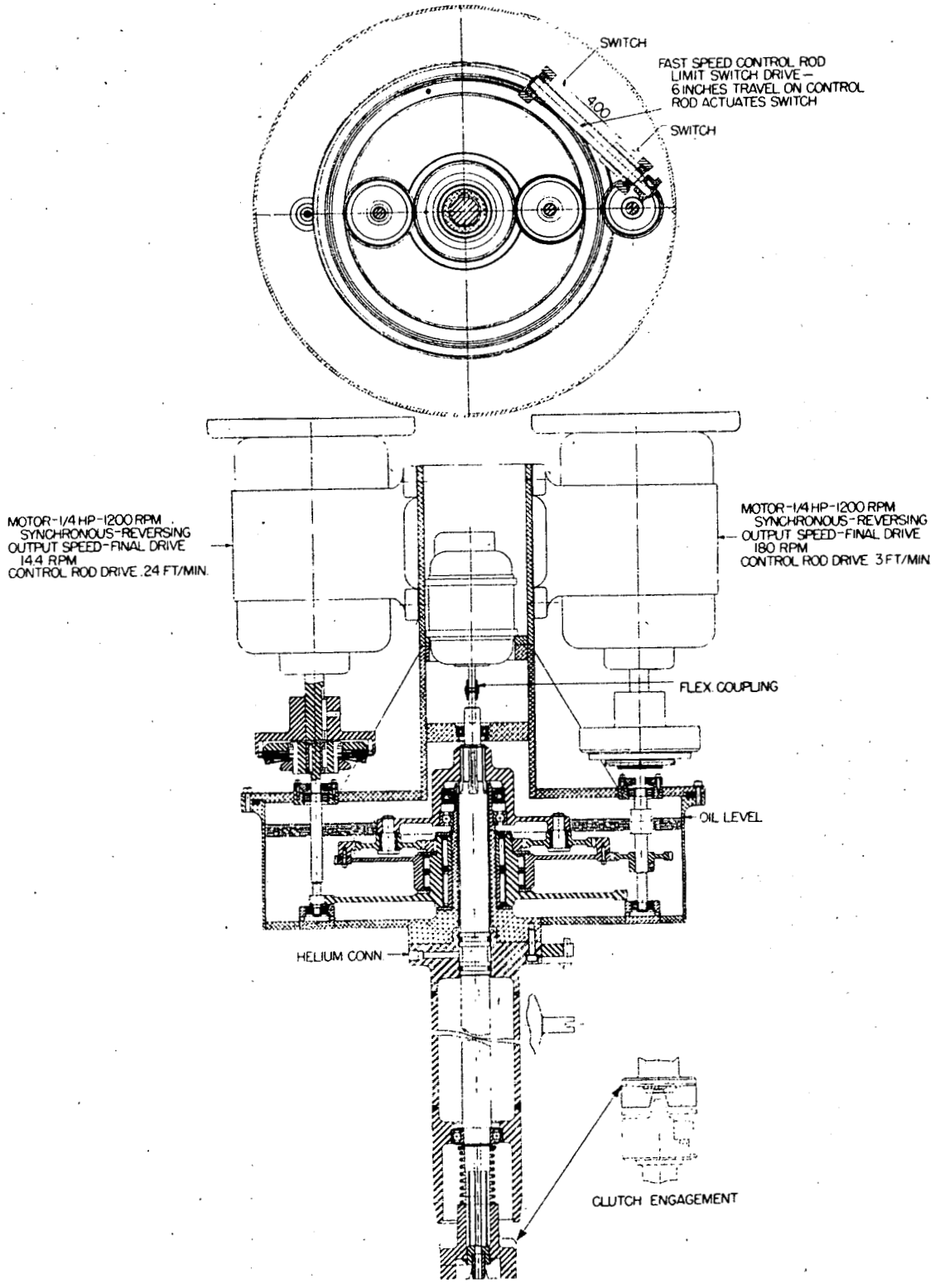

Fig. 36. Control Rod Drive Assembly (Two Speed)

motors are made to drive a single shaft at different speeds and in reversible directions of rotation.

The regulating rod travel is limited to plus or minus 6 inches beyond the normally controlled position established by the shim rod drive. An Acme screw is driven by the high speed input shaft. A cam travels on this screw and actuates limit switches at each end of the twelve-inch travel. A center switch is provided for indicating the position of the regulating movement at the center of travel.

The slip couplings are of the spring loaded, friction disc type with an adjustment nut regulating the spring pressure to give a fixed torque limit. Loads in excess of this limit cause the coupling to slip. This provides a safety stop against driving the ball nut and worm in the pull tube beyond the limits of the worm thread and other jamming due to faulty manual control.

A selsyn unit direct driven from the main shaft supplies intelligence for indicating the position of the pull tube.

The main shaft drives a two-tooth clutch which in turn drives the ball nut-screw shaft. The clutch is spring loaded for engagement and a maximum of one-half turn is allowed before positive engagement.

The two control rods that are not provided with an overriding movement for regulation, will be driven at a single speed with a single motor under manual control (Fig. 37). The required speed is obtained using a worm and worm gear reduction driving at right angles through miter gears. The spring loaded clutch is used and the drives are removed merely by lifting from the control rod recess.

2. Development of Control Rod Elements (H. Strahl) - Four centrifugally cast control rod rings have been received (Fig. 38). It was requested the cylinders be cast in steel molds instead of graphite molds, as several test castings indicated the higher the carbon content, the harder the material became. Trouble was encountered in removing the finished castings, so ultimately graphite molds were used. From the analysis of the finished cylinders, it appears that the graphite mold causes only a skin effect which disappears when the outside is machined to size.

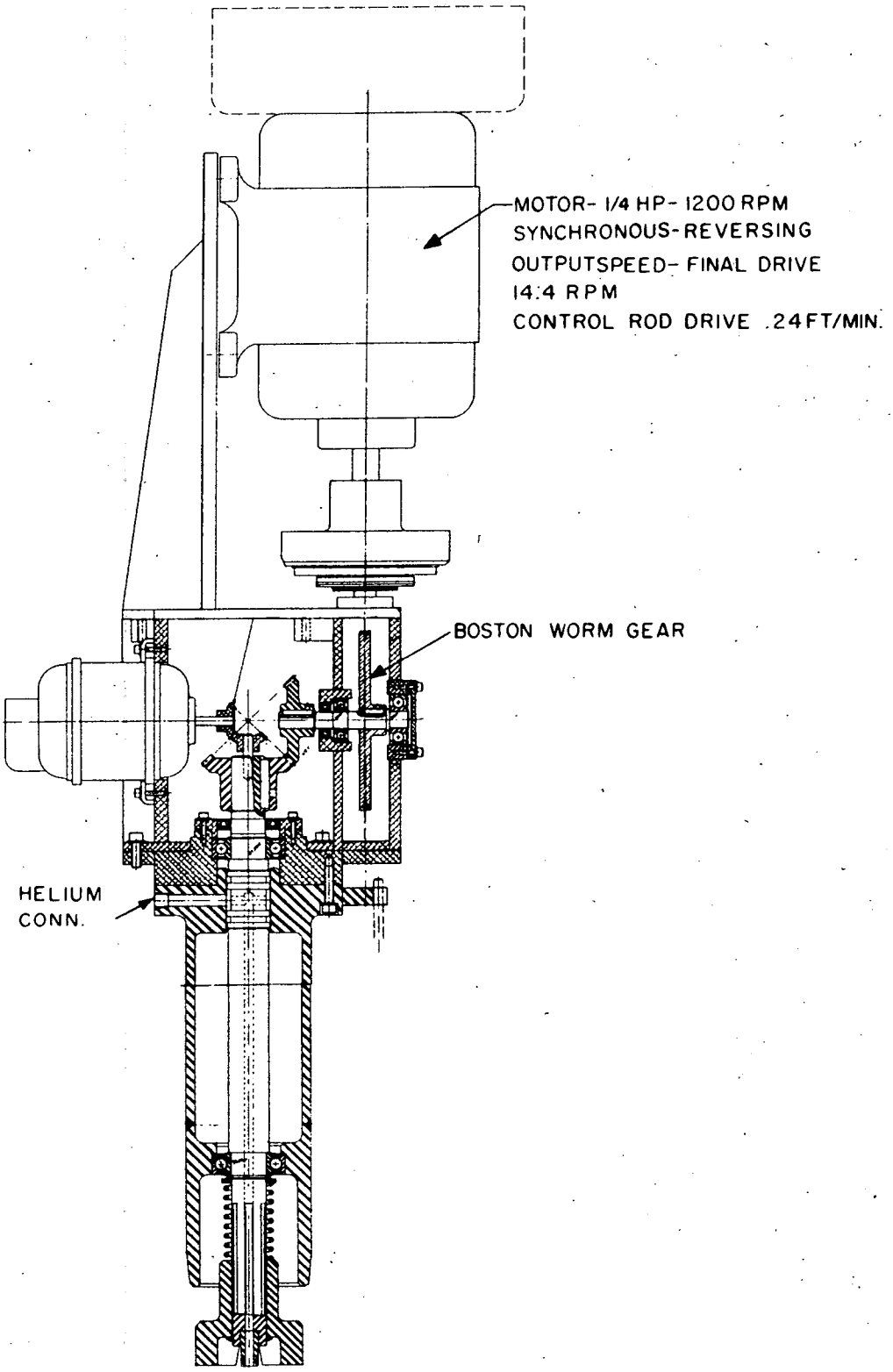

Fig. 37. Control Rod Drive Assembly (Single Speed)

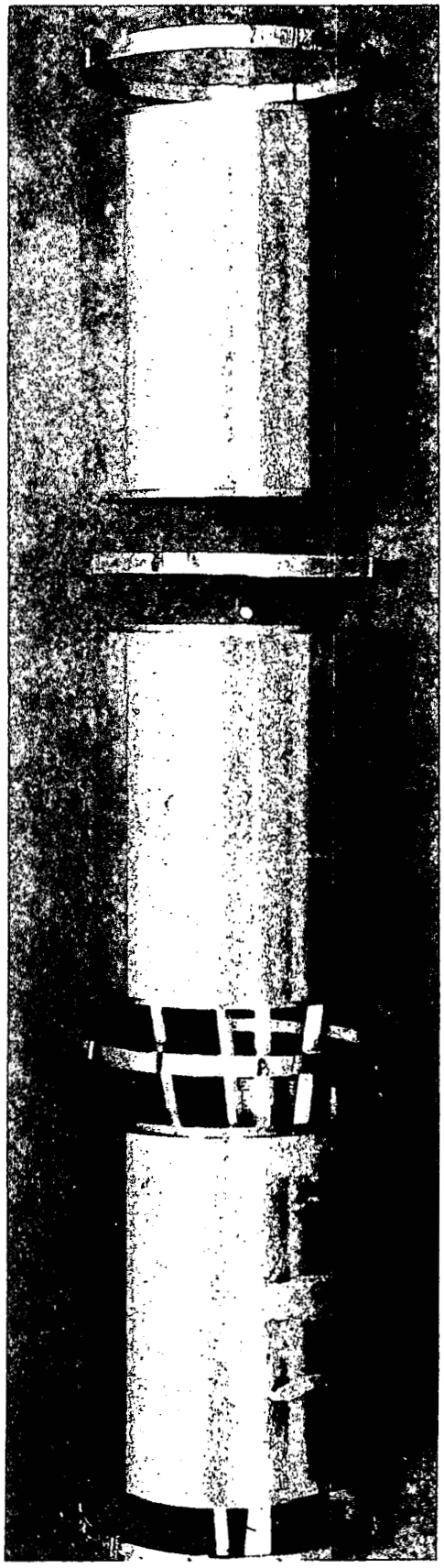

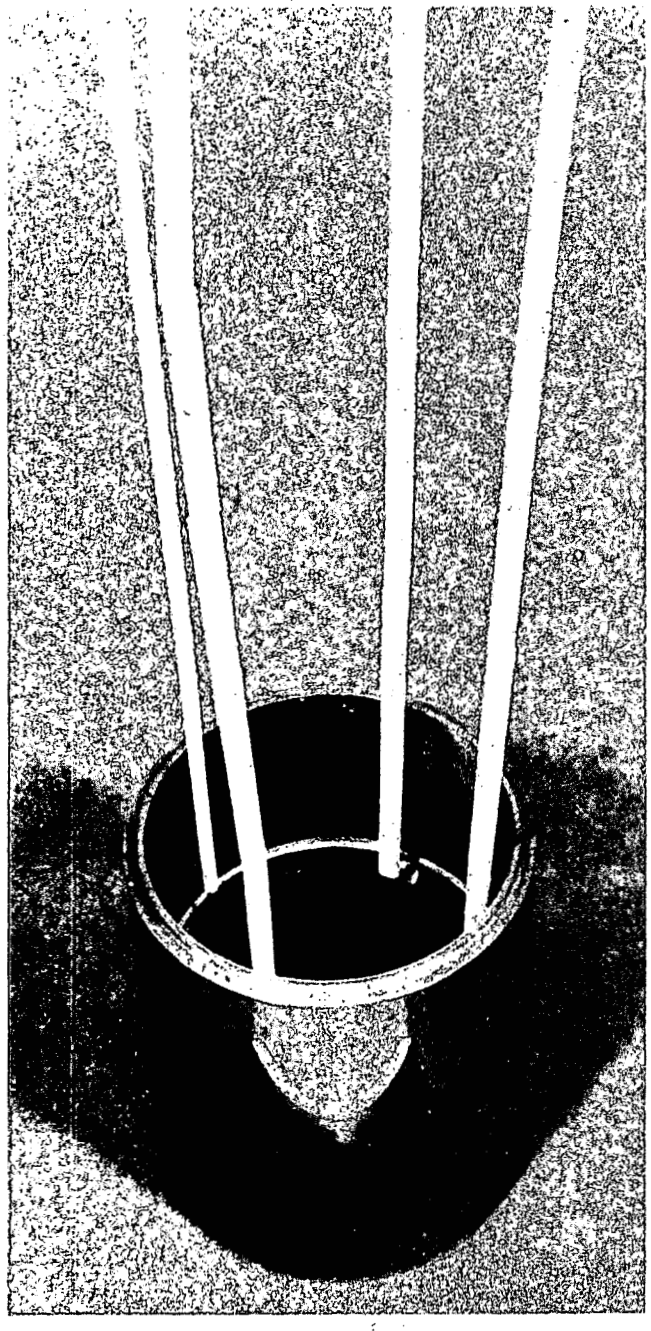

B

A

Fig. 38. Boron Steel Control Rod Rings

Unclassified
SRP25-83B

Following is an analysis of the finished cylinders:

Ni	80.48%*	C	0.10, 0.11*
Cr	10.00%	Si	0.71*
Fe	3.57%*	Mn	0.22
B	3.61%*	Co	0.68*

These cylinders appear to be softer than any fabricated thus far, the Rockwell hardness being C-53.

One of the cylinders was thermally cycled 500 times from 400 to 1200° F under a load of 25 pounds. The dimensions were the same after cycling. A piece of a cylinder was heated to 1200° F in contact with stainless steel to make sure the two would not stick together. No bonding or sticking effect was observed.

3. Control Rod Heat Transfer Experiment (J. D. Howell) - As previously described and illustrated (NAA-SR-956, p. 49; NAA-SR-1027, p. 40), the experimental system for the heat transfer experiment has been completed. During the last quarter the system was completed and put into operation. Initial runs were made with a nominal radial clearance between the boron rings and the thimble of 10 mils, the boron rings being held concentric with the thimble tube by means of spacer rings (Fig. 38-A). Power input into the boron rings (by the graphite heater) was increased to 8.3 kilowatts per foot, and the thimble temperature was varied from 650 to 825° F; the temperatures were recorded by thermocouple imbedded in the rings as shown in Fig. 38. This simulated conditions expected along the central control rod of the SRE between points one-half and three-quarters the distance from the bottom. This area is considered the most critical, due to the combination of high heat fluxes and relatively high thimble temperatures.

Under these conditions the highest boron ring temperature measured was 1100° F.

The next set of runs will be made with the same nominal annulus, but with the boron rings held against the side of the thimble. This is the most likely position of the rings in the control rod since they fit loosely in the draw tube. It is also the worst condition for heat transfer, and will indicate whether difficulties with excessive local temperatures in the rings may occur.

*These determinations are quantitative. The remaining analyses are spectrographic and accurate to plus or minus 10 per cent of the given values.

B. Safety Device System

1. Ball Release Studies (E. C. Phillips, E. B. Hecker) - As previously reported (NAA-SR-1027, p. 88), an experiment is being designed to determine the release time and the manner in which boron steel balls would be released from a storage hopper into a thimble in the core of the reactor. The experiment was designed mocking-up all internal working parts as shown in Fig. 39. Due to a racheting effect of the balls between the sliding hopper wall and the internal tubes of the device, it was necessary to add a sleeve between the hopper wall and the balls. A reflector which separates the balls from the air stream has been redesigned and fabricated of high impact strength die steel. This was found necessary because of severe damage to the reflector caused by the peening action of the returning balls.

Light compression springs have been added to the spider supporting the ball hopper in order to increase the release speed following the solenoid action. The important factor is the time transfer between the release of the solenoid and the arrival of the first balls at the core reflector interface, which is two feet below the hopper gate. This time varies between 407 and 394 milliseconds. The first balls reach the bottom of the core in 805 to 764 milliseconds. Approximately 10 seconds are required to completely fill the safety thimble with the boron steel balls. The hopper gate is completely open in less than 112 milliseconds. However, balls are falling from the hopper before it is completely open. The method of observing these measurements is as follows: Plastic windows were placed two feet and eight feet below the hopper gate. Since the center tubes of the Ball Safety Device are made of stainless steel, the outer one was polished in order to obtain high light reflectivity. A set of three phototube and exciter lamps were placed in a housing in this plastic section. The phototubes were placed 120° apart and the exciter lamps placed next to them but shielded in such a way that the phototubes could see only light reflected from the center tube of the device. An amplifier was designed and constructed to feed into a dual-beam oscilloscope. Measurements were taken of the time between solenoid release and the interruption of the light beam at either the two-foot level or the eight-foot level. The hopper gate opening was determined by a sensitive sound pickup.

An air flow rate of 29.5 cfm and 16 psig removes the balls in about one and one half minutes. The pressure on the air piston in the latch is higher than 16 psig before the latch air valve opens.

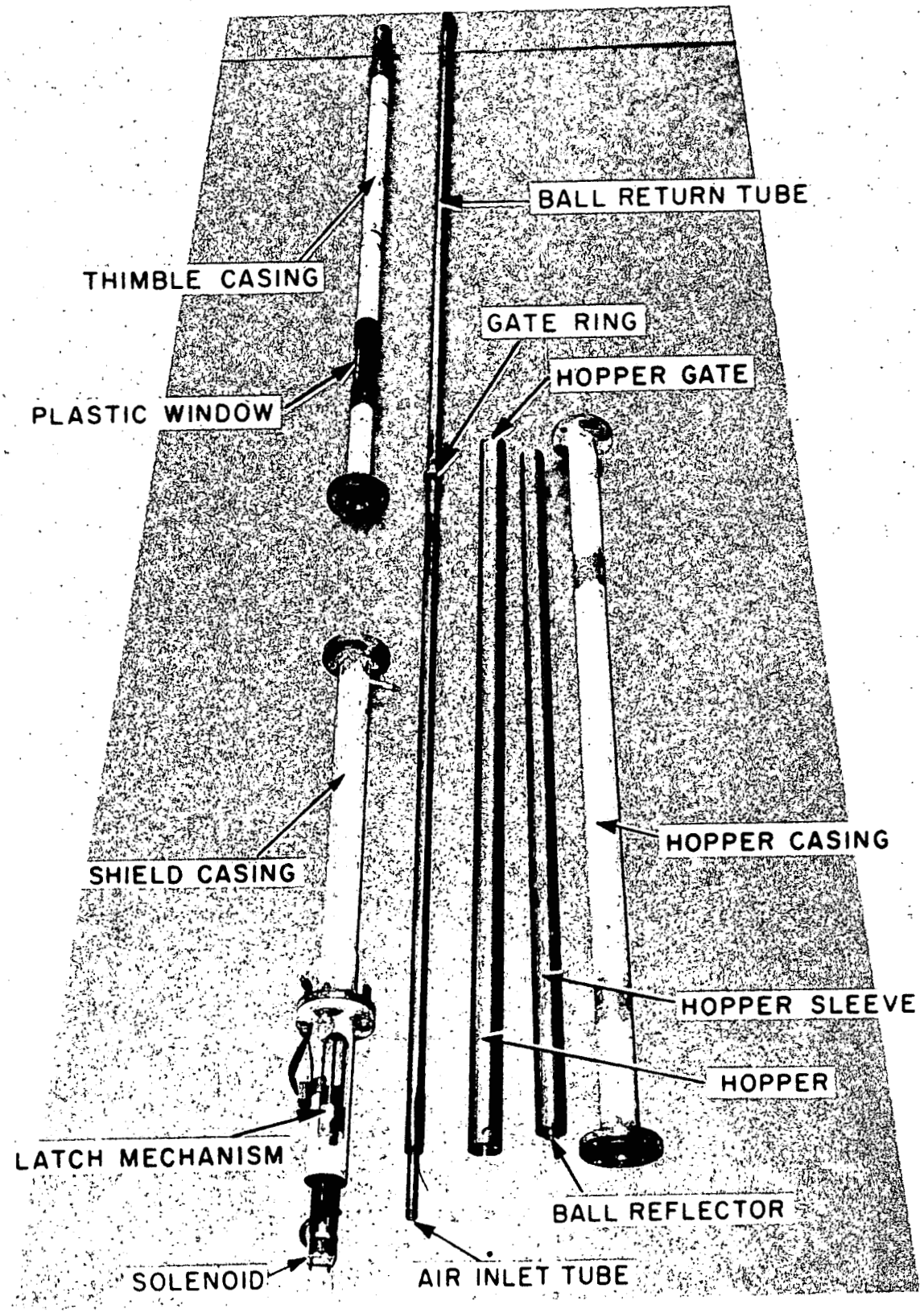

Fig. 39. Ball Safety Device - Mock-Up

Unclassified
SRP25-79A

The tests have been made with 1/8-inch chrome steel bearing balls. An attempt to use stainless steel shot with 3 per cent boron content resulted in jamming and severe scoring of the hopper, hopper sleeve, and ball return tube by fragments of the shot which shattered.

In order to operate the test over several hundred cycles, a sequence timer was incorporated into the Ball Safety Device. This (a) latched and set the hopper gate, (b) energized the holding relay, (c) emitted air to lift the balls from thimble to hopper, (d) de-energized the holding relay, and (e) dropped the balls into the thimble.

2. Boron Steel Ball Procurement (A. E. Miller, W. J. Hallett) - Inquiries have been made to metal and ceramic ball manufacturers to determine the feasibility of producing boron containing balls suitable for the Ball Safety Device. In addition to having a minimum boron content of 1.5 per cent in steel or an equivalent weight in a ceramic, these 1/8-inch diameter balls must not sinter or pressure weld under a load of a 10-foot column of balls at 1500° F. Also, they must be capable of withstanding impact against the steel reflector when moving with a velocity of 100 ft/sec.

A sample batch of 50 pounds of 2.97 per cent boron 18-8 stainless steel balls made by shotting techniques was obtained. These balls were unsuitable, as they were neither round, solid, constant in size, nor did they have a continuous surface. These defects appear to be characteristic of balls produced by a shotting process. Thus, it appears that if metallic spheres are to be used, they will have to be manufactured using methods more nearly approaching those used in the manufacture of ball bearings.

Steel balls containing 1.7 to 2.0 per cent boron are available. These 0.125 $\pm$ 0.005 inch balls have a sphericity tolerance of $\pm$0.001 inch. Pressure welding experiments will be performed on 3/8 inch spheres of the same alloy. A sample of 3/8 inch, 4 per cent boron nickel balls fabricated for Savannah River have been obtained. It is felt that 1/8 inch spheres of this alloy can be made, but the vendor is not presently equipped to do so.

Thus far only two manufacturers capable of fabricating suitable ceramic balls have indicated interest in doing so. A sample of 1/4 inch balls has been ordered. These balls will have a bulk density of 1.95 gm/cc and contain 0.16 gm/cc of boron.

3. Ball Sintering Experiments (A. Omo) - Ball sintering experiments previously reported (NAA-SR-1049) are being continued as new types of balls are received. The shot technique balls were placed under an atmosphere of 5 psia of helium to test for pressure welding. Samples of the balls were heated to 1120 and 1320° F under weights giving pressures equivalent to a 7-foot column of balls.

Since it was thought that nitriding of the balls would prevent sticking, nitrided samples were also tested under the same conditions. Nitriding was accomplished by heating the balls to 1075° F in an atmosphere of anhydrous ammonia for 5 hours.

After being tested under the above conditions for 21 days, none of the samples showed any tendency to stick together. It is probable that there was a small amount of oxygen in the helium atmosphere since the weights and cups in some of the sintering retorts showed discoloration. The retorts and ball samples are shown in Fig. 40.

4. Pressure Bonding Tests on Nickel-Boron Alloy - Square samples of three types of nickel boron were tested for pressure bonding in contact with stainless steel 304L samples. The samples were heated at 1200° F for 21 days in an atmosphere of helium. A pressure of 25 psi was held on the contact faces by a weight, as shown in Fig. 41.

The nickel boron samples were placed between alternate samples of 304L stainless, so that there were two contact faces for each type of metal. There was no pressure bonding at any of the contact faces. There seemed to be a slight oxide coating on the weight and cup which was thought to be due to oxygen in the helium.

Samples of stainless 304 tubes and stainless 347 were also tested for pressure bonding (Fig. 42). Tubes of 304 stainless were placed under 347 stainless weights in a helium atmosphere. Samples were heated at both 1120 and 1320° F for a period of 21 days. Nitrided samples were also tested under the same conditions. None of the samples showed any tendency to weld. There was a light-blue film on one sample and a light-gray film on another; this was probably due to oxygen impurities in the helium.

Fig. 40. Sintering Retorts for Boron Steel Balls

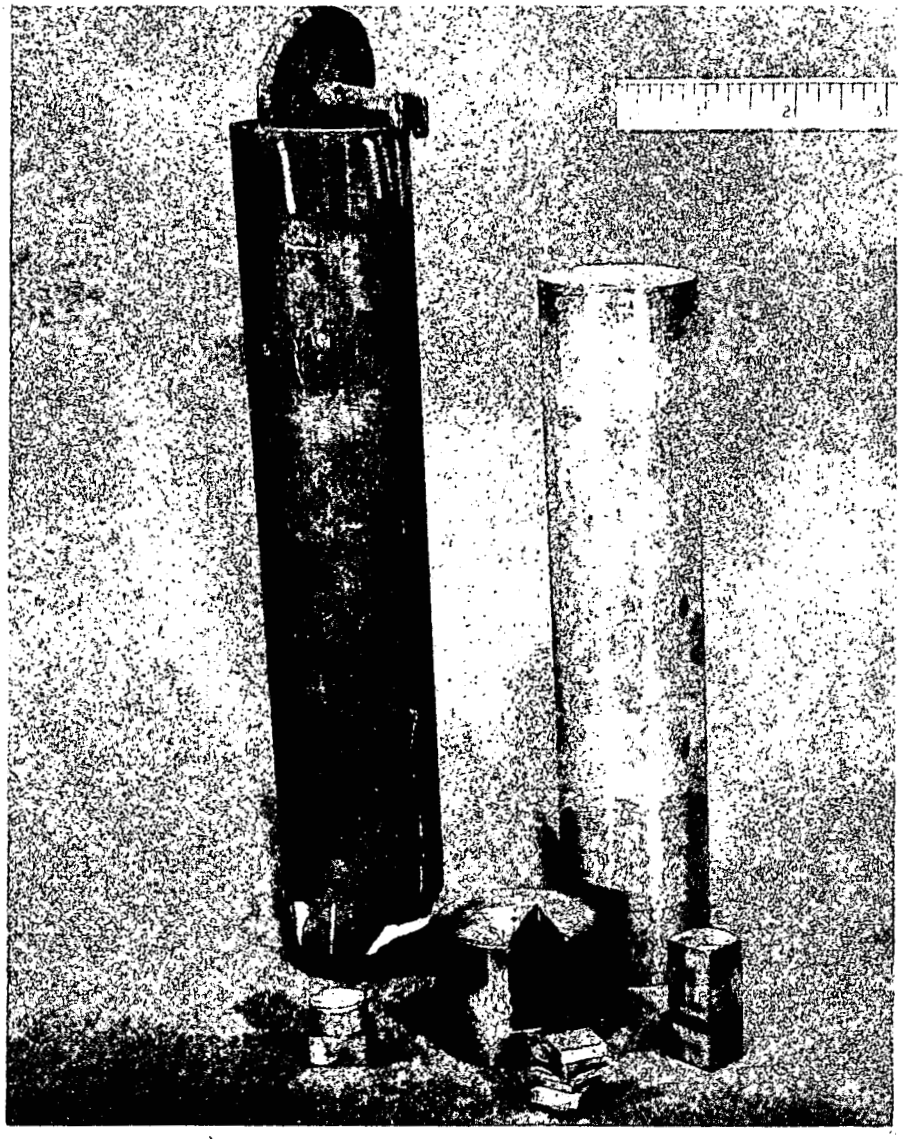

Fig. 41. Specimens and Retort for Pressure Bonding Tests of Nickel Boron Alloy and 304L Stainless Steel

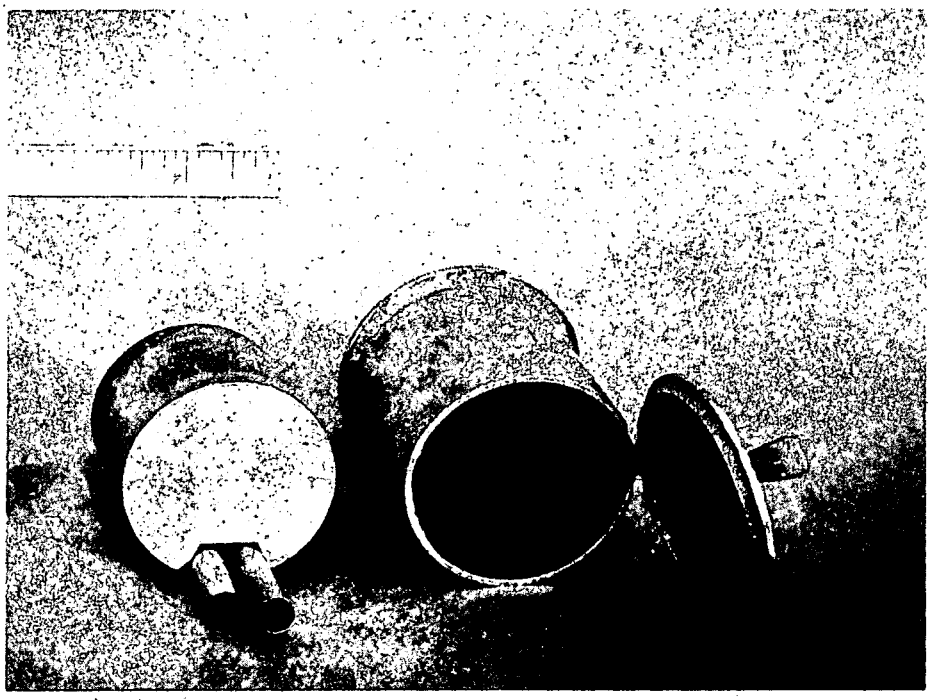

Fig. 42. Retort and 304 Stainless Steel Tube Specimens for Pressure Bonding Tests

Unclassified
SRP25-78A

X. SHIELDING

A. Top Rotating Shield

1. Arrangement (J. Churchill) - The small removable plug was increased from 16 to 19 inches in diameter and repositioned to allow greater clearance during moderator cell removal.

Two additional tubes were located in the rotating shield for neutron beam experimental facilities.

Tubular heaters will melt the metal seal between the ring shield and the rotatable shield allowing the shield to rotate freely without breaking the gas seal.

The bottom of the shield consists of a layer of lead sandwiched between a thin layer of stainless steel on the bottom and a thick layer of low carbon steel on top. Coolant tubes are imbedded in the lead. Hexagonal cans containing stainless steel wool for thermal insalation cover the bottom of the rotatable shield.

The over-all thickness of the rotatable shield is 6 feet-9 1/2 inches of which 5 feet-4 inches are high density magnetite iron ore concrete.

2. Radiation Dose Rates at Top Surface of Rotating Shield

a. Neutron Dose Rate at the Surface of the Top Shield (R. L. Ashley) Calculations to determine the neutron dose rate at the surface of the top shield have been completed. The method used was to plot a histogram of leakage neutron data considering 6 neutron groups: 2 Mev to 30 kev, 30 kev to 10 kev, 10 kev to 1 kev, 1 kev to 10 ev, 10 ev to thermal, and thermal. A smooth curve drawn through the histogram yielded a more detailed neutron spectrum. This was necessary since a large fraction of the total leakage was composed of neutrons in the 30 kev to 2 Mev range, where neutron tolerance changes by a factor of about 15. The neutron dose rate at the surface of the shield was then computed. For a 5 foot 4 inch magnetite ore concrete shield (231 lbs/ft^3) a dose rate of 0.33 mrem/hr was obtained. It should be mentioned that the value of γ used in these calculations for the highest energy group is 0.12 cm^{-1}. This value was obtained by extrapolating experimental data obtained from measurements performed on the Brookhaven shield. The slope of the neutron attenuation in the concrete, after about the first foot, is determined by this value.

b. Gamma Ray Dose Rate at the Surface of the Top Biological Shield (R. C. Gerber) - Detailed calculations to obtain the gamma ray dose rate at the surface of the top shield have been completed. The shielding materials above the reactor reflector are 5 feet 9 inches of sodium, 10 inches of thermal insulation, 1 inch of stainless steel, 1.25 inches of lead, 4 inches of iron, and 5 feet 4 inches of magnetite ore concrete (231 lbs/ft^3). The sources of gamma radiation were analyzed assuming exponential neutron attenuation through each of the materials listed above, isotropic gamma ray generation, quadratic dose buildup factors, and infinite plane source geometry. The gamma ray emission spectrum was in each case grouped to represent the dominant energies. The results of these calculations are tabulated as follows:

GAMMA RAY DOSE RATE AT SURFACE OF TOP SHIELD

Source	Gamma Ray Energies (Mev)	Dose Rate (mr/hr)
Concrete capture	9.3; 7.6; 6.0; 3.0	0.25
Iron capture	9.3; 7.6; 6.0; 3.0	0.05
Core and reflector	7.0; 5.0; 3.0	0.03
Sodium capture	6.4; 5.0; 3.0	0.02
Sodium decay	2.76; 1.38	0.0003
	Total =	0.35

The sources of error in the calculation were examined by placing limits on the microscopic data utilized in the analysis, (e.g., the gamma ray and neutron absorption coefficients and the spectral form of the capture gammas) the predicted neutron leakage from the core, source geometry, etc. The results indicate that the gamma ray dose rate can be no more than a factor of 2 above the computed value nor a factor of 10 below this value.

3. Heat Generation in the Top Shield (R. C. Gerber) - Calculations analyzing the heat generation in the top thermal and biological shields have been completed. The data from the previous section was used to obtain the sources of radiation as well as the heat generation. The results of the calculations are tabulated below.

HEAT GENERATION IN THE TOP THERMAL AND BIOLOGICAL SHIELDS

Source	Heat Generated (in Btu/hr-ft^2) in Thermal Shield	Heat Generated (in Btu/hr-ft^2) in Biological Shield
Sodium capture	48	0.5
Sodium decay	102	1.0
Iron capture	13	0.6
Core and reflector	9	0.1
Concrete capture	-	0.7
Totals	172	2.9

B. Coolant Pipe Trench and Gallery Shielding

1. General - Layout drawings have been completed for the pipe trenches in the reactor building which will carry the toluene being used as an auxiliary coolant. Toluene lines will be used for cooling the hot dry storage cells for irradiated fuel.

In order to determine the shielding requirements for the toluene, it was necessary to investigate the inorganic materials in the toluene. Specimens of toluene were irradiated in the North American Aviation Inc. water boiler reactor to measure the concentration of the impurities. The results of the experiments indicate that the resultant dose rates from the toluene impurities are so low that no shielding will be required.

2. Shielding Required for Gas Lines and Toluene Pipes in Gallery Shield (A. R. Vernon) - The trench for gas lines entering the sodium gallery has been examined to determine the required shielding. Two alternative methods of shielding have been considered. The top of the seal box, located on top of the gallery shield, may be covered with lead to attenuate the scattered gamma rays streaming up the passage, or the lower end of the passage (in the gallery) may be shielded from direct radiation. The calculations indicate that 2 inches of lead is required for the seal box in order to reduce the radiation level to 10 per cent of AEC tolerance. In order to achieve an equivalent reduction in the primary gamma-radiation reaching the important scattering region, five inches of lead would be required around the lower end of the passage. These calculations apply for a minimum scattering angle of 60°.

For pipes carrying toluene coolant from the sodium galleries it was calculated that 3.75 inches of lead were required over the floor trench where the pipe exits from the shield. Here again, the minimum scattering angle is 60°. If the toluene pipe were pointing directly at one of the sodium coolant lines in the gallery, about 8 inches of lead shielding would be required.

3. Radiation Level in Gallery due to Neutron Leakage (A. R. Vernon) - The radiation level in the gallery area due to induced activity from neutrons leaking through the regions where sodium coolant lines pass through the thermal shield has been examined. Using estimates of the neutron flux and current at the thermal shield it was possible to estimate the amount of activity induced in the gallery. After several years of continuous reactor operation, the radiation

level one meter from the sodium lines was calculated to be of the order of 20 mr/hr. It is expected that the radiation level will be greater than this value in the region of the expansion bellows. Calculations are in progress to determine the radiation level due to induced activity in the thermal shield. The effects of mass transfer from stainless steel and also the corrosion of zirconium will have to be considered as sources of additional radioactivity.

XI. REACTOR SERVICES

A. Irradiated Fuel Storage System (W. Alderson, C. W. Cook)

A new dry storage system shown in Fig. 43 has replaced the previously described water storage pond. Three different types of cells are installed into the reactor floor; namely, fuel storage, fuel cleaning, and new fuel storage. All cells are capable of receiving full length fuel elements, control mechanisms, control rod mechanisms, or any other components which can be withdrawn from the reactor. The top of all cells are level with the reactor loading face and are serviced by the fuel handling coffin.

Fuel storage cells are provided for spent fuel or irradiated elements. These cells have an external toluene cooling system for removing the afterglow heat.

Fuel cleaning cells are provided with a water spray system for removing sodium from fuel elements.

New fuel storage cells serve the purpose of storing new elements before they are placed in the reactor. Helium and vacuum lines are connected to these cells for establishing the proper helium atmosphere before the new fuel is transferred into the handling coffin.

The shielding requirements for the hot dry fuel storage tubes has been investigated. The shielding was arranged such that the radiation level in the immediate vicinity during loading and unloading operations would be less than that due to the presence of the loaded fuel handling coffin itself. The results of the calculations indicate that the floor should contain at least 1.5 feet of magnetite ore concrete (230 lbs/ft^3). Also, a 4-inch lead flange, 2 inches thick, should be attached to the bottom of the fuel handling coffin skirt. This shielding

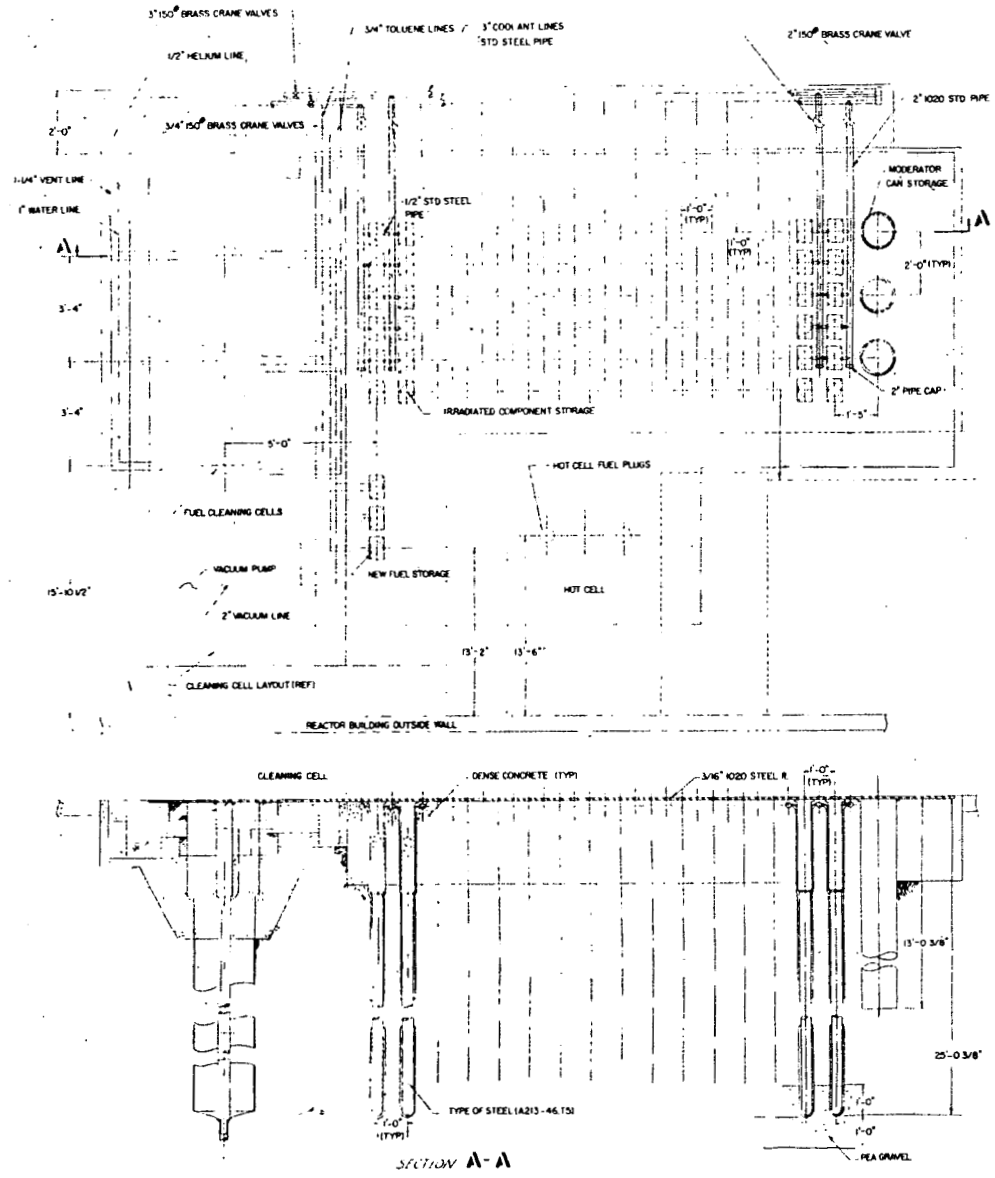

Fig. 43. SRE Dry Fuel Storage Layout

arrangement is such that the maximum radiation level 4 feet from the surface of the coffin would be about 60 mr/hr.

B. Fuel Element Handling Coffin (R. O. Crosgrove, R. L. Ashley, A. R. Vernon)

Final design layout drawings have been completed on all of the components of the fuel element coffin.

The shielding calculations for the section of the handling coffin adjacent to the active fuel have been checked. The maximum dose rate at the operator for a 9-inch lead shield was found to be 280 mr/hr. A 2.8 inch thick lead shadow shield will reduce the radiation level at the operator to just tolerance.

The shielding requirements for the bottom of the fuel handling coffin have been investigated. The results of preliminary calculations indicate that 4 inches of lead will reduce the dose rate at the operator to about 15 per cent of AEC tolerance. The dose rate 6 feet from the coffin will be about 12 mr/hr, while at 12 feet the intensity is down by about a factor of 4. Calculations to determine the shielding requirements for the section of the handling coffin above the fuel are in progress. It appears that this portion of the shield is determined by the fission product activity of the fuel and the activity induced in the control rod housing. The following shielding scheme for the side of the coffin has been proposed:

a. 9.0 inches of lead up to the top of the fuel element
b. Taper to 4.0 inches of lead six feet above the fuel element
c. Taper to 0.5 inch of lead 15 feet above fuel element
d. 0.5 inch of lead from 15 foot mark to top of coffin

All of these lead thicknesses are in addition to the 0.5 inch steel of the coffin container.

In addition, a 0.5-inch shadow shield should be placed above and a 0.25-inch shield below the operator.

Calculations have also been performed regarding the use of the fuel handling coffin for handling the reactor startup neutron source. For an antimony-beryllium source of 2×10^8 neutrons/sec the dose rate at the operator will be about 2.5 times AEC tolerance. This is considered adequate since such manipulations will certainly take place at very infrequent intervals.

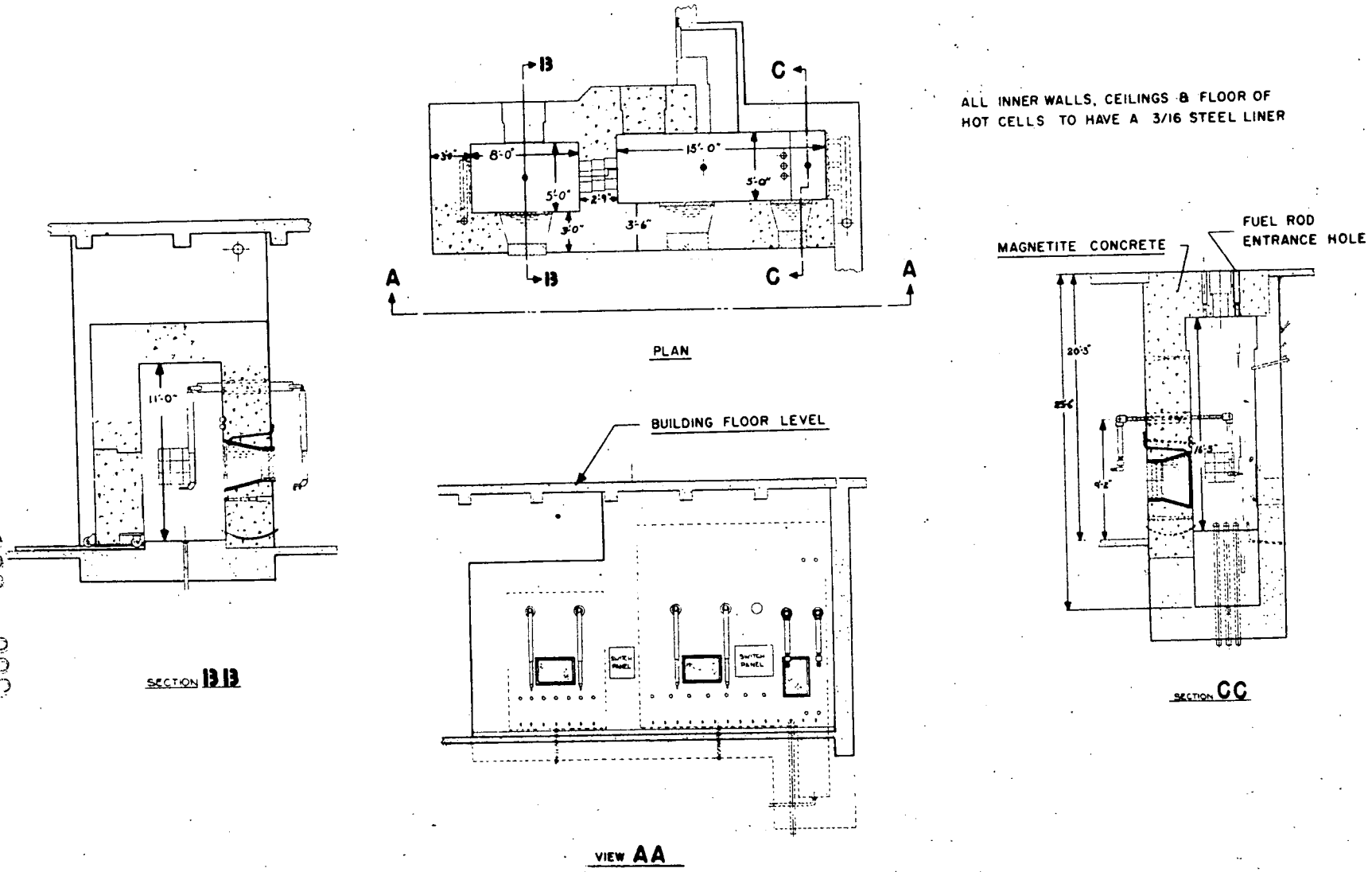

Fig. 44. Moderator Cell Coffin

C. Moderator Cell Handling Coffin (R. Crosgrove, H. DeWaid, R. L. Ashley, C. W. Cook)

A design has been completed of a handling coffin for removing and replacing the hexagonal moderator cells of the SRE. Some of the possible reasons for removal and replacement after the reactor has been operating are the following:

(a) Visual inspection for mechanical defects or failures and damage caused by installing techniques.
(b) Evaluation of probable useful cell life based on chemical or physical deterioration.
(c) Evaluation and redesign of the spacing established for maintenance of cooling film.
(d) Measurement of thermal expansion and deviation from original tolerances.
(e) Determination of the maximum permissible manufacturing tolerances based on operating experience.

The arrangement of the coffin is shown in Fig. 44. The principle of coffin operation is quite simple. The coffin is positioned over the desired (20-inch or 40-inch) reactor plug, and the plug is engaged and lifted up into the coffin. The internal mechanism of the coffin then rotates 180 degrees on the vertical axis of the coffin. This operation positions the moderator cell coffin over the hole in the reactor top. A grapple is lowered to engage and withdraw the moderator cell into the coffin. The roof plug is then replaced in the reactor. The coffin is then moved by the bridge crane to the cell washing area where the cell is removed from the coffin. A new cell is picked up by the coffin, the coffin is positioned over the reactor plug, the plug is removed, and the new cell is charged into the reactor.

Calculations to determine the shielding requirements for the moderator can removal system were completed. The following assumptions were used in the analysis:

a. All fuel is removed from the reactor prior to removal of either the 20 or 40-inch plugs.
b. The 20-inch and 40-inch plugs in the top shield will not be removed until at least 48 hours after shutdown.
c. The level of the sodium pool will be dropped to the top of the moderator cans.

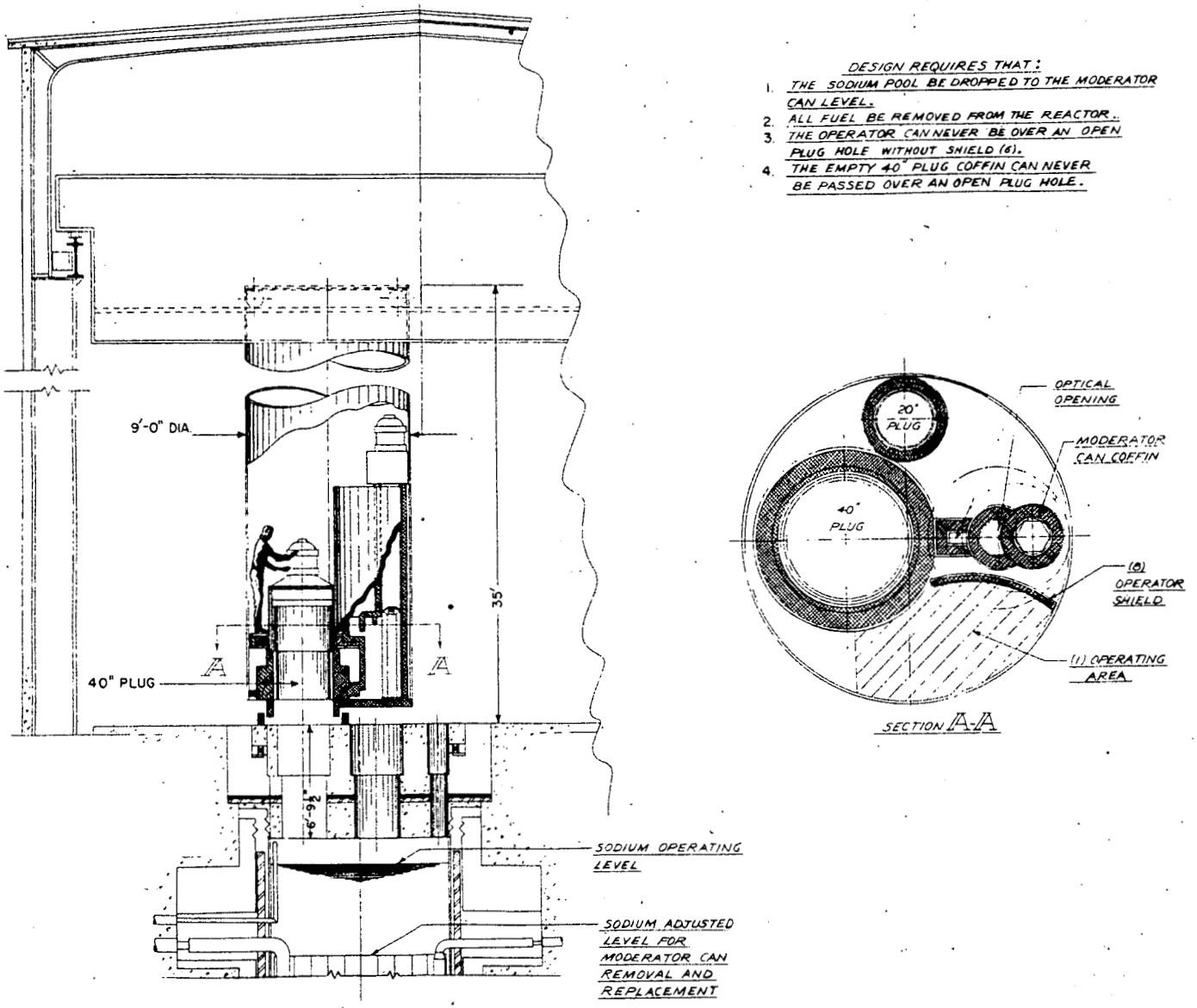

Fig. 45. Arrangement of SRE Hot Cells

d. The operator can never be positioned over any part of an empty shield plug hole.
e. The coffin for the 40-inch plug, when empty, can never pass over an open plug hole.
f. The operator is subject to gamma radiation from 3 sources:
   (1) an open plug hole
   (2) a shielded (withdrawn) plug
   (3) a shielded (withdrawn) moderator can

All shielding calculations were based on the gamma dose rates (in the area occupied by the operator) at a height of 3 to 5 feet above the top shield.

When the operator is in a position such that he does not have a direct line of sight with the reflector, the shielding over the open 40 inch diameter hole must be 1 inch of iron and 4 inches of lead. This will reduce the radiation level at the operator to 1/3 of AEC tolerance. Most of this radiation comes from scattering off the sides of the hole and from air scattering. If the operator occupies a position over the empty 40-inch hole, he must be shielded by at least 1 inch of iron and 9.7 inches of lead. Most of the direct gamma dose rate from the open hole is due to radioactive sodium when the wait time is taken as 48 hours. However, should a 9-day wait time be allowed, the major contribution to the direct dose rate would be from the activity induced in the stainless steel fittings located on top of the moderator cans. For the 9-day wait period the shielding over the hole should be 1 inch of iron and 7.3 inches of lead. Stainless steel fittings contribute most of the scattered dose rate for both wait times, therefore 1 inch of iron and 4 inches of lead are required when the operator is not in direct line of sight with the reflector.

The shielding for the 20 and 40-inch plug coffins was designed to provide a gamma dose rate of 1/3 AEC tolerance at the operator position or 250 mr/hr at the surface of the coffin, whichever requires the more shielding. The minimum shielding required for these plugs was found to be

a. 3.5 inches of lead or 1 inch of iron and 3.1 inches of lead around the bottom 2 feet of the plug.
b. 2.0 inches of lead or 1 inch of iron and 1.6 inches of lead from 2 feet to 3 feet from the bottom
c. 0.4 inches of lead or 1 inch of iron from 3 feet to the top of the plug.

d. no shielding is needed on top of the plug

A plate consisting of 1 inch of iron and 4 inches of lead should be situated within the coffin for the 20-inch plug such that it is positioned near the bottom of the coffin. This will prevent the operator from being overexposed when the empty 20-inch plug coffin passes over an open plug hole. When the plug is drawn into the coffin the plate will serve as the top shield. (No such plate is required in the coffin for the 40-inch plug as long as it will never pass over an open plug hole.)

The shielding for the moderator can coffin was designed to provide a maximum gamma dose rate of 250 mr/hr at the surface. A shadow shield has been added to provide a dose rate of 1/3 AEC tolerance at the operator. A shield consisting of 1 inch of iron and 4.5 inches of lead is required both around and on the top of the moderator can, while a 2.75-inch lead shadow shield is required between the coffin and the operator.

D. Hot Cells

The layout of the primary hot cell has been made compatible with the latest hot dry storage design. As a result of this, the hot cell is now underground with the top surface level with the hot dry storage section. The fuel elements will now be introduced into the hot cell through a hole in the ceiling (Fig. 45). The fuel coffin will be used for this operation.

A metallurgical hot cell has been attached to the side of the primary hot cell. This will be used for polishing, etching, and metallographic studies of fuel specimens. There will be specimen transfer mechanisms between the cells.

The metallurgical hot cell has one pair of master slave manipulators and the primary hot cell has two master slave manipulators plus a 1000 pound bridge crane. The metallurgical hot cell will have 3-foot walls of magnetite ore concrete (231 lb/cu ft). The primary hot cell walls will be 3.5 feet thick.

E. Radioactive Liquid Waste Disposal System (F. W. Dodge)

The method and equipment for the disposal of irradiated liquid waste has been reviewed and modified during the past quarter. The major change results from the elimination of the fuel storage pond and the use of dry storage tubes. This greatly reduces the volume of liquid which must be handled. The objective of the study was to provide the simplest and most economical arrangement with the provision for installation of separation and concentration equipment in the future.

Insofar as possible, high activity waste will be segregated from low activity waste liquids. This will be accomplished by draining all waste solutions into a sump tank, individually monitoring the solutions, and then transferring to the disposal system. Low activity liquids will be pumped directly to a large storage tank for future disposal. High activity solutions will be transferred to small hold-up tanks to allow for further decay. The solutions will then be placed in small shielded containers for final disposal. A schematic drawing of the radioactive liquid waste disposal system is shown in Fig. 46.

1. Fuel Cleaning Waste - The chief source of radioactivity in waste liquids will be the sodium washed off the discharged fuel elements during the cleaning operation. In order to allow the sodium activity to decay to a practicable level, the fuel elements will be stored for 10 days after removal from the reactor before they are washed with water. This arrangement will also permit immediate monitoring of the waste water solutions to determine their ultimate disposal. This procedure has the additional advantage of detecting a ruptured fuel rod jacket by indicating an unanticipated amount of activity in the wash water.

2. Metallurgical Hot Cell Waste - Liquid wastes from the Metallurgical Hot Cell will be isolated from liquid wastes produced in the fuel cleaning operation. Liquid wastes from the Hot Laboratory will result largely from the decanning and cleaning of fuel rods, and they will be more radioactive than wastes from the fuel cleaning operation. These wastes will also exist in a more concentrated volume, and transfer through the reactor liquid waste system would result in undesirable dilution. In addition, these wastes will be largely alcoholic, and it is not felt desirable to mix these organic wastes with water. These wastes will be disposed of in small shielded containers.

Low activity wastes from floor drains and cell decontamination will be directed to the sump tank for disposal.

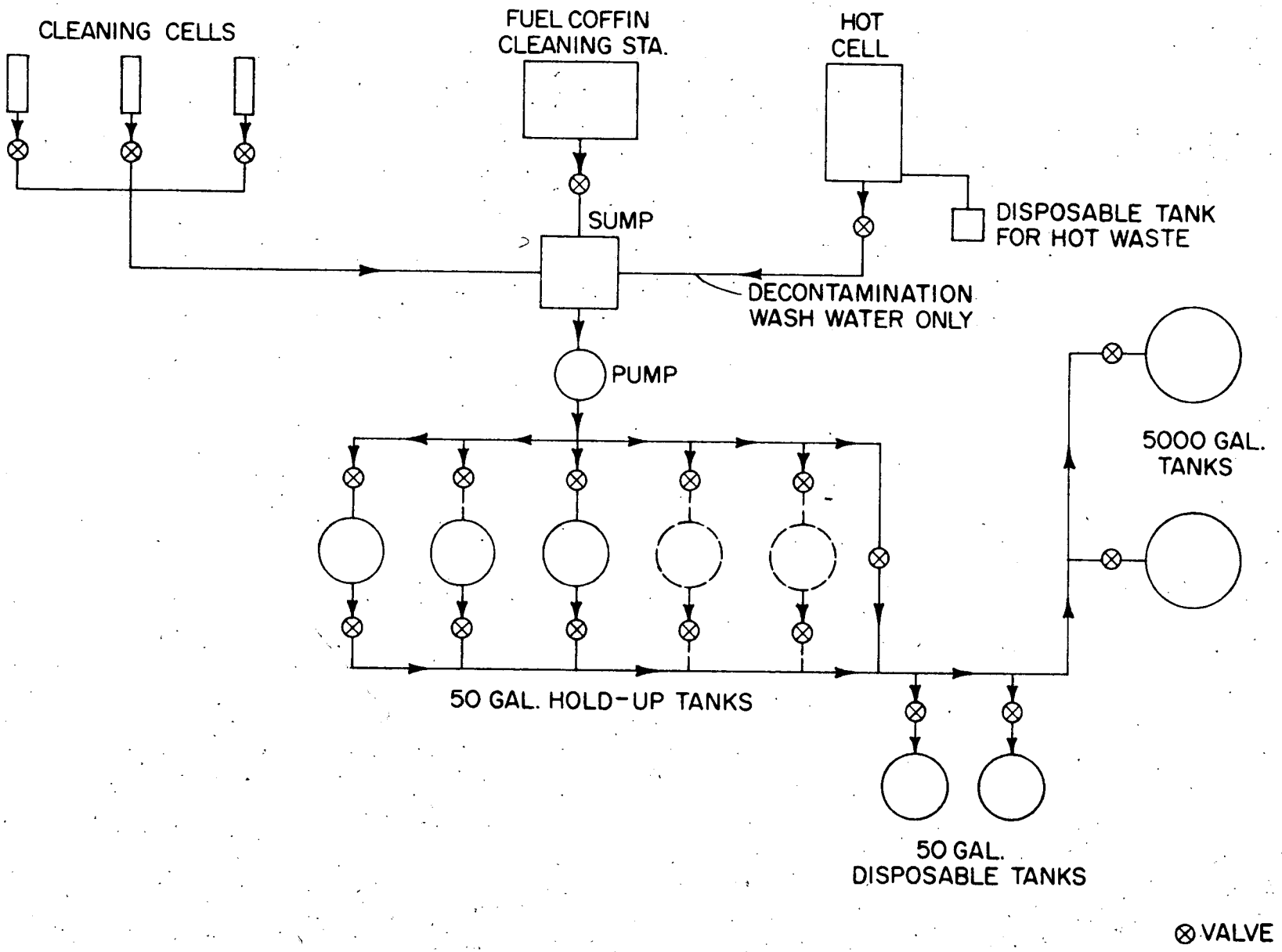

Fig. 46. Schematic of Radioactive Liquid Waste Disposal System